

2

Martin-CR-64-47 Copy No.

FACILITY FORM 802

N64-33287

(ACCESSION NUMBER)

158

(PAGES)

NASA CR 59255

(NASA CR OR TMX OR AD NUMBER)

(THRU)

(CODE)

(CATEGORY)

CONTRACT NAS8-5417

**STUDY OF TERMINAL DRAINING FOR
LIQUID OXYGEN AND
LIQUID HYDROGEN PROPELLANTS,
FINAL SUMMARY REPORT**

AUGUST 1964

OTS PRICE

XEROX

\$

5.00

MICROFILM

\$

1.00

prepared for

National Aeronautics and Space Administration
George C. Marshall Space Flight Center
Huntsville, Alabama 35812

prepared by

MARTIN COMPANY

Denver Division
Denver, Colorado 80201

Martin-CR-64-47

Copy No. 2

Contract NAS8-5417

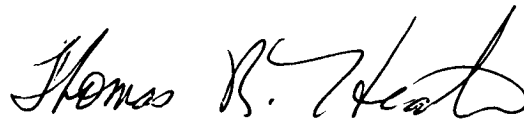
STUDY OF TERMINAL DRAINING FOR
LIQUID OXYGEN AND LIQUID HYDROGEN PROPELLANTS,
FINAL SUMMARY REPORT

August 1964

Author

J. J. Traxler
A. P. Lane

Approved

A handwritten signature in cursive script, reading "Thomas R. Heaton".

Thomas R. Heaton, Program Manager

MARTIN COMPANY
Denver, Colorado
Aerospace Division of Martin-Marietta Corporation

FOREWORD

This report is submitted in accordance with Contract NAS8-5417.

CONTRACT WORK STATEMENT

The primary objective of this study is to determine propellant residuals peculiar to tank design and to study methods of reducing residuals without significant interference with other parameters important to efficient vehicle design. The study is to be experimental and desired information is: vortex formation and surface depressions for cylindrical and toroidal tankage and tank slosh influence on toroidal tank outflow. Model tanks will be used for the investigations and toroidal tank shape, toroidal and cylindrical tank suction line arrangements, anti-vortex devices, and drainage rates will be variables studied. Water will be used as the working fluid and evidence will be provided to demonstrate applicability to liquid oxygen and liquid hydrogen propellants. The test tanks should permit visual observation whenever possible and draining phenomena should be photographed by motion picture. Tank configurations to be considered should be similar to stage propellant tanks such as a cylindrical tank with a concave bottom containing suction lines at one or more points around the periphery and a toroidal tank with one or more suction lines situated in a sump and non-sump bottom configuration.

CONTENTS

	<u>Page</u>
Foreword	ii
Contract Work Statement	iii
Contents	iv
Summary and Conclusions	ix thru xi
I. Introduction	I-1
II. Phase I -- Analysis	II-1
A. Model-Prototype Similitude Criteria . .	II-2
B. Vortexing in a Central Symmetrical Outlet	II-3
C. Tank Outlet Design	II-8
D. Dropout Residual Predictions	II-19
E. Toroidal Tank Liquid Slosh Resonant Frequencies	II-23 thru II-27
III. Phase II -- Design, Procurement and Fabri- cation	III-1
A. Design	III-1
B. Fabrication and Procurement	III-2
C. Calibration	III-3
IV. Phase III -- Test	IV-1
A. Test Objectives	IV-1
B. Test Plan	IV-2
C. Test Results	IV-6 thru IV-16

V.	Data Analysis and Correlation	V-1
	A. Liquid Residuals	V-1
	B. Toroidal Tank Liquid Slosh Resonant Frequencies	V-2
	C. Data Repeatability	V-3
VI.	Future Studies	VI-1 and VI-2

Appendixes

A.	References and Bibliography	A-1
B.	Symbols	B-1 thru B-6
C.	Engineering Drawings	C-1 thru C-34
D.	Figures and Tables	D-1 thru D-47
E.	Computer Programs	E-1 thru E-18

Distribution

Figure

1	Simulation Parameters, Cylindrical Tank . . .	D-1
2	Simulation Parameters, Toroidal Tank, Hydrogen	D-2
3	Simulation Parameters, Toroidal Tank, Oxygen	D-3

4	Influence of Friction on Nondropout Outlet Contour, Hydrogen	D-4
5	Influence of Friction on Nondropout Outlet Contour, Oxygen	D-5
6	Influence of Acceleration on Nondropout Outlet Contour, Hydrogen	D-6
7	Influence of Acceleration on Nondropout Outlet Contour, Oxygen	D-7
8	Dropout Parameter, Toroidal Tank, Nonsump Bottom	D-8
9	Dropout Parameter, Cylindrical Tank with Con- cave Lower Dome and Side Outlets	D-9
10	Toroidal Tank Sloshing Natural Frequency, Cylindrical Ring Tank	D-10
11	Toroidal Tank Sloshing Natural Frequency, Circular Canal	D-11
12	Predicted Dominant Modes, Toroidal Model Tank .	D-12
13	Model Cylindrical Tank, Concave Lower Dome . .	D-13
14	Model Toroidal Tank	D-14
15	Test System Schematic	D-15
16	Terminal Draining Study Test Setup, Cylindrical Tank Installed	D-16
17	Calibration Chart, Cylindrical Tank, Concave Lower Dome	D-17
18	Calibration Chart, Toroidal Tank	D-18
19	Calibration Part 1, 1 1/4-in. Flowmeter	D-19
20	Calibration Part 2, 1 1/4-in. Flowmeter	D-20
21	Calibration, 1/2-in. Flowmeter	D-21

22	Cylindrical Tank Baffle Configurations	D-22
23	Cylindrical Tank, Concave Lower Dome - Influences of Flowrate, Outlet Configuration, and Baffle Design on Residuals	D-23
24	Influence of Slosh and Number of Outlets on Toroidal Tank Residuals	D-24
25	Toroidal Tank Baffle Configurations	D-25
26	Selected Baffle Performance in Toroidal Model Tank	D-26
27	Toroidal Tank Residuals as a Function of Bottom Type, Number, and Size of Baffled Outlets . . .	D-27
28	Antislosh Solid Baffles Installed in Toroidal Model Tank Half	D-28
29	Antislosh Screen Baffles Installed in Toroidal Model Tank Half	D-29
30	Sump Bottom Modification Details	D-30
31	Predicted and Test Observations, Stable Planar Resonance Mode, Toroidal Model Tank	D-31
32	Predicted and Test Observations, Stable Non-planar Resonance Mode, Toroidal Model Tank . . .	D-32
33	Toroidal Tank Full-Scale Outlet Contours	D-33
34	Cylindrical Tank with Concave Lower Dome Model .	D-34
35	Calibrated Cylindrical Model Tank	D-35
36	Toroidal Model Tank	D-36
37	Outlet Inserts for Toroidal Model Tank	D-37
38	Toroidal Model Tank-Sump Bottom View	D-38
39	Terminal Draining Study Test Setup, Toroidal Tank Installed	D-39

Table

1	Toroidal Tank Outlet Design - Nondropout Outlet Computer Program Input	D-40
2	Pertinent Outlet Dropout Parameter Calculations, Cylindrical Tank - Concave Lower Dome	D-41
3	ξ_n Factors for Cylindrical Ring Tank	D-42
4	Natural Frequency Parameter, λ_n , for Circular Canal	D-43
5	Prototype and Model Tank Design Parameters . . .	D-44
6	Toroidal Tank, Sloshing Resonant Frequency Stable Planar Resonance	D-45
7	Toroidal Tank, Sloshing Resonant Frequency Stable Nonplanar Resonance	D-45
8	Comparison of Analytical and Test Results for Residuals of Selected Cylindrical Tank Outflow Tests - No Baffles, No Prerotation	D-46
9	Analytical Predictions for Residuals for Toroi- dal Tank Outflow Tests - No Sump Bottom, Baffled Outlets, No Prerotation, No Slosh	D-46
10	Selected Toroidal Tank Nonsump Bottom Test Data	D-47

SUMMARY AND CONCLUSIONS

33287

Analysis - A mathematical model is derived for describing vortexing outflow behavior in a central outlet of a cylindrical tank with a convex lower dome. The derivation is based on the constancy of circulation and on the value of the gravitational potential gradient.

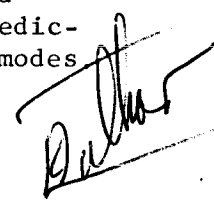
Two methods of designing propellant tank outlets to minimize propellant residuals are presented. The first, the noncavitating outlet concept, defines an outlet profile that maintains the flowing liquid static pressure constant throughout the outlet. The second concept, the nondropout outlet approach, employs the solution of the two-dimensional Bernoulli equation with the constraint that maintains a flat velocity profile in the outlet, i.e., insures a geometrically flat liquid surface as terminal draining occurs.

All mathematical models requiring automatic machine computation have been programed for the IBM 1620 computer, and sample program listings are presented in this report.

Outlet profiles designed from the nondropout approach are physically shallower than those computed using the noncavitating assumption. Since the outlet slopes of the nondropout approach are the absolute minima allowable to maintain flat velocity profiles, the longer, and hence steeper, noncavitating outlets will also prevent dropout. In actual practice, the outlet contour selected is determined by additional considerations of tank pressure, propellant volatility, and space allocations in the propellant feed system-engine interface region.

Analysis of tank residuals resulting from tank outlets not strictly amenable to the design methods discussed above is also presented. Side outlets in a cylindrical tank with concave lower dome and outlets in the toroidal tank bottom were examined. A dropout parameter, $A_s^3 \frac{dA_s}{dy}$, is derived from two-dimensional, open-channel flow theory. Critical depth values and tank residuals are analytically predicted from this parameter.

Slosh modes for the toroidal tank under lateral excitation are investigated. Two dominant modes are found, stable planar and stable nonplanar motions. Equations are presented for the prediction of the resonant response frequency of the torus to both modes



Test - Model tank outflow test data simulating residuals for full-scale cylindrical and toroidal tanks are presented here.

1. Cylindrical Tank (Concave Lower Dome)

The concave lower dome completely eliminated vortexing (even under induced prerotation) and, for all practical purposes, drop-out. A condition termed "spillover" occurred that was manifested by a localized dropout at the horizontal side outlets. Residuals were not quantitatively great, being proportional to $(\text{flowrate})^n$, where n varies from 0.47 to 0.93. None of the antivortex baffles significantly improved draining. Residuals predicted by open-channel flow analysis for unstable flow were in excellent agreement with test results.

2. Toroidal Tank

Substantial vortex-induced residuals were experienced in the toroidal tank when the outlet ports were unprotected by baffles, regardless of bottom type, slosh mode, or number and size of outlets. Correlation of residuals with analytic predictions was satisfactory.

All antivortex baffle designs tested, including the flat plate, cruciform, combination plate and cruciform, and upright cone, succeeded in materially reducing residuals. The baffle showing greatest promise was the circular flat plate with a diameter 2.5 times the outlet diameter. Further improvements were noted when this ratio was increased. Tests using the circular flat plate baffle under nonslosh and slosh modes revealed:

- 1) Outlet port uncovering is a major cause of two-phase flow;
- 2) Sump bottoms improve toroidal tank draining over non-sump bottoms;
- 3) Residuals are proportional to $(\text{flowrate})^n$ -

Nonsump bottom, $n = 0.425 - 0.838$,
 Sump bottom, $n = 1.33 - 2.25$;
- 4) Tank draining using one outlet is generally better than for two outlets, although the residual differences are minor.

Secondary objective test data analysis yields the following conclusions:

- 1) Two dominant slosh modes exist under lateral excitation. These are adequately predicted by equations derived for a circular canal and circular ring tank;
- 2) When vortex-initiated two-phase flow is absent, increasing the depth of the sump decreases toroidal tank residuals;
- 3) Antislush baffles, such as four total gradient sectors of solid or screened construction, effectively dampen fluid motions but do not significantly affect residuals unless near the outlet ports.

Conclusions - Toroidal tank residuals remain quantitatively large despite the improvement evidenced when sump bottoms and vortex inhibitors are used. The logical next phase in reducing residuals in toroidal tanks would be to develop low-level slosh-inhibiting devices for the outlet ports and to optimize sump contours.

The mathematical model programed for vortex outflow behavior is restricted to cylindrical tanks with convex lower domes. Future effort should concern application to other tank shapes, such as the toroidal tank. This is advisable because these tests have shown that vortexing two-phase flow is the prime cause of excessive residuals in toroidal tanks.

I. INTRODUCTION

Efficient design of propellant tankage requires that the maximum amount of the loaded propellant be used by the rocket engine. Stringent requirements of the power plant demand a prescribed net positive suction head (NPSH) for a pump-fed propulsion system, or at least vapor-free liquid for either pump-fed or pressure-fed systems. When these requirements are not satisfied, system malfunction will result.

NPSH supply is generally achieved by tank pressurization and the pressurizing effects of liquid elevation and vehicle acceleration. Even under conditions of adequate positive head, however, vapor inclusion in the outflowing liquid may still occur. Factors promoting this relate to certain hydrodynamic phenomena that arise in the propellant tank, such as vortexing, dropout, cavitation, and slosh. It is the investigation of these phenomena and their influence on tank residuals that constitutes the basis of this study.

This program is primarily experimental and covers outflow tests from two scaled plexiglas tanks. The first, simulating the Saturn SIVB hydrogen tank, is a cylinder with a concave lower spherical dome with side outlets. The second is a torus with outlets situated in a sump or nonsump bottom.

The program effort is divided into three phases. Phase I constitutes the analytical effort. This phase includes the derivations of equations and mathematical models describing efficient outlet design, vortex flow behavior, tank residual predictions, and toroidal tank slosh characteristics.

Phase II is the test design phase, and includes the design, fabrication, and installation of all test equipment and instrumentation.

Phase III encompasses the actual testing and data evaluation and, together with Phase II, constitutes the bulk of the program effort.

The work detailed here was funded by the National Aeronautics and Space Administration under Contract NAS8-5417. The program manager was Mr. James L. Moses of the George C. Marshall Space Flight Center Propulsion and Vehicle Engineering Division Laboratory (P&VE - PT), Huntsville, Alabama.

II. PHASE I -- ANALYSIS

Certain phenomena related to the propellant feed subsystems of liquid rocket propulsion systems have been identified as causative factors that result in unused propellant. These phenomena promote the entrainment of vapors in the liquid propellant (two-phase flow) in the outlet, particularly during terminal draining. This condition may result in a catastrophic pump-fed system malfunction, at worst, or at best, will require premature engine shutdown, resulting in excess propellant residuals.

This program investigates the vortexing, dropout, slosh, and cavitation flow phenomena.

Vortexing - Under certain outflow conditions, such as with high outflow rates and low viscosity fluids, a vortex of fluid can form over the outlet of the propellant tank. This is a localized circulatory motion of fluid with the central core depressing and moving downward toward the outlet.

Vapor entrained in the vortex core generally enters the outlet before tank depletion.

Dropout - During propellant outflow, the main liquid surface body lowers until a critical height is reached. At this height a portion of the liquid surface over the outlet dips and allows vapor to enter the tank outlet. Dropout results from a nonuniform velocity gradient across the fluid flow area in the converging tank outlet section; the height at which it occurs is termed dropout height.

Slosh - Slosh is unrestricted fluid surface oscillation within the propellant tank, which may result from motions of the vehicle or normal structural, flight control, and rocket engine system excitations.

In addition to promoting flight control, structural, and tank pressurization problems, sloshing may cause tank residuals by uncovering the tank outlet.

Cavitation - Tank outlet and baffle configurations may cause localized high propellant velocities with a resulting decrease of static pressure. When local stream static pressure falls below the liquid vapor pressure, cavitation will result. Besides this cavitation phenomenon, a dynamic flow separation can result whenever a streamline is required to change direction rapidly to follow intricate baffle or flow channel geometries. The presence of the cavitation or the flow separation may result in the admission of vapor bubbles to the tank outlet.

A. MODEL-PROTOTYPE SIMILITUDE CRITERIA

The analyses concerning the behavior of liquids in a tank during outflow and under slosh or rotation modes are based in part on certain simplifying assumptions, and therefore require experimental verification. Furthermore, the relative influence of different baffle designs and outlet configurations can only be determined with certainty by experimentation. Modeling laws permit the use of scaled tanks and substitute liquids to simplify an otherwise costly test program. Such laws may be derived from a dimensional analysis of the variables that govern the phenomena under investigation and result in the dimensionless parameters shown in the following tabulation.

Predominant Force Field	Dimensionless Control	Dimensionless Group
Gravity	Froude No.	$\frac{v^2}{La}$ or $\frac{\dot{w}^2 L}{a}$
Viscosity	Reynolds No.	$\frac{\rho VL}{\mu}$
Gravity-Viscosity	Reynolds No./ $\sqrt{\text{Froude No.}}$	$\frac{L^{3/2} a^{1/2} \rho}{\mu}$
Surface Tension	Weber No.	$\frac{\rho V^2 L}{\sigma}$

For tank draining behavior and related slosh studies under a gravity field, both gravitational and viscosity forces are effective. Thus, to achieve dynamic similarity, the Reynold No./ $\sqrt{\text{Froude No.}}$ should be constrained. To accomplish this requires very large scale models if water or gasoline are to be used as the test fluid. This, however, normally defeats the purpose of model testing. To circumvent this difficulty, a smaller scale may be selected, but this would require test fluids of unusually low kinematic viscosity that are not available.

It is evident, therefore, that some compromise must be made for these tests. While it is recognized that both gravity and viscosity forces are effective, the gravity forces normally predominate. This dominance is particularly noticeable in liquid oxygen and liquid hydrogen, which have relatively low absolute viscosities and, therefore, reduced fluid friction and drag effects. In addition, analyses of certain fluid behavior phenomena such as slosh and dropout indicate a negligible effect from viscous forces. Consequently, a Froude No. constraint should be the basis for dynamic similarity in this program.

Test values are computed as follows: (S = scale factor; g = acceleration)

$$\text{Model volume flowrate} = \frac{(\text{prototype volume flowrate})}{g^{1/2}} (S)^{5/2};$$

$$\text{Prototype residual (volume)} = \text{model residual (volume)} (S)^3;$$

$$\text{Prototype linear event} = \text{model linear event} (S);$$

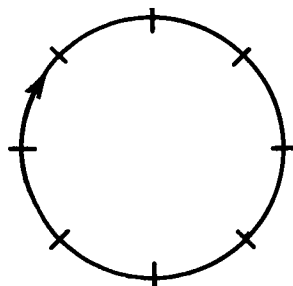
$$\text{Prototype slosh frequency} = \text{model slosh frequency} (gS)^{1/2}.$$

Figures 1, 2, and 3 present the model water flowrate as a function of propellant flowrate and prototype acceleration for both the cylindrical and toroidal tanks.

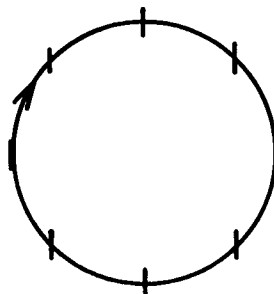
B. VORTEXING IN A CENTRAL SYMMETRICAL OUTLET

The dynamics of vortex action occurring in propellant tanks in response to external perturbances is based on Kelvin's Theorem on the conservation of circulation in an incompressible, nonviscous fluid. As derived in classical hydrodynamic texts (Ref 1 and 2), Kelvin's Theorem explains that the circulation along a closed curve is not destroyed under the influence of an irrotational field of force such as gravity. If the curve were under the influence of a potential function, such as the gravity potential function, the vortex tube itself would respond to the potential gradient, but the circulation within the vortex tube would not be changed. In other words, if a fluid is moving through a cylindrical tube, such as the upper portion of a propellant tank, and if vortex tubes are initially present in the fluid, they will simply translate along with the moving fluid. If, however, the vortex tube were suddenly forced to assume a smaller radius, a momentum balance would demand that the circulation increase to maintain the original angular momentum. This is demonstrated by the increased angular speed as a rotating fluid flows through a constriction.

In the following discussion, it will be important to distinguish between two types of rotational flow, forced vortexing and free vortexing. The first type is that experienced when the fluid is forced to vortex by a paddle rotating the fluid. The orientation of any general particle in vortex flow is shown in the following sketch.



a. Forced Vortexing



b. Free Vortexing

Note that the fluid in forced vortexing rotates as a solid body. This type of vortexing is often called solid-body rotation. In contrast to solid-body rotation, the mechanism of free vortexing shows that the natural undisturbed mode takes over after the removal of the paddle.

Imagine a circular plate of thickness dh composed of a large number of fluid particles, and imagine a paddle forcing the differential plate to rotate as a solid body as in (a) of the preceding sketch. The kinetic energy input to the differential element is the sum of the kinetic energies of the individual particles:

$$KE = \sum_{n=1}^N \frac{1}{2} m_n (r_n \omega_n)^2 = \frac{1}{2} \omega_o^2 \sum_{n=1}^N m_n r_n^2, \quad [1]$$

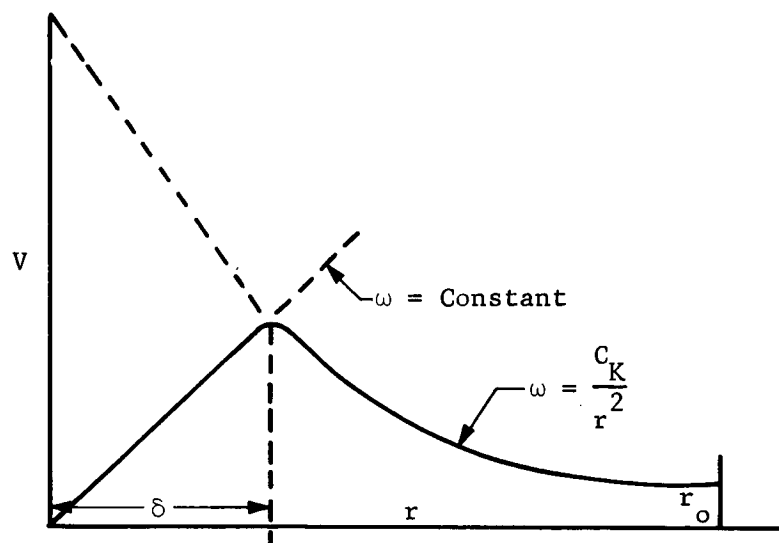
where N = number of particles in the plate and ω_o = the initial angular rotation of the particles. Other symbols are defined in Appendix B. Now, if the paddle is removed,

$$\text{Torque} = \frac{d \left(\sum_{n=1}^N m_n r_n V_n \right)}{dt} = 0. \quad [2]$$

Since m_n is constant with time,

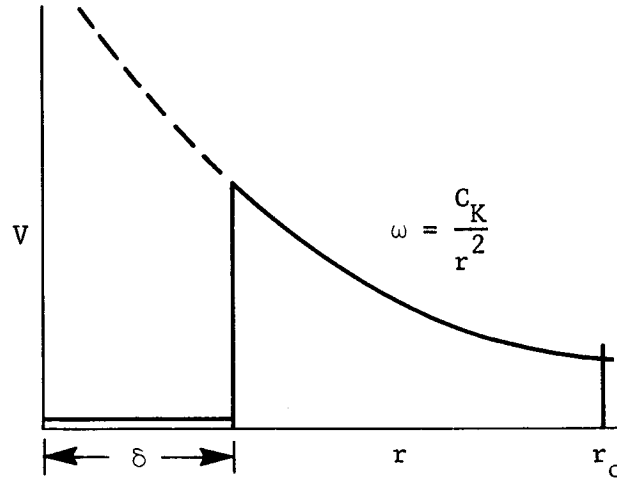
$$\frac{d(r_n V_n)}{dt} = 0, \text{ or } r_n V_n = C_K \text{ (a constant), and } \omega_n = \frac{C_K}{2r_n^2}. \quad [3]$$

Equation [3] gives the ω -distribution of the free vortex as a function of radius. However, the formula predicts an infinitely large ω for particles at the origin, which is not physically possible. This difficulty may be resolved in one of three ways. First, if vortexing is severe enough, an "air pipe" or vapor core will descend through the element, as is often observed in vortexing. The core of radius prevents the radius of any particle from becoming infinitely small and permits the velocity distribution as given in Eq [3] to prevail. Second, if we hypothesize a central core of the element rotating as a solid body, the velocity distribution may prevail up to the perimeter of the solid-body core. This case is illustrated in the following sketch.



Free Vortexing with a Solid-Body Rotating Core

The third possibility for reconciling the free-body velocity distribution with an actual physical system is by the insertion of an artificial core of radius δ , which physically prevents any fluid from getting closer to the origin than δ . This scheme is represented in the following sketch.



Free Vortexting with a Stationary Core

No matter what the particular manner of establishment of a core δ , the redistributed velocity function of the differential element must yield the same kinetic energy for the element as the input energy. Therefore,

$$\frac{1}{2} \omega_o^2 \sum_{n=0}^N m_n r_n^2 = \frac{1}{2} \sum_{n=0}^N m_n r_n^2 \frac{C_K^2}{r_n^4},$$

$$C_K = \omega_o \sqrt{\frac{\sum_{n=0}^N (r_n^2)}{\sum_{n=0}^N \left(\frac{1}{r_n}\right)^2}}. \quad [4]$$

Knowing ω_o , and location of the particles, we may calculate C_K . Then from Eq [3], the resultant velocity distribution may be determined.

The velocity redistribution, however, if unaccompanied by any compensating factors, would give rise to the phenomenon of adjacent annuli with unequal energies. The kinetic energy of any particle

at a radius r_n from the origin is $1/2 m_n r_n^2 \omega_n^2 = 1/2 \frac{C_K^2}{r_n^2} m_n r_n^2$,

$$KE = 1/2 \frac{m_n C_K^2}{r_n^2}, \quad [5]$$

which is clearly a function of r . But note that adjacent particles do not exist with unequal energies; they adjust their height until their energies are equal. The total energy of any particle is given by

$$E_m = KE_n + m_n g h_n.$$

Taking the height of a particle at r_o to be zero, the energy of any particle must be

$$E_m = KE_{(r_o)},$$

and

$$KE_n + m_n g h_n = KE_{(r_o)},$$

$$h_n = \frac{KE_{(r_o)} - KE_n}{m_n g} = 1/2 \frac{\left[\frac{m_{(r_o)} C_K^2}{(r_o)^2} - \frac{m_n C_K^2}{(r_n)^2} \right]}{m_n g}.$$

Since all the particles are assumed to be of the same mass, the expression for the height of any particle, relative to the particles at r_o , is

$$h_n = c_K^2 \frac{\left[\left(\frac{1}{r_o} \right)^2 - \left(\frac{1}{r_n} \right)^2 \right]}{2g} \quad [6]$$

A mathematical model describing the vortex phenomenon can be set up rather simply if one assumes that the tangential velocity distribution of rotating outflow is superimposed on the normal streamline velocity profiles of nonrotating outflow. In this way a particle's radial position is known by a proportionality factor and the actual outlet contour. Based on this assumption, the angular rotation history of any particle can be readily determined at any time during the outflow, since the conservation of angular momentum demands that for any particle n , at a known level K ,

$$(\omega_{k,n})(r_{k,n})^2 = (\omega_{k+1,n})(r_{k+1,n})^2 \quad [7]$$

The tank is divided into vertical "K" levels and radial bands. In proceeding from the K^{th} to the $K + 1^{\text{st}}$ level, the height of each band adjusts to maintain an energy balance as expressed by Eq [6]. This adjustment of the height of each band is repeated until the tank is depleted. Two-phase flow is assumed to occur when the height profile, determined by heights of adjacent bands, lies tangent to the hypothetical vortex core.

This mathematical model is programed for the IBM 1620 computer and is discussed in Appendix E.

C. TANK OUTLET DESIGN

There are several methods of designing propellant tank outlets to minimize and even preclude two-phase flow from the tank. These methods have been derived to prevent cavitation and/or dropout in the tank outlet, and they are simplified by assuming the absence of flow perturbations such as vortexing or sloshing. These methods are described below.

1. Noncavitating Outlet

Assuming one-dimensional flow theory applies, and neglecting frictional pressure losses, the static pressure is maintained at some value greater than the liquid vapor pressure throughout the outlet. On the basis of this constraint, the pressure relationship between two horizontal levels is

$$\frac{P_1}{\rho} + \frac{ah_1}{g_c} - \frac{V_1^2}{2g_c} = \frac{P_2}{\rho} + \frac{ah_2}{g_c} - \frac{V_2^2}{2g_c}. \quad [8]$$

When the applied ullage pressure is constant, as is often the case, $P_1 = P_2$, and Eq [8] reduces to

$$\frac{ah_1}{g_c} - \frac{V_1^2}{2g_c} = \frac{ah_2}{g_c} - \frac{V_2^2}{2g_c} = \text{constant}. \quad [9]$$

The origin of the fluid height is taken at the entrance to the outlet where the fluid velocity is still relatively small and Eq [9] is essentially zero. Thus, in all other outlet points, (2, 3, ..., n), the required velocity is

$$V_n^2 = 2ah_n, \quad [10]$$

where h_n is measured with the positive sense in the direction of flow. From the continuity equation applied to a circular cross section, an expression for the outlet diameter is obtained as a function of the distance below the entrance to the outlet,

$$D_n = 0.949 \sqrt[4]{\frac{Q^2}{ah_n}} \text{ ft.} \quad [11]$$

2. Nondropout Outlet

The liquid dropout point is defined as that instant during outflow when two-phase flow is initiated in the outlet while liquid remains in the tank. To assure that dropout does not occur, the tank wall surface about the outlet should be contoured so that the axial velocity component of a streamline adjacent to the wall surface is identical to the average velocity in the center of the outlet at the same elevation. Thus with equal axial velocity vectors, the fluid surface remains geometrically flat throughout the outlet. In practice the tank pressure is also usually maintained high enough to prevent cavitation in the nondropout outlet.

These assumptions are made in this analysis:

- 1) Axially symmetrical outlet;
- 2) Vortex-free outflow;
- 3) Slosh-free outflow.

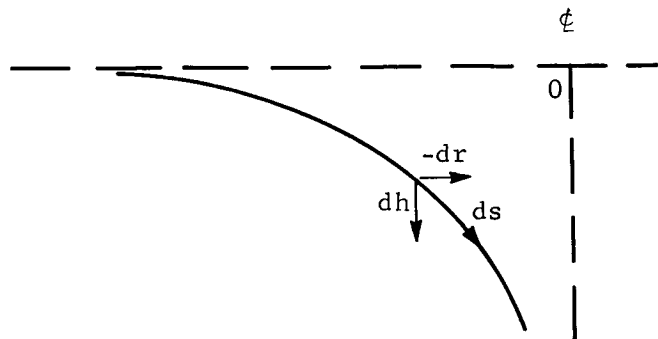
Bernoulli's equation applied to the stream line adjacent to the outlet wall, with no external work, expressed in total differential form is

$$\frac{dP}{\rho} + a dh + \frac{1}{2} d(v_s^2) + g_c dE_f = 0. \quad [12]$$

To simplify, set $dP = 0$. Equation [12] can now be expressed as a differential equation with respect to the variable "r"

$$a \frac{dh}{dr} + V_s \frac{dV_s}{dr} + g_c \frac{dE_f}{dr} = 0. \quad [13]$$

Circular Cross Section - Examine the stream line, taking the origin at the elevation of the point of tangency of the outlet to the tank.



$$\text{Slope} = - \frac{dh}{dr}$$

$$ds^2 = dr^2 + dh^2$$

$$\left(\frac{ds}{dr}\right) = - \sqrt{1 + \left(\frac{dh}{dr}\right)^2}$$

$$\left(\frac{ds}{dr}\right) = \sqrt{1 + \left(\frac{dh}{dr}\right)^{-2}}$$

$$V_s = V_h \frac{ds}{dh} = V_h \sqrt{1 + \left(\frac{dh}{dr}\right)^{-2}}$$

The average fluid velocity is

$$V_{avg} = \frac{Q}{\pi r^2}$$

Equating this to the axial component at the wall stream line:

$$V_h = Q/\pi r^2,$$

$$V_s = (Q/\pi r^2) \sqrt{1 + \left(\frac{dh}{dr}\right)^{-2}}.$$

Differentiating this expression with respect to r,

$$\frac{dV_s}{dr} = -2 \frac{Q \sqrt{1 + \left(\frac{dh}{dr}\right)^{-2}}}{\pi r^3} - \frac{Q}{\pi r^2} \frac{\left(\frac{dh}{dr}\right)^{-3} \frac{d^2h}{dr^2}}{\sqrt{1 + \left(\frac{dh}{dr}\right)^{-2}}}. \quad [14]$$

For incompressible flow, the friction loss at the wall is

$$\frac{E_f}{s} = \frac{V_s^2}{Ch^2 R} = \frac{2V_s^2}{Ch^2 r}, \quad [15]$$

where R, the hydraulic radius, is $r/2$ for circular outlet and Ch, the Chezy loss coefficient, is $\sqrt{\frac{8g_c}{f}}$.

Differentiating with respect to \underline{s} ,

$$\frac{dE_f}{ds} = \frac{d}{ds} \left(\frac{2V_s^2}{Ch^2 r} \right) = \frac{2Q^2}{\pi^2 r^5 Ch^2} \left(1 + \left(\frac{dh}{dr} \right)^{-2} \right)$$

Differentiating the friction loss with respect to r and substituting known values,

$$\frac{dE_f}{dr} = \frac{dE_f}{ds} \frac{ds}{dr} = - \frac{2Q^2}{\pi^2 r^5 Ch^2} \left(1 + \left(\frac{dh}{dr} \right)^{-2} \right) \sqrt{1 + \left(\frac{dh}{dr} \right)^2} \quad [16]$$

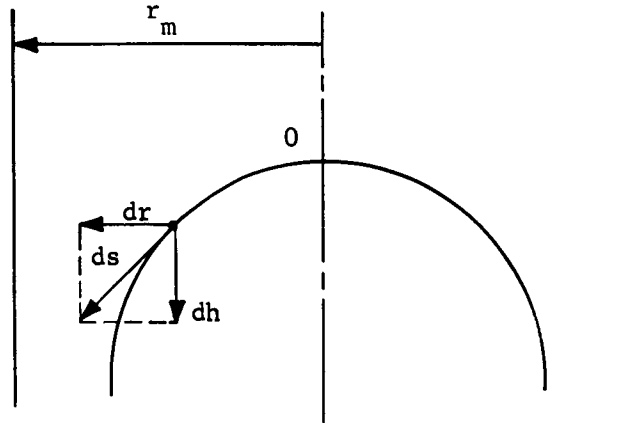
It is now possible to substitute known values for V_s , $\frac{dV_s}{dr}$, and $\frac{dE_f}{dr}$ into Eq [13] to get

$$\begin{aligned} a \frac{dh}{dr} - \frac{2Q^2}{\pi^2 r^5} \left(1 + \left(\frac{dh}{dr} \right)^{-2} \right) - \frac{Q^2}{\pi^2 r^4} \left(\frac{dh}{dr} \right)^{-3} \frac{d^2 h}{dr^2} \\ - \frac{2g_c Q^2}{Ch^2 r^5 \pi^2} \left(1 + \left(\frac{dh}{dr} \right)^{-2} \right) \sqrt{1 + \left(\frac{dh}{dr} \right)^2} = 0. \end{aligned} \quad [17]$$

Simplifying by dividing by $-\left(\frac{Q^2}{\pi^2 r^4} \left(\frac{dh}{dr}\right)^{-3}\right)$ a second order differential equation in h and r as obtained.

$$\frac{d^2 h}{dr^2} + \left(\left(\frac{dh}{dr} \right)^3 + \frac{dh}{dr} \right) \left(\frac{2}{r} + \frac{2g_c}{Ch^2 r} \sqrt{1 + \left(\frac{dh}{dr} \right)^2} \right) - \frac{\pi^2 r^4}{Q^2} a \left(\frac{dh}{dr} \right)^4 = 0. \quad [18]$$

Circular Annular Cross Section - Examining as before the stream line adjacent to the wall and taking the origin at the apex of the concave lower dome, a similar procedure results in the following equations:



$$\text{Slope} = \left(\frac{dh}{dr} \right)$$

$$\left(\frac{ds}{dh} \right) = \sqrt{1 + \left(\frac{dh}{dr} \right)^2}$$

$$\left(\frac{ds}{dr} \right) = \sqrt{1 + \left(\frac{dh}{dr} \right)^2}$$

At the outer wall,

$$v_h = v_s = \frac{Q}{\pi(r_m^2 - r^2)}$$

At the inner wall,

$$v_s = v_h \left(\frac{ds}{dh} \right) = \frac{Q \sqrt{1 + \left(\frac{dh}{dr} \right)^2}}{\pi(r_m^2 - r^2)}$$

[19]

Since we are concerned with the inner wall contour, Bernoulli's equation is applied to the stream line adjacent to the inner wall. Differentiating Eq [19] with respect to r ,

$$\frac{dV_s}{dr} = \frac{2rQ\sqrt{1 + \left(\frac{dh}{dr}\right)^{-2}}}{\pi(r_m^2 - r^2)^2} - \frac{Q\left(\frac{dh}{dr}\right)^{-3} \frac{d^2h}{dr^2}}{\pi(r_m^2 - r^2)\sqrt{1 + \left(\frac{dh}{dr}\right)^{-2}}}. \quad [20]$$

Friction loss at the wall is governed by Eq [15]. The hydraulic radius for the annular cross section is

$$R = \frac{\pi(r_m^2 - r^2)}{2\pi(r_m + r)} = \frac{r_m - r}{2},$$

Differentiation of E_f of Eq [15] with respect to r similar to the procedure followed for Eq [16], and substituting appropriate values for R , ds/dr , and V_s , we obtain

$$\frac{dE_f}{dr} = \frac{dE_f}{ds} \frac{ds}{dr} = \frac{2V_s^2}{Ch^2(r_m - r)} \frac{ds}{dr} = \frac{2Q^2}{\pi^2 Ch^2} \frac{\left(1 + \left(\frac{dh}{dr}\right)^{-2}\right)\sqrt{1 + \left(\frac{dh}{dr}\right)^2}}{(r_m^2 - r^2)^2 (r_m - r)}. \quad [21]$$

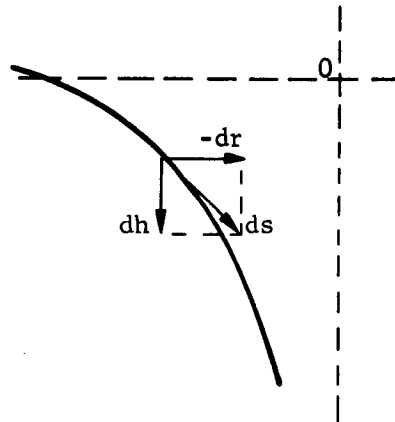
Substituting Eq [19], [20], and [21] into Eq [13]

$$\begin{aligned} a \frac{dh}{dr} + \frac{2Q^2 r \left(1 + \left(\frac{dh}{dr}\right)^{-2}\right)}{\pi^2 (r_m^2 - r^2)^3} - \frac{Q^2 \frac{d^2h}{dr^2} \left(\frac{dh}{dr}\right)^{-3}}{\pi^2 (r_m^2 - r^2)^2} + \\ + \frac{2g_c Q^2 \left(1 + \left(\frac{dh}{dr}\right)^{-2}\right)\sqrt{1 + \left(\frac{dh}{dr}\right)^2}}{Ch^2 \pi^2 (r_m^2 - r^2)(r_m - r)}. \end{aligned} \quad [22]$$

Simplifying by dividing by $\frac{-Q^2(dh/dr)^{-3}}{\pi^2(r_m^2 - r^2)^2}$, a second order equation in h and r similar to Eq [18] is obtained.

$$\frac{d^2h}{dr^2} - \left[\left(\frac{dh}{dr} \right)^3 + \frac{dh}{dr} \right] \left[\frac{2r}{r_m^2 - r^2} + \frac{2g_c \sqrt{1 + \left(\frac{dh}{dr} \right)^2}}{Ch^2 (r_m - r)} \right] - \frac{\pi^2 a (r_m^2 - r^2)^2 \left(\frac{dh}{dr} \right)^4}{Q^2} = 0. \quad [23]$$

Rectangular Central Outlet -



We examine the stream line adjacent to the wall of this rectangular outlet (total depth = δ) taking the origin at the elevation of the point of tangency of the outlet to the tank.

$$\text{Slope} = - \frac{dh}{dr}$$

$$ds^2 = dr^2 + dh^2$$

$$V_s = V_h \frac{ds}{dh} = V_h \sqrt{1 + \left(\frac{dh}{dr} \right)^{-2}}$$

$$\frac{ds}{dr} = \sqrt{1 + \left(\frac{dh}{dr} \right)^2}$$

The average fluid velocity is

$$V_{\text{avg}} = \frac{Q}{2\delta r}.$$

Equating this value to the axial component at the wall stream line,

$$V_h = V_{\text{avg}},$$

$$V_s = \frac{Q \sqrt{1 + \left(\frac{dh}{dr}\right)^{-2}}}{2\delta r}. \quad [24]$$

Differentiating V_s with respect to r

$$\frac{dV_s}{dr} = \frac{Q \sqrt{1 + \left(\frac{dh}{dr}\right)^{-2}}}{2\delta r^2} - \frac{Q \left(\frac{dh}{dr}\right)^{-3} \frac{d^2h}{dr^2}}{2\delta r \sqrt{1 + \left(\frac{dh}{dr}\right)^{-2}}}. \quad [25]$$

Friction loss at the wall is governed by Eq [15]. The hydraulic radius for the rectangular cross section is

$$R = \frac{2\delta r}{2(\delta + 2r)} = \frac{r\delta}{\delta + 2r}.$$

Differentiation of E_f in Eq [15] with respect to r similar to the procedure followed for Eq [16], and substituting appropriate values for R , ds/dr , and V_s we obtain

$$\frac{dE_f}{dr} = \frac{dE_f}{ds} \frac{ds}{dr} = \frac{-Q^2 \left(1 + \left(\frac{dh}{dr}\right)^{-2}\right) (\delta + 2r) \sqrt{1 + \left(\frac{dh}{dr}\right)^2}}{4\delta^3 r^3 Ch^2}. \quad [26]$$

Substituting Eq [24], [25] and [26] into Eq [13]

$$\begin{aligned} a \frac{dh}{dr} - \frac{Q^2 \left(1 + \left(\frac{dh}{dr}\right)^{-2}\right)}{4\delta^2 r^3} - \frac{Q^2 \left(\frac{dh}{dr}\right)^{-3} \frac{d^2h}{dr^2}}{4\delta^2 r^2} - \\ - \frac{g_c Q^2 (\delta + 2r) \left(1 + \left(\frac{dh}{dr}\right)^{-2}\right) \sqrt{1 + \left(\frac{dh}{dr}\right)^2}}{4\delta^3 r^3 Ch^2} = 0. \end{aligned} \quad [27]$$

Simplifying by dividing by $-\frac{Q^2 \left(\frac{dh}{dr}\right)^{-3}}{4\delta^2 r^2}$, a second order differential equation in h and r , similar to Eq [18] and [23], is obtained.

$$\begin{aligned} \frac{d^2 h}{dr^2} + \left(\left(\frac{dh}{dr} \right)^3 + \frac{dh}{dr} \right) \left(\frac{1}{r} + \frac{g_c (\delta + 2r) \sqrt{1 + \left(\frac{dh}{dr} \right)^2}}{Ch^2 \delta r} \right) \\ - \frac{4a\delta^2 r^2 \left(\frac{dh}{dr} \right)^4}{Q^2} = 0. \end{aligned} \quad [28]$$

Method of Solution - Solutions of Eq [18], [23] and [28] describe the contour of a nondropout outlet for the appropriate outlet arrangement. This has been accomplished by a computer program detailed in Appendix E.

3. Simplified Design Approach

Recognizing that solutions of the previous equations are extremely difficult to solve manually and require machine-oriented numerical computation procedures, a simplifying assumption has been considered to enable rapid calculation. Assuming that the resulting slope of the contour is relatively constant, then

$$\frac{d^2 h}{dr^2} = 0.$$

These equations will then reduce to easily solvable forms for the circular, circular annular, and rectangular outlets.

$$r = \sqrt[5]{\frac{2Q^2 \left(1 + \left(\frac{dh}{dr} \right)^2 \right)}{\pi^2 a \left(\frac{dh}{dr} \right)^3} + \frac{g_c \left(1 + \left(\frac{dh}{dr} \right)^2 \right)^{3/2}}{Ch^2}}. \quad [18a]$$

$$\begin{aligned} \left(r_m^2 - r^2 \right)^2 \left(r_m - r \right) = - \frac{2Q^2}{\pi^2 a \left(\frac{dh}{dr} \right)^3} \left[\frac{1 + \left(\frac{dh}{dr} \right)^2}{r_m + r} r + \right. \\ \left. + \frac{g_c \left(1 + \left(\frac{dh}{dr} \right)^2 \right)^{3/2}}{Ch^2} \right] \end{aligned} \quad [23a]$$

$$r = \sqrt[3]{\frac{Q^2}{4a\delta^2} \left(1 + \left(\frac{dh}{dr}\right)^2\right) + \frac{g_c (\delta + 2r) \left(1 + \left(\frac{dh}{dr}\right)^2\right)^{3/2}}{Ch^2 \delta}}. \quad [28a]$$

Unfortunately, the actual slope is not even remotely constant, so certain inaccuracies are inevitable.

4. Applications

A typical design case has been calculated by both of the design methods. The nondropout outlet rigorous solution produces a comparatively shallow outlet contour, because it generates the absolute minimum slope condition for preventing dropout. The outlet contour calculated from the noncavitating criterion (first method) has a slope in excess of the minimum required to prevent dropout. The latter criterion, therefore, generates a contour which is also a nondropout shape, but which may suffer from excessive longitudinal space requirements.

The outlet contours for the toroidal tank model tanks were designed in accordance with the mathematical model developed in Appendix E for the circular symmetrical nondropout outlet. Prototype parameters were used and the resultant contour scaled to model dimensions. A minimum acceleration condition was used since this resulted in the maximum contour length, and thus would perform satisfactorily under higher acceleration levels. Pertinent design parameters include:

- 1) Hydrogen flowrate - 14 lb_m/sec;
- 2) Oxygen flowrate - 7 lb_m/sec;
- 3) Acceleration - 16.1 ft/sec²;
- 4) Outlet line size based on 25 fps nominal velocity.

The Chezy loss coefficient, Ch, for both liquid oxygen and liquid hydrogen was computed on the basis of an outlet wall surface smoothness of 10⁻⁵ ft. This resulted in Ch values of 151 and 160 for lox and hydrogen, respectively. Conservatively, a Ch value of 150 was used throughout. Program input constants are listed in Table 1. The results of these calculations are illustrated (Fig. 33). This figure depicts the outlet contour for both hydrogen and oxygen before the 1/4 scaling for the water outflow tests.

5. Effect of Parametric Variations on Nondropout Outlet Contours

The effects of a variation in certain parameters on the nondropout outlet contour have been investigated. The exact solution for a circular outlet, Eq [18], was used in this investigation. The principal parameter studies include the Chezy loss coefficient $\sqrt{\frac{8g_c}{f}}$, and tank acceleration. Wide variations were considered despite the fact that these parameters are normally constrained by physical laws or specification tolerances. However, parametric influence evaluation is still useful, especially for application studies.

Figures 4 and 5 show that the influence of friction in outlet contour is minimal for both hydrogen and lox propellants. In fact no change in contour is evidenced for Ch values greater than 100. This corresponds to a friction factor less than 0.0257. Actual calculation of friction factors for these propellants based on Poiseuille flow theory and normal flow channel materials are of the order of 0.01. It is therefore concluded that reasonable variations of friction factor will have negligible effect on tank draining for a given outlet contour.

Figures 6 and 7 show that the length of the tank outlet has an inverse relationship with longitudinal acceleration. Although the influence is small, outlets should be designed on the basis of the minimum acceleration. Thus, while the longest contour will be generated, this will assure adequacy for the range of accelerations anticipated.

D. DROPOUT RESIDUAL PREDICTIONS

In many applications propellant tank bottoms and outlet configurations are such that (1) the nondropout outlet design equations do not apply, or (2) the precise nondropout outlet contour cannot be fabricated. Two cases in point are the model tanks being evaluated in this program. These tank shapes are not exactly covered by the derived equations.

The toroidal tank outlet contour can be approximated by the theory for a central circular outlet, Eq [18], although it is expected that there should be some effect from the noncylindrical tank geometry. Likewise the cylindrical model with concave bottom dome and horizontal side outlets is not exactly covered by the design theory for a circular annular cross section, Eq [23]. Nevertheless, a calculation of the outlet contour of a circular annular outlet was completed and showed that the actual concave dome slope was more than sufficient to prevent dropout.

Outflow tests verified the above conclusion regarding the bulk of the cylindrical tank dropout residuals, but residuals still were sustained because of the flow behavior at the horizontal side outlets. A liquid surface depression immediately above the side outlet(s) is noted at terminal draining. This spillover condition, i.e., side outlet dropout, is immediately followed by two-phase flow in the outlet.

Since both tank configurations are unique and do not lend themselves to the exact analysis mentioned above, an attempt has been made to predict actual tank residuals.

The analysis that follows has been previously used with great success in predicting dropout height for nonideal circular outlets in cylindrical tanks with convex lower domes.

Frictionless, uniform, incompressible, two-dimensional open-channel flow is assumed. Open-channel flow theory is considered since the flow at or near the dropout point is primarily parallel to the tank bottom and the fluid surface is free.

Applying Bernoulli's equation to the flow, but modifying it by the specific energy concept with the datum at the bottom of the outlet, the following expression is obtained.

$$e = \frac{ah}{g_c} + \frac{V_s^2}{2g_c} \quad [29]$$

Since V_s is the circumferential velocity, the continuity equation is applied noting that the channel flow consists of two approaches to the outlet. A_s is the area sum of the two approaching channels.

$$e = \frac{ah}{g_c} + \frac{Q^2}{2g_c A_s^2} \quad [30]$$

It has been established that fluid surface dropout arises from the unstable flow conditions existing in open-channel flow at the interface of the tranquil and rapid flow regimes. The height at this interface is usually termed critical depth and is the height at which dropout occurs. This interface is defined by the condition of minimum specific energy. To obtain the minimum energy, the derivative of e with respect to h is set equal to zero, noting that A_s is also a function of h . Thus,

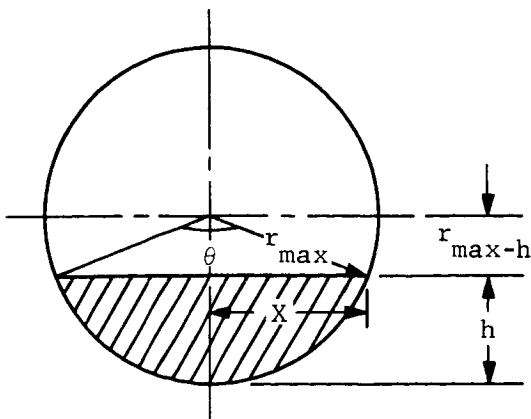
$$\frac{de}{dh} = \frac{a}{g_c} - \frac{Q^2}{g_c} \frac{\frac{dA_s}{dh}}{A_s^3} = 0. \quad [31]$$

Therefore, the condition of critical depth occurs when

$$\frac{A_s^3}{\left(\frac{dA_s}{dh}\right)} = \frac{Q^2}{a}. \quad [32]$$

The parameter $\left(A_s^3 / \frac{dA_s}{dh}\right)$, which is a function of fluid depth, is called the dropout parameter since dropout occurs at a depth where this parameter is equal to (Q^2/a) . The variation of the dropout parameter with fluid depth is plainly a function of the tank geometric configuration. In the toroidal tank, for example, this parameter may be obtained from a simple calculation as follows.

For the nonsump bottom, the area A_s is twice the cross-hatched area shown in the following sketch.



$$d\left(\frac{A_s}{2}\right) = 2 X dh$$

$$\frac{dA_s}{dh} = 4X$$

$$X^2 + (r_{\max} - h)^2 = r_{\max}^2$$

$$X = \sqrt{2r_{\max}h - h^2}$$

$$\frac{dA_s}{dh} = 4\sqrt{2r_{\max}h - h^2}$$

From conventional mensuration formulas,

$$\frac{A_s}{2} = \frac{r_{\max}^2 \theta}{360} - \frac{r_{\max}^2 \sin \theta}{2},$$

where

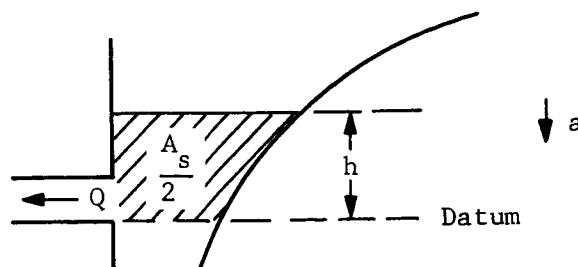
$$\theta = 2 \cos^{-1} \frac{(r_{\max} - h)}{r_{\max}}.$$

The dropout parameter in the toroidal tank becomes

$$\frac{A_s^3}{\left(\frac{dA_s}{dh}\right)} = \frac{2\left(\frac{r_{\max}^2 \theta}{360} - \frac{r_{\max}^2 \sin \theta}{2}\right)^3}{h\sqrt{\frac{2r_{\max} - 1}{h}}} \quad [33]$$

and this is shown as a function of depth in Fig. 8.

For the cylindrical tank with concave lower dome, the geometrical configuration is such that a simple mathematical expression does not exist for the dropout parameter.



Cylindrical Tank, Concave Lower Dome
Channel Flow Arrangement

In the procedure actually employed, the area A_s as shown in the accompanying illustration is computed by geometric means as a function of h . Graphical differentiation of this curve gives $\frac{dA_s}{dh}$ also a function of h . It is then a simple matter to calculate the dropout parameter $A_s^3 / dA_s / dh$. Table 2 presents a tabulation of these calculations for the cylindrical tank with concave lower dome. These results are shown as a function of depth in Fig. 9.

E. TOROIDAL TANK LIQUID SLOSH RESONANT FREQUENCIES

An objective of this program is to determine slosh influences on toroidal tank outflow, and specifically on propellant residuals. Because model tank testing is the primary investigating tool, it is of considerable import to analytically examine toroidal tank wave propagation characteristics and especially the slosh resonances.

The basic theory concerning the dynamic effects of liquid sloshing has been well detailed by many researchers (Ref 3 thru 6). These analyses assume that, for small amplitudes of motion, the natural frequencies of oscillations of a free liquid approximate resonant sloshing frequencies. Based on ideal potential flow theory for an incompressible nonviscous liquid in a rigid tank, past analyses of the resonant frequencies have been applied to a variety of tank shapes. These include vertical cylinders and annular ring cylinders (lateral excitation), spheres, and circular canals (diametral excitation). Most of these theoretical results have been confirmed by tests.

The analytical solution is an eigenvalue problem involving the solution of the Laplace equation describing the irrotational motion of free fluid particles,

$$\nabla^2 \varphi = 0, \quad [34]$$

The Laplace equation is solved subject to certain boundary conditions relating to the specific tank configuration. For example, the condition of zero radial flow at the tank wall

$$\frac{\partial \varphi}{\partial r} = 0, \quad [35]$$

the condition of zero axial velocity at the tank bottom

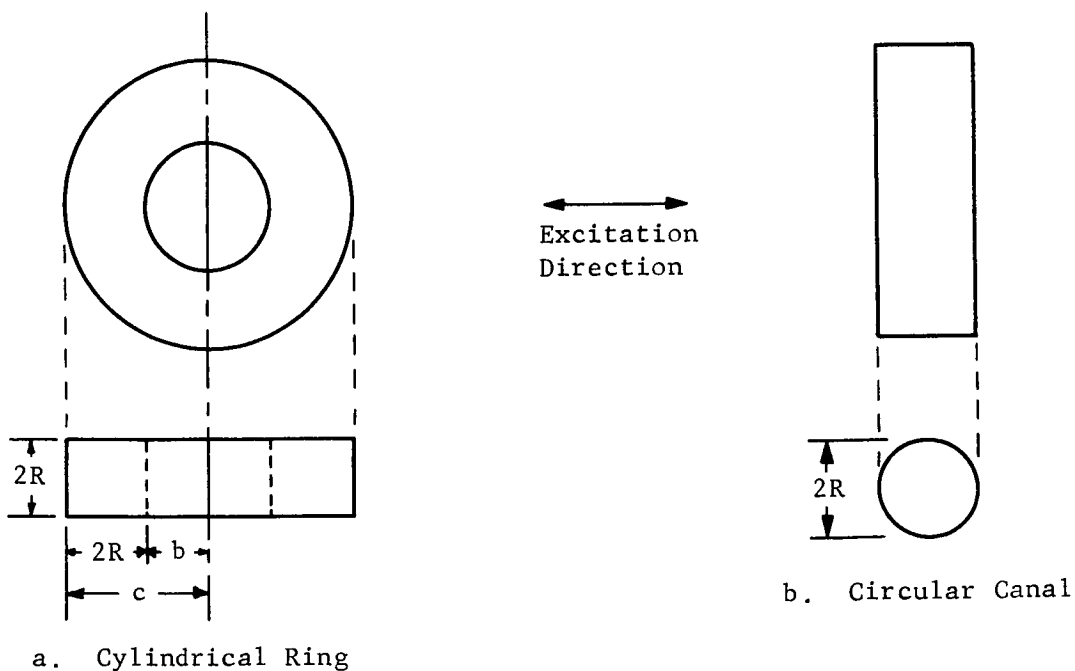
$$\frac{\partial \varphi}{\partial Z} = 0, \quad [36]$$

and the condition of constant pressure at the free fluid surface

$$\frac{\partial^2 \varphi}{\partial t^2} = -g \frac{\partial \varphi}{\partial Z} \quad [37]$$

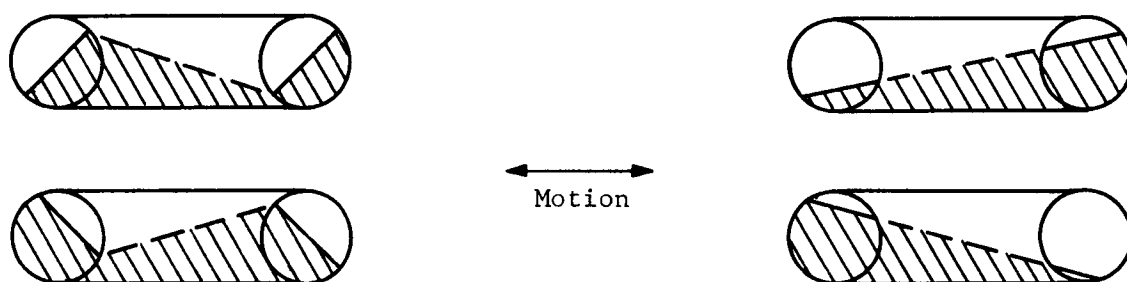
must hold.

The solution has been derived for both the cylindrical ring tank (Ref 4) and the circular canal (Ref 3) depicted schematically below.



The idealized tank shapes in the preceding sketch appear to represent reasonable models for evaluating the fluid responses of the toroidal tank to lateral excitation.

Investigation of the toroidal tank wave forms revealed that two fundamental types of fluid motions are involved for the toroidal tank response, stable planar and stable nonplanar motions. Stable planar motion occurs when each half of the torus cross section oscillates individually. View a. shows the extremes under this condition.



a. Stable Planar Motion

b. Stable Nonplanar Motion

Stable nonplanar motion occurs when the entire fluid body sloshes in unison. This is a rotational form of steady state fluid motion with a single nodal diameter that circulates about the torus channel at a constant rate. View b. shows the extremes under this condition. It is evident that equations derived for both the cylindrical ring tank and circular canal (of appropriate dimensions) would be reasonable approximations for the stable nonplanar and stable planar motions, respectively, of the toroidal tank.

The solution covering the cylindrical ring tank has been developed by Bauer (Ref 4). The natural frequency f_n , and the frequency parameter λ_n , are expressed by

$$f_n = \frac{1}{2\pi} \sqrt{\frac{a\xi_n}{c}} \tanh \frac{(\xi_n h)}{c} \quad [38]$$

$$\lambda_n = \frac{\omega_n^2 c}{a} = \xi_n \tanh \frac{(\xi_n h)}{h} \quad [39]$$

where ξ_n are the roots of the determinant $\Delta_1(\xi)$,

$$\Delta_1(\xi) = \begin{vmatrix} J_1'(\xi) & Y_1'(\xi) \\ J_1'(K\xi) & Y_1'(K\xi) \end{vmatrix} = 0. \quad [40]$$

$J_1'(\xi)$ = first derivative of Bessel function first kind, first order.

$Y_1'(\xi)$ = first derivative of Bessel function second kind, first order.

The roots of the determinant $\Delta_1(\xi)$ are listed in Table 3 for the first three modes ($n = 1, 2, 3$) as a function of tank diameter ratio, $k = b/c$. For the vertical cylinder, b and therefore k are zero so that the roots reduce to the zeros of the first derivative of the Bessel function of the first kind.

To apply these results to the toroidal tank, the cylindrical ring tank should have dimensional equivalence to the toroidal tank in the following manner. The cylindrical ring tank should have a height and radial width equal to the diameter ($2R = 1.46$ ft) of the ring of the torus. In addition, the inner and outer wall radii of the cylindrical ring tank should also be identical to the toroidal tank, and thus for the test model $k = 0.3$. The sloshing natural frequencies for an equivalent cylindrical ring tank have been calculated on this basis, and are shown in Fig. 10 as a function of fluid height. Both first and second modes are shown.

The solution for the circular canal (Ref 3) is also obtained from a solution of the differential equation describing the fluid motion and the appropriate boundary conditions. A matrix formulation was employed for the solution, and this was evaluated numerically.

III. PHASE II -- DESIGN, PROCUREMENT AND FABRICATION

A. DESIGN

Tanks - Two scaled plexiglas nonpressurizable propellant tanks were tested.

The cylindrical tank, shown in Fig. 13, was modeled after the Saturn SIVB hydrogen tank. However, it has two outlet arrangements, a single 1-in. diameter side outlet or three 13/32-in. diameter side outlets radially spaced at 60 deg.

The second tank, illustrated in Fig. 14, is a torus modeled after a hydrogen or lox tank for an upper stage application. The latter was constructed in two halves, incorporating a sump bottom or a nonsump bottom configuration. This permits a choice of outflowing from either half. Two outlets, located 180 deg apart, are available for either bottom. Special inserts are provided for each of these outlets and are contoured for nondropout outflow performance for two line sizes, 11/16 in. and 1 3/16 in. ID (see App D).

Feedline sizes for both models were obtained by considering a nominal prototype feedline velocity of 25 fps, which was then appropriately scaled for the model.

Prototype and model design parameters are listed in Table 5, which also shows the variations of the tank outlet configurations. Model flow rates, obtained on the basis of Froude No. constraint, can be readily determined from Fig. 1, 2, and 3.

Test Fixture - A schematic and photograph of the complete outflow system are shown in Fig. 15 and 16. This design permits outflow under gravity head alone or as boosted by a drain pump. The motor-driven centrifugal pumping unit is capable of draining 120 gpm from two 1 3/16-in. outlets (the peak requirement). By certain hand valve adjustments, the same pump can refill the tank from the catch basin.

The valves shown are all manual (globe-type) except for a remotely controlled pneumatic actuated rapid shutoff valve. This valve was selected to obtain a greater accuracy for residual calculations because its high-speed operation reduced outflow occurring during the closing operation. This outflow had to be accounted for in the residual computations. The valve-closing response was such that a virtual linear flow profile resulted over a time span of 1 1/2 sec.

The calibrated reservoirs installed between the tank outlets and the flowmeters served as catch reservoirs, and prevented the flowmeter from uncovering during outflow.

The support structure for the toroidal tank was connected to an adjustable amplitude crank and thence to a variable speed electric drive system. Possible excitation amplitudes ranged up to 1 1/2-in. double amplitude with frequencies from 0.3 to 2 cps.

A camera support arrangement was also provided so that high speed cameras could be mounted in different positions above and around the model tank.

Figure 33 thru 39 present photographic views of the overall test fixture, tankage, tank outlets, and baffles.

B. FABRICATION AND PROCUREMENT

The major design items and their drawing numbers (Martin-Denver Division identification) are listed below. All drawings are included in Appendix C.

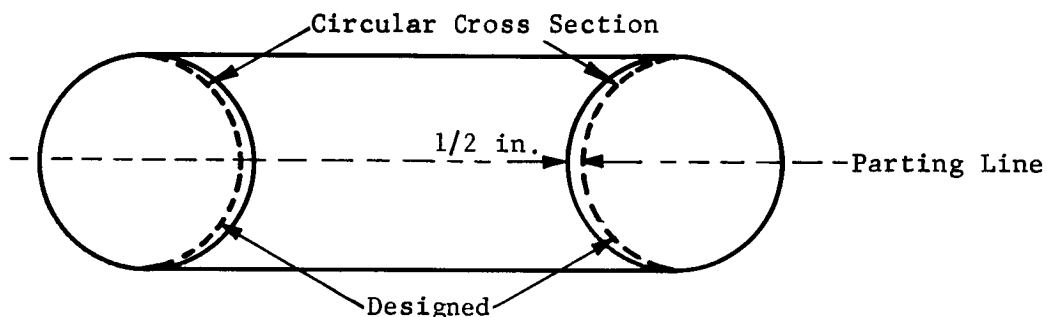
<u>Item</u>	<u>Drawing Number</u>
Cylindrical Tank, Installation	CFL 6100590
Toroidal Tank, Installation	CFL 6100591
Tank, Plastic, Cylindrical	CFL 6100592
Tank, Plastic, Toroidal	CFL 6100593
Slosh Fixture, Installation	CFL 6100594
Support Tank	CFL 6100595
Camera Mount	CFL 6100596
Support, Cylindrical Tank	CFL 6100597
Slosh Fixture Drive Mount	CFL 6100599

The frequency parameter, λ_n , for the first three modes of the circular canal are listed in Table 4. Unlike the behavior for the cylindrical ring tank, λ_n does not become zero for the nearly empty cylindrical canal nor is it bounded for the full tank. The sloshing natural frequency for a circular canal of radius R is shown as a function of fluid depth in Fig. 11. Both first and second resonant modes are shown.

It is now possible to predict the resonant slosh frequencies of the toroidal tank under lateral excitations of small amplitudes. The first mode slosh frequencies are shown in Fig. 12 for a 1 g acceleration field. The upper curve depicts stable planar motion, the lower curve shows stable nonplanar motion. The determination of which type of sloshing motion will be dominant must be accomplished under an experimental test program because the analysis itself does not indicate the relative strength of the wave forms.

In addition to these items, component items, such as valves, pump, catch tank, flowmeters and miscellaneous hardware, were obtained. The majority of these items were fabricated by laboratory support groups or otherwise requisitioned from company supplies. Procured items were the plexiglas tanks, certain flowmeters, valves, pump, and structural steel.

A difficulty was encountered in the molding of the toroidal tank. The inner wall of the torus expanded radially during cool-down after the molding process. A minor dimensional variation of the inside radius of 1/2 in. resulted.



Perfect matching of both halves was achieved, however, so that no misalignment existed at the mating periphery. Evidently the only effect from this enlargement was in the tank volume, which was accounted for during calibration.

C. CALIBRATION

The model tanks, and all flowmeters were calibrated before test use. The results are shown in Fig. 17 thru 21. The model tanks were calibrated with a 1000-cc graduated cylinder. Estimated accuracy is $\pm 1\%$. The flowmeter signal accuracy was laboratory checked to within $\pm 0.3\%$, and the corrected flowrate-signal variation is shown in the appropriate calibration chart.

IV. PHASE III -- TEST

A. TEST OBJECTIVES

Test objective are outlined for both the cylindrical tank and the toroidal tank.

1. Cylindrical Tank

The cylindrical tank objectives are:

- 1) Determine the effect of outlet size and outlet flow interaction on tank residuals;
- 2) Determine the effect of outflow rates (simulating prototype vehicle acceleration) on tank residuals;
- 3) Evaluate the influence of several antivortex devices on tank residuals.

2. Toroidal Tank

The primary objectives for the toroidal tank are:

- 1) Determine the effect of outlet size and outlet flow interaction on tank residuals;
- 2) Determine the effect of outflow rates (simulating prototype vehicle acceleration) on tank residuals;
- 3) Determine the effect of slosh on tank residuals;
- 4) Determine the effect of tank bottom sump on tank residuals;
- 5) Evaluate the influence of several antivortex devices on tank residuals;
- 6) Using the optimum antivortex device, demonstrate the influence of combined slosh and initial prerotation on tank residuals. Include the effects of items 1), 2), and 4).

The secondary objectives for the toroidal tanks are:

- 1) Investigate the resonant slosh frequencies (lateral excitation) of the toroidal tank;
- 2) Evaluate the influence of several high level antislosh baffles on tank residuals;
- 3) Determine the effect of bulk fluid quiescence on tank residuals;
- 4) Determine the influence of sump depth on tank residuals.

B. TEST PLAN

1. Test Description

Outflow tests constituted the major portion of the test program. These outflow tests were divided into two phases. Phase I consisted of the cylindrical tank tests, and Phase II consisted of the toroidal tank tests. In each phase, a sequence of tests was performed to achieve the primary objectives.

Phase I - Cylindrical Tank -

100 series - Evaluate the influence of side outlet size, number of outlets, and flow interaction on tank residuals.

200 series - Evaluate several antivortex devices under an initial prerotation outflow mode.

Phase II - Toroidal Tank -

100 series - Evaluate the influence of outflow rate, bottom shape, outlet size, number of outlets, and slosh on tank residuals.

200 series - Evaluate several antivortexing devices under an initial prerotation outflow mode.

300 series - Demonstrate the influence of combined prerotation and slosh, tank bottom shape, and outlet size and number on tank residuals using the optimum antivortexing device.

In addition to these, a number of secondary objective tests were performed. These included resonant slosh frequency searches, anti-slosh baffle evaluations, liquid quiescence effects, and sump contour effect.

2. Test Procedure

The test method was virtually the same for each test. A trial outflow preceded each final run to permit manual setting of the flow-control valves to attain the desired outflow rate. Instantaneous flow readings were read from Dynac recordings. The boost drain pump was available for reserve drain power. Before each test, antivortexing or antislosh baffles were installed and slosh and/or prerotation modes initiated as desired.

During outflow, the appearance of two-phase flow in any outlet was manually signalled. This resulted in the red cavitation light being recorded on film and a switch trace on the strip chart flow record. For the cylindrical tank tests, flow was stopped at the same instant that cavitation was signaled. Uncorrected tank residuals were then determined directly from the residual fluid height in the tank correlated with the tank calibration chart. For the toroidal tank tests, a greater accuracy was obtained by permitting the outflow to continue until the fluid level was in the outlet reservoir. The fluid added to bring the level to the outlet mark was recorded for each test. Uncorrected residuals were determined from the added fluid and from integration of flowrate charts.

3. Data Acquisition

a. Instrumentation

The primary instrumentation was the flowmeters that individually measured the flowrate through each outflow branch. Flowrates were recorded simultaneously on Sanborn strip chart recorders (at 5mm/sec) and Dynac tape (1 print/sec). This provided a continuous double check of flowmeter output. Recordings were always made of the direct frequency output of the flowmeters, and these readings were converted to flowrate by referring to the appropriate flowmeter calibration chart, Fig. 19, 20, and 21. Used in this way, estimated flowrate inaccuracy was less than $\pm 1\%$ for the Sanborn, and less than ± 1 cps for the Dynac recorder.

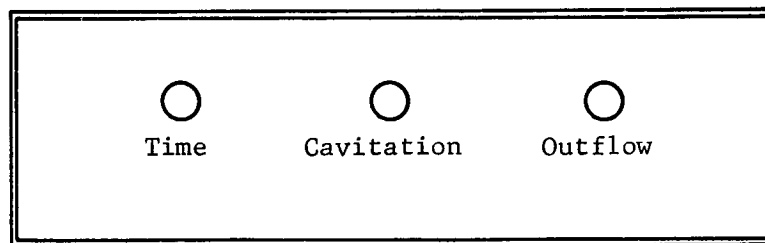
In addition to flowrate signals, certain test timing events, such as run start, cavitation, and shutdown times, were recorded on the Sanborn recorder.

The initial prerotation mode was accomplished by paddle or by tangential filling from the top. A floating object timed during rotation certified the rotational speed.

No special instrumentation was required for the slosh rig. The adjustable amplitude setting was read directly from scale marks adjacent to the roller mounts. A stop watch was used to certify the frequency.

b. Camera Coverage

Test coverage by a high speed camera (16 mm color) was used for most outflow tests. Film speed was normally 128 frames/sec, although for the two outlet toroidal tank tests 64 frames/sec was used for the second outlet. An event indication display, as shown in the following sketch, was provided in the camera field for simultaneous camera coverage during the outflow tests. This provided precise correlation of event occurrence in all film sequences with flow records. It also permitted correction of computed residuals for the human error incurred during test conduction.



Indicator Display

- Note:
1. Time: "red", time of day or real time in coded 1-sec intervals.
 2. Cavitation: "red" on, when cavitation is manually signalled.
 3. Outflow: "green" on, when shutoff valve is open.

When two side cameras were used, only the cavitation event signal from the indicator display was provided for the second camera field.

c. Data Requirements

Outflow test data consisted of the flowrate history through all outlets and the event and real time signals as recorded on Sanborn charts and the Dynac tape. Readings of the fluid height in the cylindrical tank or the additive volume for zeroing the level in the outlet in the toroidal tank were also required for each run. In addition to these data, test particulars, such as slosh frequency-amplitude, prerotation rate, baffle type, etc, were also required.

The instant of two-phase flow in the outlet is signaled by the test conductor. The shutdown signal for the pump and the shutoff valve closure signal followed. The residuals for any test were then computed as follows.

Cylindrical Tank - Uncorrected residuals are equal to the sum of the fluid volume remaining (corresponding to the tank calibration mark) and the time-integrated flow occurring between the signalled cavitation event and actual shutdown.

Toroidal Tank - Uncorrected residuals are equal to the differences between the time-integrated flow occurring between the signalled cavitation event and actual shutdown, and the volume of fluid required for zeroing the level in the tank outlet.

Residuals obtained for either tank were corrected for the human error in detecting cavitation, which generally amounted to a 0.2- to 0.4-sec lag from actual cavitation, as evaluated from the film sequences. The flowrate is integrated with respect to time over the time lag interval and added to the uncorrected residual (subtracted if the event signal was early) to obtain the corrected residual.

C. TEST RESULTS

Test results were analyzed for liquid residuals, toroidal tank liquid slosh resonant frequencies, antislosh baffle performance, and toroidal tank sump evaluation.

1. Liquid Residuals

a. Cylindrical Tank (Concave Lower Dome)

Outflow tests on the cylindrical tank (concave lower dome and side outlets) were performed using a 50/50 mixture of ethylene glycol-water solution (SG = 1.055, viscosity twice that of water) to avoid freezing problems. Test flowrates in accordance with Table 5 remain unchanged because mixture density was that of water. Test results follow.

Series 100 - The objective of this series was to determine the influence of flowrate and outlet location on residuals for this tank with unprotected (no baffles) side outlets. The residuals for each test were as follows:

Run No.	Outlet Configuration	Flowrate (gpm/outlet)	Antivortex Device	Prerotation (rpm)	Residuals (cu in)
101	A	7.1	No	No	59.6
102	A	14.09	↓	↓	91.3
103	B	1.22			33.9
104A	B	2.28			46.5

These tests demonstrated that the concave bottom dome does not support vortexing. In addition, normal dropout was absent, although a spillover condition, i.e., side outlet dropout, which was responsible for the residuals, existed immediately above each outlet.

Residuals are plotted as a function of volume outflow rate in Fig. 23, and a functional relationship with flowrate is evident. Tank residuals are seen to be proportional to $Q^{0.626}$ and $Q^{0.467}$ for the A and B outlet configurations, respectively. Correlation of these values with analytical predictions is discussed in the following chapter. Note that for a central symmetrical outlet in a cylindrical tank with convex lower dome the height at dropout, and therefore the quantity of tank residuals in vortex-free outflow, is theoretically proportional to $Q^{2/3}$.

Series 200 - The objective of this phase was to determine whether certain baffles could improve tank terminal draining performance, particularly under an initial prerotation mode. The antivortex baffles considered were

Baffle A - Radial vane (height = 2 outlet diameters);

Baffle B - Peripheral vane (length = 2 outlet diameters);

Baffle C - Cruciform (combination of the above two);

The baffles are shown in Fig. 22. The residuals for each of the tests, which were performed with an initial prerotation of 5 rpm, are as follows:

Run No.	Outlet Configuration	Flowrate (gpm/outlet)	Baffle	Residuals (cu in.)
201	A	7.18	A	62.3
202	A	14.45	A	68.6
203	A	7.1	B	70.54
204A	A	14.4	B	115.8
205	A	7.09	C	50.9
2-6	A	14.2	C	97.6
206-0-	A	14.27	None	110.5
207	B	1.2	A	32.44
208	B	1.2	B	17.1
209	B	1.19	C	35.3

Residuals are plotted as a function of volume flowrate in Fig. 23. Again a functional relationship with flowrate is evident, with proportionality varying from $Q^{0.47}$ to $Q^{0.93}$ for the entire test series. Although initial prerotation served to increase residuals, none of the baffles appear to significantly improve tank terminal draining performance.

b. Toroidal Tank

The planned and achieved flowranges for outlet Configurations A and B were as shown in the accompanying tabulation.

Outlet Configuration	A (hydrogen)		B (oxygen)	
	Planned	Actual	Planned	Actual
g Level Simulation	1/3-2	1/2-2	1/3-2	1/3-2
Water Flowrate (gpm)	30.3-74.3	30.2-60.6	9.62-23.5	9.62-23.5

The test results are as follows.

Series 100 - The objective of this phase was to determine the influence of tank bottoms (sump or nonsump configurations), number of outlets, and lateral slosh excitation on toroidal tank residuals. The tank outlets were unprotected (no baffles), and prerotation was absent, although absolute quiescence of the bulk liquid was not required. The measured tank residuals for each test are shown in the following tabulation:

Run No.	No. of Outlets	Bottom Type	Slosh	Flowrate (gpm/outlet)	Residuals (cu in.)
101A	1	Sump	No	30.	717.
102	1	↓	Yes	30.	186.5
103	1	↓	No	60.	1358.5
104	1	↓	Yes	61.8	2981.
105	2	↓	No	30.3	3670.2
106	2	↓	Yes	30.5	3811.5
107	2	↓	No	61.8	5025.7
108S	2	↓	Yes	61.82	4237.6
109X	1	No Sump	No	30.3	7062.8
110	1	↓	Yes	30.2	1001.
111	1	↓	No	61.5	4340.
112	1	↓	Yes	61.7	6780.
113	2	↓	No	29.8	3525.5
114	2	↓	Yes	29.17	5038.
115	2	↓	No	61.5	6426.
116	2	↓	Yes	61.8	5025.

The residuals determined in the 100-test series are plotted in Fig. 24 as a function of flowrate per outlet. Note that tank residuals increase with flowrate in much the same manner as described for the cylindrical tank.

An improvement is noted with the sump bottom, which may be attributed to the natural dampening action at the lower surface levels of the liquid in the tank.

Two flowing outlets generally result in greater residuals than one. In no two-outlet tests did dropout occur simultaneously, although the outlets and flowrates were essentially identical. Consequently, the significance of the results of the two-outlet tests is reduced in comparison with that of the one-outlet tests.

The sloshing influence on residuals is not very evident from these tests. The two-outlet tests are little affected by the frequency imposed (1 cps). Sloshing, however, tends to reduce residuals for the one-outlet tests at the low flowrate. This may be due to the fact that the sloshing is sufficient to collapse and/or delay any vortex formation. At the higher flowrates, however, the slosh frequency is apparently too low to have any significant influence on residuals.

In the above test series, the major contributing factor to two-phase outlet flow and subsequent shutdown of the outflow was the vortexing phenomenon. The vortexes formed initially with some run-to-run repeatability but dissipated and reformed in a sporadic manner.

Series 200 - As is evident in the Series 100 test program, unprotected outlets in toroidal tanks experience substantial vortexing, which results in large amounts of residuals. That test series also showed that the use of the sump bottom alone does not reduce residuals to acceptable levels and, further, that the use of an antivortex device is indicated. Many techniques have been investigated, such as screens, flat plates, floating devices, etc; the most promising appear to be the simple shapes, such as a round disc, cruciform, and cone. Based on currently available information and practices, the following baffles and dimensional criteria were adopted (see Fig. 25).

Baffle Design	Baffle Diameter Outlet Diameter	Height Outlet Diameter
Baffle A, Circular Flat Plate	2.5	1.2 (above outlet)
Baffle B, Cruciform	2.5	1.2 (to top)
Baffle C, Baffle A on Top of B	2.5	1.2 (to top)
Baffle D, 30-deg Cone (Apex Up)	2.375	1.2 (base above outlet)
Baffle A-1, Enlarged Circular Flat Plate	4.0	1.2 (above outlet)

The objective of this phase was to evaluate several anti-vortex devices and determine the optimum device. Test conditions were similar to the Series 100 tests except that an initial fluid prerotation rate of 5 rpm was applied. Only the sump bottom with outlet Configuration A was considered, and no slosh excitation was imposed. The measured tank residuals for each test were as follows:

Run	No. of Outlets	Baffle	Flowrate (gpm/outlet)	Residuals (cu in.)
201	1	A	30.2	213.4
202	1	A	61.8	781.
203	2	A	30.4	93.5
204	2	A	61.55	780.3
205	1	B	30.45	562.
206	1	B	60.7	650.5
207	2	B	30.35	479.3
208	2	B	61.	1124.
209	1	C	30.15	269.5
210	1	C	61.	1107.5
211	2	C	29.8	536.7
212	2	C	61.2	914.
213	1	D	30.4	248.
214	1	D	61.	799.5
215	2	D	30.4	297.9
216	2	D	61.4	629.4

The residuals determined in the Series 200 tests are plotted in Fig. 26 as a function of volume flowrate per outlet. A comparison with the results from the Series 100 tests (Fig. 24) reveals that all of the baffles that were considered significantly reduced residuals. Baffles A and D, the circular flat plate and upright cone, are superior. These baffles reduce residuals by at least 40% of the Series 100 results. Baffle A was selected for the Series 300 confirmation tests.

Series 300 - Upon selection of Baffle A as the most promising antivortex baffle, verification tests were performed to examine the influence of slosh, bottom type, and outlet size on residuals. As in the previous baffle evaluation tests, an initial prerotation of 5 rpm was applied; in addition, a slosh frequency of 1 cps was also imposed. The measured tank residuals for each test were as follows:

Run	No. of Outlets	Bottom Type	Outlet Configuration	Flowrate (gpm/outlet)	Residuals (cu in.)
302	1	Sump	A (1 3/16-in. dia)	30.	262.5
304	1	↓	↓	61.2	639.4
306	2	↓	↓	30.05	280.9
308	2	↓	↓	60.8	927.6
310	1	No Sump	↓	30.	1437.
311	1	↓	↓	61.45	1927.8
313X	2	↓	↓	29.95	1472.
315	2	↓	↓	61.45	2280.6
317	1	Sump	B (11/16-in. dia)	9.6	75.7
318X	1	↓	↓	23.2	540.1
320	2	↓	↓	10.	63.65
321	2	↓	↓	22.1	473.6
323X	1	No Sump	↓	9.6	603.6
324	1	↓	↓	23.5	1211.72
326	2	↓	↓	9.55	731.1
327	2	↓	↓	22.45	1187.5
324X	1	↓	↓	23.5	984.8 (Baffle A-1)

These results are plotted in Fig. 27 as a function of volumetric outflow rate per outlet.

In most instances, vortexing was virtually eliminated by the baffle until the liquid level dropped below the baffle. The two-phase flow in the outlet was primarily caused by an uncovering action due to sloshing liquid. Sump bottoms performed significantly better than the nonsump bottoms. This is attributed to the natural dampening action of the tapered sump to the slosh-induced liquid motion. It is apparent that the reason such improvement was not noted in the Series 100 tests is that, for unprotected outlets, two-phase flow was initiated by vortexing well before the benefits of the sump could be realized. Two-outlet tests were only slightly poorer than the similar one-outlet tests, and even then this trend was reversed in some instances. Residuals in all cases increased with flowrate, although the rate of increase was less with the nonsump bottom. Although corresponding test points are shown not connected in Fig. 27, the inclination of a connecting line would vary from 53 to 66 deg for the sump bottom and 23 to 40 deg for the nonsump bottom. Thus, flowrate dependencies varying from $Q^{1.33}$ to $Q^{2.25}$ for the sump bottom and $Q^{0.425}$ to $Q^{0.838}$ for the nonsump bottom are indicated.

2. Toroidal Tank Liquid Slosh Resonant Frequencies

Two types of stable fluid motions are involved in the response of the toroidal tank (horizontal position) to lateral excitation, as described previously. These are stable planar and stable non-planar motions. A dominant slosh frequency search was undertaken for each of these motion types.

Stable planar motion was examined initially by employing a 3/4-in double amplitude on the slosh fixture. The results of the search are shown in Table 6. The dispersion at the low fluid depths reflects the influence of the dampening action of the sump. Such behavior explains the improvement in terminal draining associated with the sump bottoms. The increase in resonant frequency as fluid depth increases is also evident. This trend is typical for most tank configurations including cylindrical, spherical, and circular shapes.

An investigation of the stable nonplanar resonance was also undertaken. Since the resulting fluid motions were more violent, the double amplitude for these tests was decreased to 7/16-in. Resonant points were found to be at a much lower frequency, as anticipated, but because of the slosh fixture minimum speed limitation and the large turbulent motions of the fluid, only a narrow range of liquid depths was examined. These results are shown in Table 7.

3. Toroidal Tank Antislosh Baffle Evaluation

It has been demonstrated that, in the absence of vortexing, two-phase outlet flow is caused primarily by outlet port uncovering under the action of slosh-induced liquid motion. Other undesirable facets of such fluid perturbations are vehicle instability and control difficulties, large ullage gas temperature fluctuations leading to pressurization system problems, potential tank structural failure, etc.

Large baffles to reduce sloshing activity have had many applications in cylindrical propellant tanks. The guiding principle involves partitioning the tank into a number of compartments and permitting the increased eddy current energy and the reduced compartment dimensions to dissipate and reduce the major flow perturbances. In accordance with this theory, baffles were designed for the toroidal tank. These were circular flat shapes, designed to fit in the torus channel, and spaced 90 deg apart. Figures 28 and 29 show the installation of two designs, the solid plate with weight reducing cutouts and the screen (20 mesh).

The results of special antislosh baffle tests, which were performed with antivortex Baffle A installed in the nonsump bottom, are listed in the following tabulation and are compared with similar tests performed without the antislosh baffle.

Runs No.	No. of Outlets	Outflow Rate (gpm/outlet)	Residuals (cu in.)	Comment
311	1	61.45	1927.8	No Antislosh Baffle
315	2	61.45	2280.6	No Antislosh Baffle
315H	2	61.55	2000.6	Solid Plate Baffle
315S	2	61.55	1767.7	Screen Baffle

It is evident from these results that only minor improvement results from the use of total diametric antislosh baffles in reducing tank residuals. Other baffles are needed that would concentrate the dampening action near the tank outlet where the problem of port uncovering exists. In conformance with this theory, it is apparent that the tank sump should have a major influence in reducing tank residuals arising from the slosh-induced port uncovering. If a diametric slosh baffle is used, it is intuitively apparent that a screen device is superior to a solid device, even with cutouts, because it would dissipate the slosh energy more efficiently.

4. Toroidal Tank Sump Evaluation

Sumps in toroidal tank bottoms reduce residuals, especially when the vortex phenomenon has been sufficiently suppressed. The sump of the toroidal model was approximately 3 in. deep. To further evaluate the sump influence, a second design 50% as deep but tapering to the same peripheral intersection with the tank wall (Fig. 30), was tested. No baffle was installed, and no sloshing was imposed in these one-outlet (outlet Configuration A) tests.

The residual for one test (Run B) was 12,152 cu in. for an outflow rate of 61.5 gpm. This is considerably larger than residuals from corresponding nonsump bottom and full sump tests (Runs 111 and 103, respectively) and is due to vortex-initiated two-phase outlet flow.

It is suspected that, for the no-slosh tests, repeatability of test results will be poor because results are influenced by motions existing in the liquid before test. Sloshing tends to destroy any ordered liquid motion such as a vortex so that greater repeatability is possible, especially for the sump bottom configuration tests. On the other hand, tests performed with an initially quiescent* liquid would be a better measure of the sump influences since initial motions would virtually not exist. Such tests were performed with both full and half sump under reasonably identical, initially quiescent conditions. In the half sump test, residuals were 948.5 cu in. at 61.5 gpm (Run A). In comparison, for the full sump case (Run 108), residuals were 554.8 at 61.7 gpm. Tabulated results of these tests follow.

*Quiescence of liquid was achieved after a hold period exceeding 1 hr.

Run No.	No. of Outlets	Bottom Type	Slosh	Flowrate (gpm/outlet)	Residuals (cu in.)	Comment
B	1	1/2 Sump	No	61.5	12,152	Normal
111	1	Nonsump	No	61.5	4340.	Normal
103	1	Sump	No	60.	1358.5	Normal
A	1	1/2 Sump	No	61.7	948.	Quiescent
108	2	Sump	No	61.7	554.8	Quiescent

Thus certain advantages arise from the employment of a sump in the toroidal tank. The slosh-dissipating characteristic is only part of the benefit. The relationship of sump depth in reducing residuals is also evident, although it seems likely that these benefits exist in a limited range.

V. DATA ANALYSIS AND CORRELATION

A. LIQUID RESIDUALS

Liquid residuals were analyzed for a cylindrical tank and toroidal tank for several liquid outflow conditions.

1. Cylindrical Tank (Concave Lower Dome)

The dropout analysis developed in Section D of Chap. II permits certain analytical predictions relating to the depth at which two-phase flow commences and can thus be used to estimate tank residuals. The effects, if any, of baffle installation and pre-rotation modes were not considered. A comparison between the calculated and measured data has been undertaken in an attempt to verify the analytical method.

Actual dropout heights, with respect to the lower extremity of the outlet, were determined from test data by inspection of the test films under a Boscaw viewer. This equipment permitted precise measurement of liquid heights since tank calibration marks were in the camera field. Because of camera orientation to the field and tank surface curvature, some error is expected in these measurements, though the magnitude of these errors is not expected to be significant.

Computed dropout heights (above the outlet lower extremity) were determined by evaluating the ratio (Q^2/a) for a particular test case. The dropout parameter is then evaluated from the rela-

tion $\frac{A^3}{dA} = \frac{Q^2}{a}$. The calculated critical depth is the height of

liquid found in Fig. 9, which satisfies this relationship. Residual computations were accomplished with the tank calibration chart, Fig. 17, and the correlation of the tank scale to actual tank depth as follows:

	Tank Scale	Tank Depth (in.)
Upper Extremity Outlet A	38.656	2
Upper Extremity Outlet B	37.468	0.812

Table 8 presents the results of these calculations and compares them with the actual test measured data. Fair agreement is shown between the two methods.

2. Toroidal Tank

Predictions of critical depth (Section D of Chap. II), and thus tank residuals, are valid only for vortex-free unperturbed outflow. For the toroidal tests, these conditions did not exist because substantial vortexing occurred during the nonbaffle tests; even with antivortex baffles present, a prerotation or slosh mode existed. Consequently, direct correlation with analytical results should be invalid. Recognizing this, critical depth calculations are made for the four basic outflow rates that are applicable to the two-outlet configurations. Using the critical depths thus calculated, tank residuals can be computed from the tank calibration chart (Fig. 18). These results are shown in Table 9.

It is evident when comparing these analytical results with the appropriate nonsump test data of the 300 test series, Table 10, that the influence of the imposed slosh significantly increases tank residuals.

B. TOROIDAL TANK LIQUID SLOSH RESONANT FREQUENCIES

Toroidal tank slosh response characteristics to lateral excitation have been analyzed in Section E of Chap. II. This analysis considers two types of stable motions, planar and nonplanar, but makes no judgement regarding the strength or dominance of each motion type. These motions can be adequately represented by equations derived for a circular canal and cylinder ring tank.

Figure 31 shows the test data points obtained for the stable planar resonance. Excellent agreement with the theoretical curve derived from the first mode circular canal shape equations is indicated. Figure 32 shows the test data points obtained for stable nonplanar resonance. Excellent correlation with the theoretical curve derived from the first mode equivalent cylindrical ring shape is indicated.

C. DATA REPEATABILITY

The degree of data repeatability is difficult to ascertain because unmeasured liquid viscous forces and resulting liquid motions undoubtedly influenced the test results. As an example, residuals obtained in tests where the liquid initial conditions were absolutely quiescent were far less than the normal, apparently "still fluid" test condition residuals. This is one of the reasons why the joining of the plotted test data points on figures illustrating tank residuals was omitted. Although a scattering of points was observed, the primary residual influences could still be evaluated with reasonable certainty. Naturally a greater number and range of test points would be of increasing value in quantitative evaluations. It is more than likely, however, that the scatter experienced would still be present, especially for the toroidal tank data, since testing of this system involves the complicating slosh and prerotation effects.

Certain other test data, notably the toroidal tank fundamental slosh frequency relations with liquid depth, were quite repeatable, as is seen in Fig. 31 and 32.

VI. FUTURE STUDIES

Mathematical models describing vortex outflow behavior in other than cylindrical tanks and convex lower domes are needed. These models should enable analytic design and evaluation of vortex inhibitors, which appear to be mandatory for high usable mass fraction toroidal tanks. In addition, the influence of the sump contour and tank contour should also be analytically evaluated.

The test program on the toroidal tank was limited in degree and scope. Despite this, the relatively few runs performed were sufficient to show trends. Undisputedly, the unknown internal flow perturbances and uncontrollable test conditions demand a greater number of tests to guarantee proper interpretation of results. Certainly future programs in this area should encompass a greater bracketing of intermediate test points.

Vortex and low level slosh inhibitors and sump contouring demand more thorough test evaluation. It is in these three areas where proper design would lead to substantial benefits in tank draining. The studies to date have served their purpose well in highlighting this. But a greater number of different antivortex designs with dimensional variations should be evaluated to determine the optimum design. In addition, low level antislosh baffles and sump contouring effects should be studied. Scant information is available at present on such designs as applied to toroidal tanks.

The present toroidal tank model is ideally suited for these tests. The use of paraffin in effecting sump contour changes has been most successful. Baffle fabrication and installation procedures are such that baffle configuration changes are rapid and exceptionally inexpensive.

This test program was restricted to a toroidal tank constrained to a horizontal plane, outflowing from either a sump of fixed dimensions or a plain bottom. Advanced mission planning indicates the possibility of other tank orientations for which draining effects have not been explained by this program. A stabilized tank inclined to the horizontal and a rotating tank are merely two orientations of the toroidal tank that hold promise for advanced missions.

It is evident that the continuing interest in toroidal tanks for space applications indicates that a program of substantially greater degree and scope is urgently needed to investigate and improve tank draining behavior so that usable mass fractions of toroidal tanks are not compromised.

APPENDIX A

REFERENCES AND BIBLIOGRAPHY

A. REFERENCES

1. Prandtl and Tietjens: Fundamentals of Hydrodynamics and Aeromechanics. Dover Publications, 1934.
2. D. H. Menzel: Mathematical Physics. Prentice Hall, 1953.
3. B. Budiansky: "Sloshing of Liquids in Circular Canals and Spherical Tanks." Journal Aerospace Sciences, V27, March, 1960.
4. H. F. Bauer: Theory of the Fluid Oscillations in a Circular Cylindrical Ring Tank Partially Filled with Liquid. NASA TND-557.
5. H. Lamb: Hydrodynamics Sixth Edition, Dover Publications, 1945.
6. H. F. Bauer: Propellant Sloshing. ABMA DATR-18-58, 5 November 1958.

B. BIBLIOGRAPHY

- Boeing Company: Experimental and Theoretical Investigation of Vortexing and Sloshing in Propellant Tanks. D2-10737.
- Dergarabedian, P.: "Behavior of Vortex Motion in an Emptying Cylinder." Proceedings, 1960 Heat Transfer and Fluid Mechanics Institute.
- Milne, W. E.: Numerical Calculus. Princeton University Press, 1949.
- Nyland, F. S.: Fluid Slosh Test Program. RL16803i, Martin Company, January 1958.
- Sutton, R. E.: "An Investigation of Resonant Non-linear, Non-planar Free Surface Oscillations of a Fluid." NASA TND-1870, May 1963.

APPENDIX B

SYMBOLS

a	Tank longitudinal acceleration (ft/sec^2)
A_s	Channel flow area (ft^2)
b	Inner radius of cylindrical ring tank (ft)
C	Outer radius of cylindrical ring tank (ft)
Ch	Chezy friction loss coefficient, $\sqrt{\frac{8g_c}{f}}$ ($\text{ft}^{1/2}/\text{sec}$)
C_K	Constant during vortexing; product of ωr^2 for any particle (ft^2/sec)
D_n	Outlet diameter at point n (ft)
$\frac{dh}{dr}, h'$	Outlet slope, rate of change of height with respect to radius
$\frac{d^2h}{dr^2}, h''$	Rate of change of slope with respect to radius (ft^{-1})
e, E	Specific energy (ft of fluid)
E_f	Friction energy loss (ft)
$E_1, E_2 \dots E_{11}$	Constants for program for nondropout outlet design
f	Darcy friction factor
f_n	Natural frequency (cps)
Fr	Froude number
g_c	Gravitational constant - $32.17 \text{ ft lb}_m/\text{lb}_f \text{ sec}^2$
g	Number of g 's of longitudinal acceleration
h_n	Fluid surface height during vortex for any point n (ft)
h, y	Height of outlet (measured from tangency point to tank), fluid height in tank (ft)
L	Length (ft)

m	Mass of fluid (lb_m)
n	Mode number
P, P_s, P_v	Pressure, static, vapor ($\text{lb}_f/\text{in.}^2$ or lb_f/ft^2)
Q	Fluid volume outflow rate (ft^3/sec)
$r(h)$	Definition of tank configuration when r is not constant (ft)
r_m	Constant outlet contour radius for annular outlet (ft)
r_n	Radius of particles undergoing energy change during vortex, Point n (ft)
r_o	Tank radius (ft)
r	Outlet contour radius (ft)
R	Hydraulic radius of outlet; canal or sphere radius (ft)
s	Distance measured tangent to outlet contour (ft)
S	Scale factor, model/prototype
$T, \Delta t$	Time, time increment (sec)
V_h, V_a	Fluid velocity in axial direction (fps)
V_s	Fluid velocity along "s" direction (fps)
We	Weber number $\left(\frac{\rho V^2 L}{\sigma}\right)$
Z	Coordinate in the vertical direction
$\omega, \omega_o, \omega_n$	Angular rotation, initial, any Point n (rad/sec)
λ_n	Frequency parameter, $\frac{\omega_n^2}{a}$ (length)

ρ	Fluid density ($\text{lb}_m/\text{cu ft}$)
σ	Surface tension (lb/ft)
$\delta(h)$	Definition of the insert and/or solid body central core configuration as a function of h (ft)
μ	Absolute viscosity ($\text{lb}_m/\text{ft-sec}$ or poise)
∇^2	Laplacian operator
Δ	Radius increment (ft)
ξ_n	Roots of the determinant $\Delta_i(\xi)$ (see text)
δ	Depth of cross section of rectangular outlet, or radius of central core in vortex field (ft)
ω_n	Natural angular frequency (rad/sec)
φ	Velocity potential
K	Constant relating equal volume horizontal levels of particle distribution during vortexing
k_n	Proportionality constant relating any particle path to the outlet radius
k	Ratio of inner to outer wall radii for cylindrical ring and toroidal tank

Computer Program Symbols - Vortexing Analysis

CIN(IN,KX)	Dummy variable
CORE	Positive - percent of radius Negative - core is read in Zero - no core
DELH	Multiplying factor for the volume increments

DELTA (M)	Core radii corresponding to R (M) (ft)
FLOW	Outflow rate (ft^3/sec)
GF	Gravity factor [$1 + 32.2$ (acceleration)]
I	Dummy variable
IN	Level number
IP	Dummy variable
IXP	Number of levels found
K	Radius number, 121 max.
KX	Point number on a level
LIST	Dummy variable
LL	Dummy variable
LLL	Dummy variable
L(N)	Levels determined for equal volume segments. An L(N) value will be one of the IN values mentioned in WRIN(IN, KX)
MM	Dummy variable
NUM	Level value
OMEGI	Initial angular velocity of liquid (rad/sec)
RIN(IN, KX)	Radius of Point KX in level IN (ft)
R(M)	Radii of the tank wall (ft)
SCALE	Scale factor to 12-ft high tank
TINTR	Time interval of outflow analysis (sec)
V	Volume of the equal volume elements (ft^3)
WRIN(IN, KX)	Angular velocity of Point KX of Level IN (rad/sec)
X	Dummy variable
Y	Dummy variable

Computer Program Symbols - Nondropout Outlet Analysis

A	Constant; function of tank outlet configuration
ACC	Tank longitudinal acceleration (ft/sec^2)
B	Constant; function of tank outlet configuration
C	Constant; function of tank outlet configuration
CH	Chezy loss coefficient, $\sqrt{\frac{8g_c}{f}}$ ($\text{ft}^{1/2}/\text{sec}$)
D	Constant; function of tank outlet configuration
DEL	Depth of cross section of rectangular outlet (ft)
DH	Height increment (ft)
$E_1, E_2 \dots E_{11}$	Constants; functions of tank outlet configuration
FC(I)	Dummy variable
GC	Gravitational constant $\left(32.2 \frac{\text{ft}}{\text{sec}^2} \frac{\text{lb}_m}{\text{lb}_f} \right)$
H	Maximum height of outlet (ft)
HIN	Height (in.)
I	Dummy variable
K	Dummy variable
Q	Volume outflow rate (cfs)
Q	Slope of outlet (dH/dR)
R	Initial radius of outlet (corresponding to H, ft)
R1	(Initial slope) ⁻¹
RIN	Outlet radius (in.)

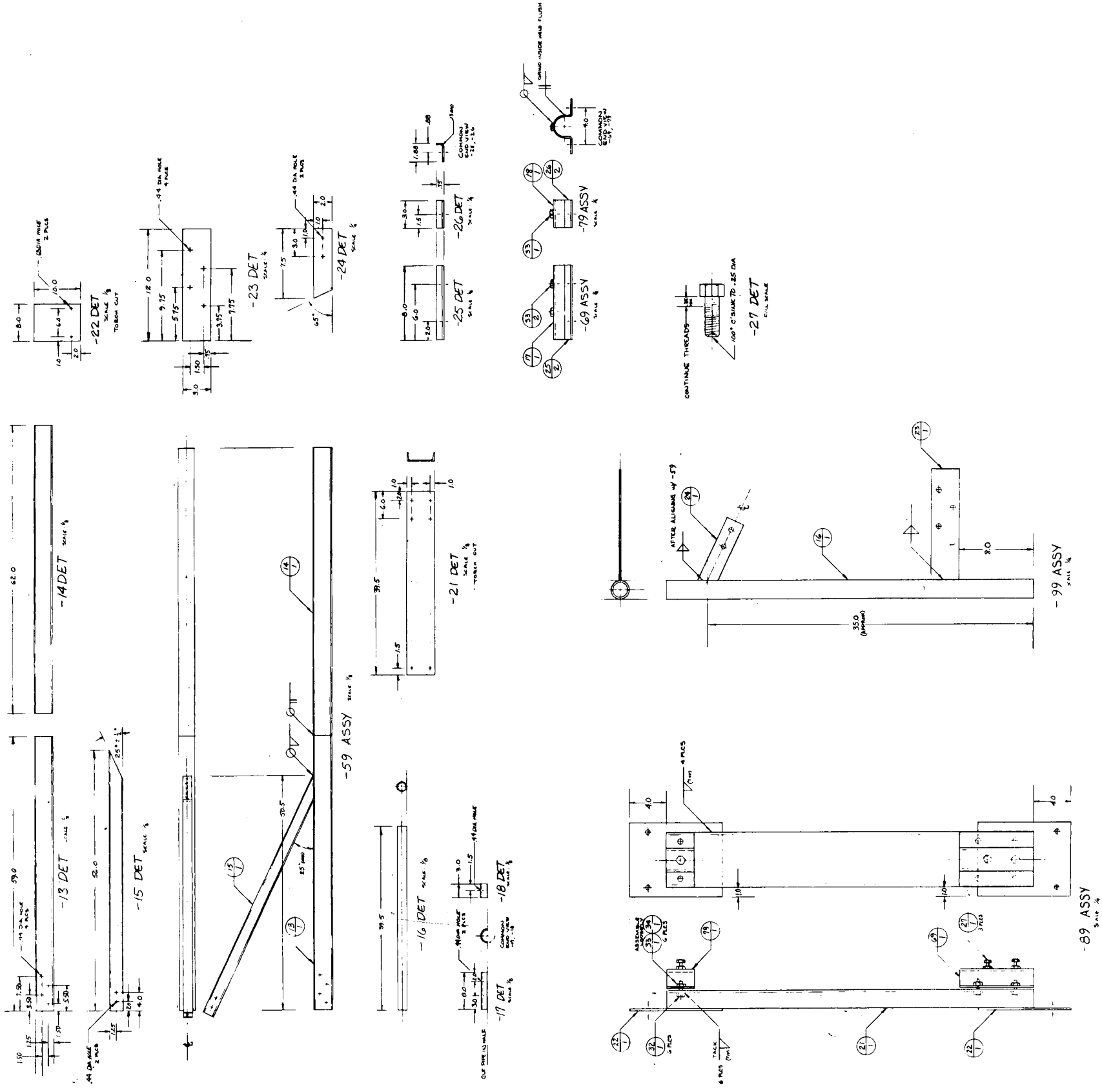
RM	Constant outlet contour radius for annular outlet (ft)
SLOPE	Maximum allowable slope (dH/dR max)
T	Dummy variable
V	Dummy variable
VP	Dummy variable
X	Dummy variable
XM	Dummy variable
XN	Dummy variable
Y	Dummy variable
Z	Dummy variable

APPENDIX C

ENGINEERING DRAWINGS

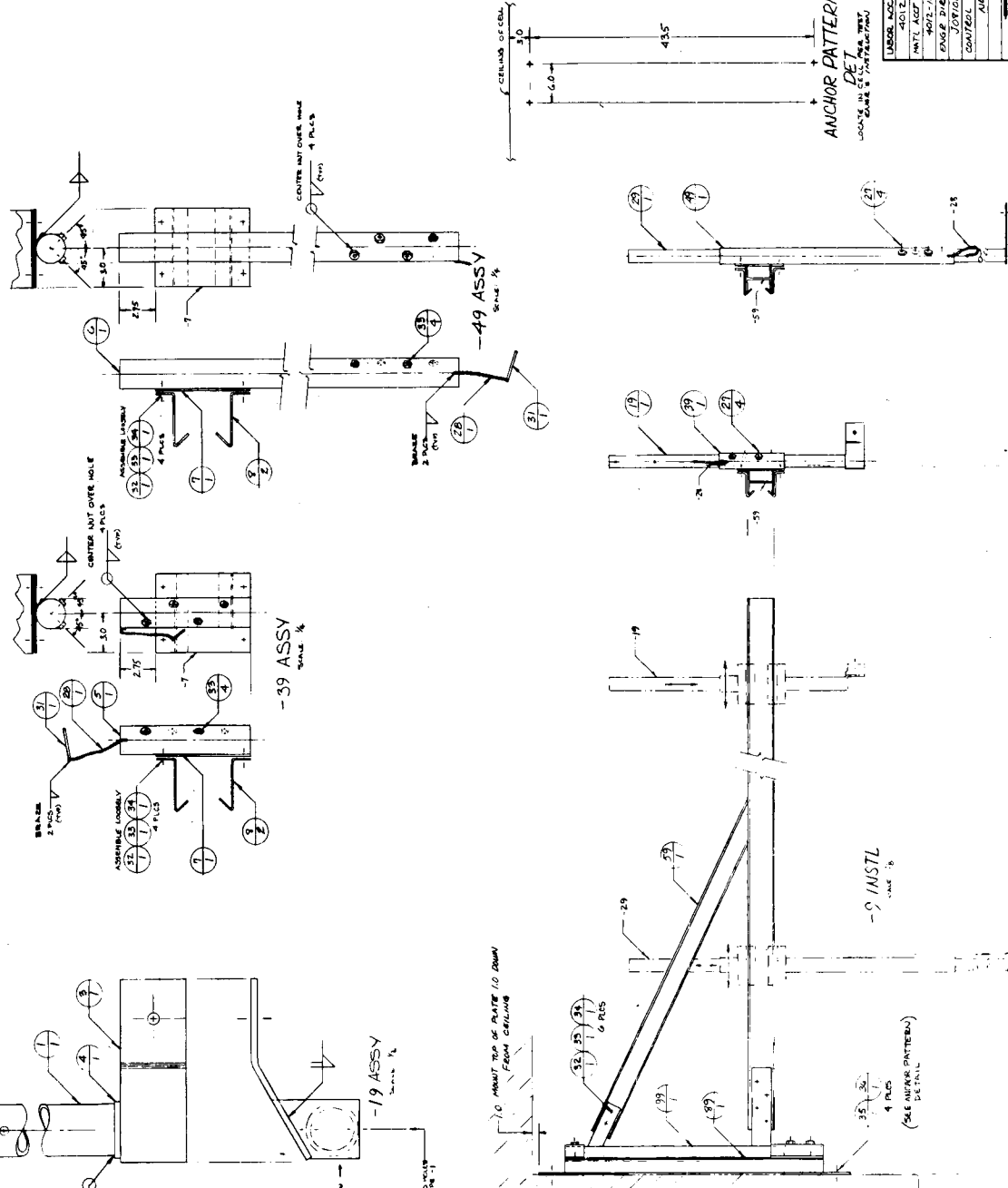
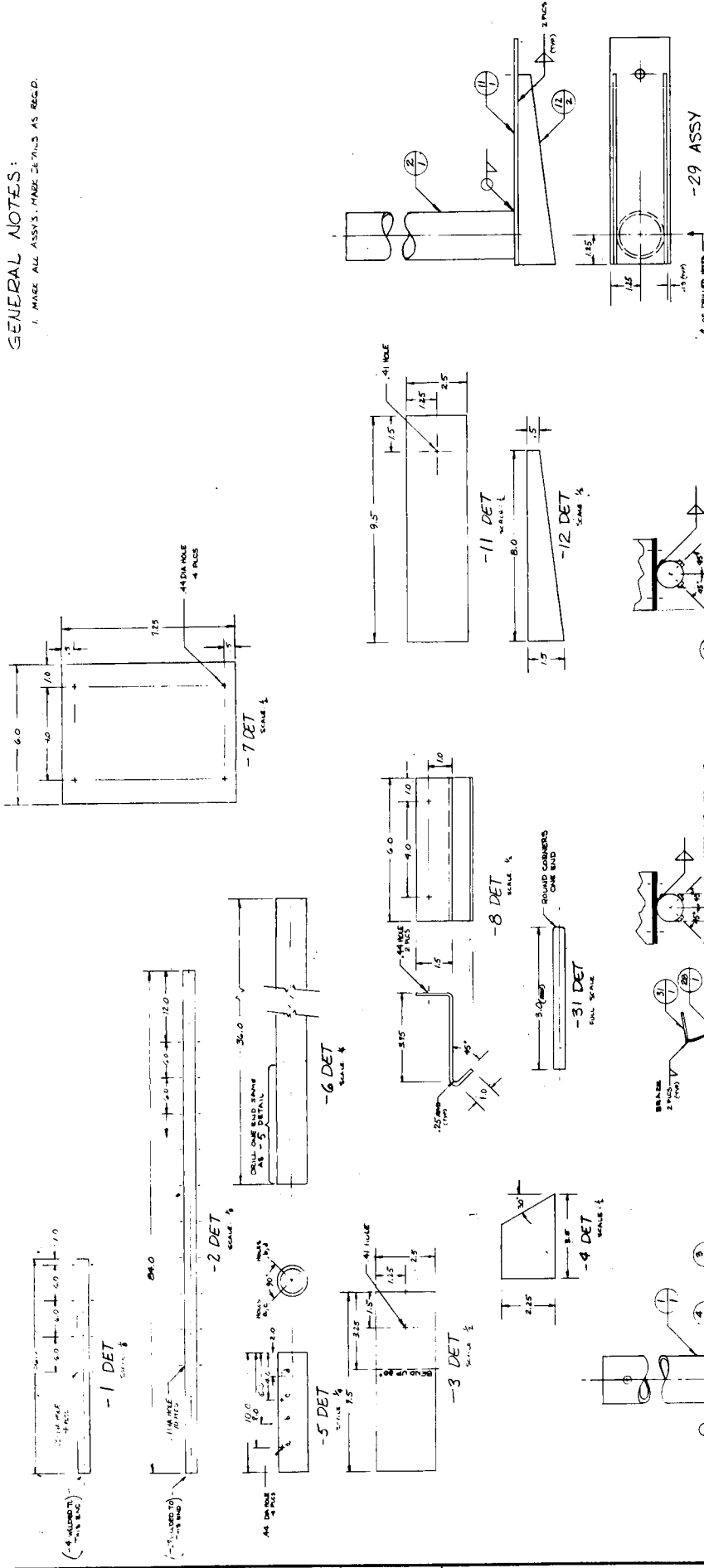
REVISIONS			
DATE	REVISIONS	BY	CHKD

DATE	38597	E	CFL6100596
SCALE	NOTED	H4003246L	SHEET 2 of 2

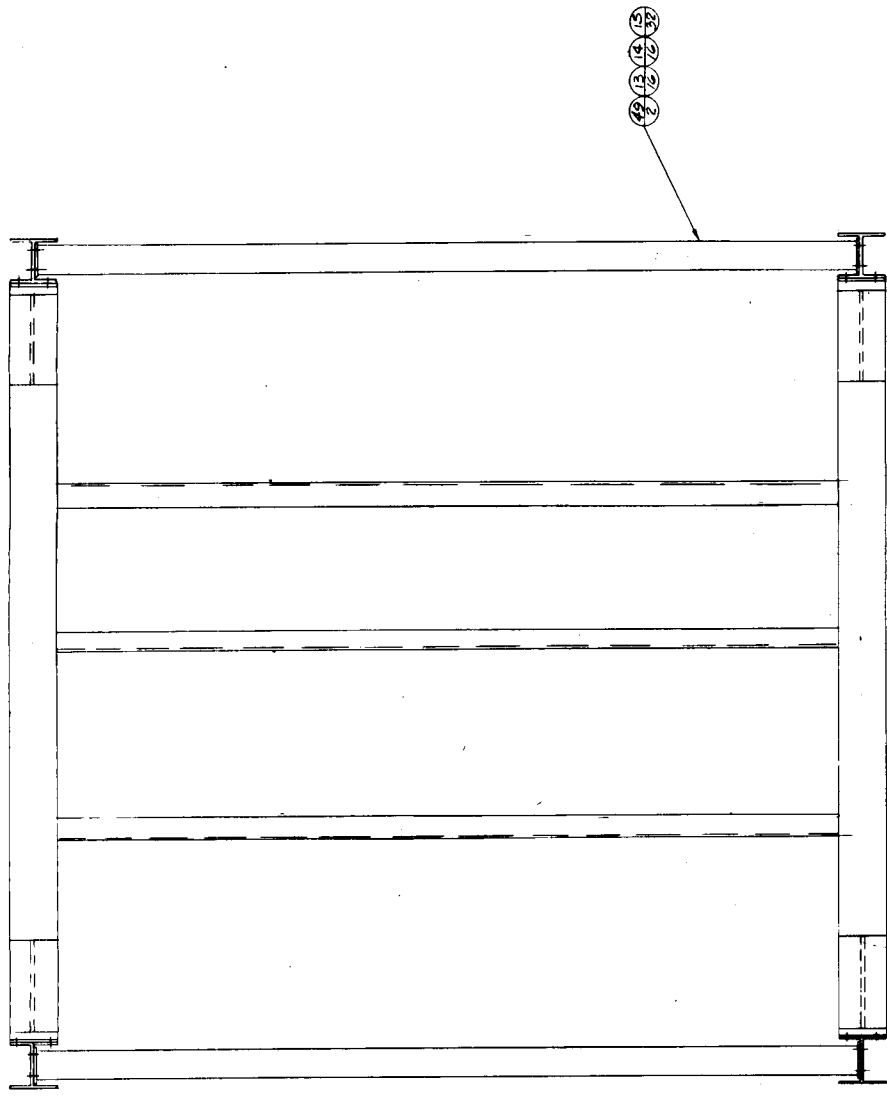


GENERAL NOTES:

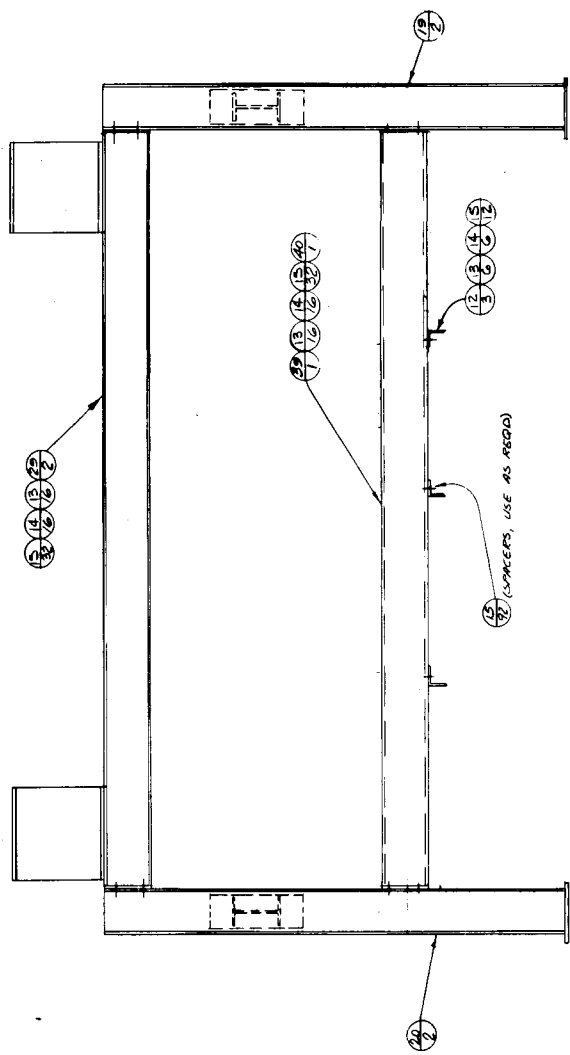
1. MAKE ALL ASSY'S. MARK SET NLS AS REG'D.

[illegible][illegible]

REVISIONS			
NO.	DATE	DESCRIPTION	BY

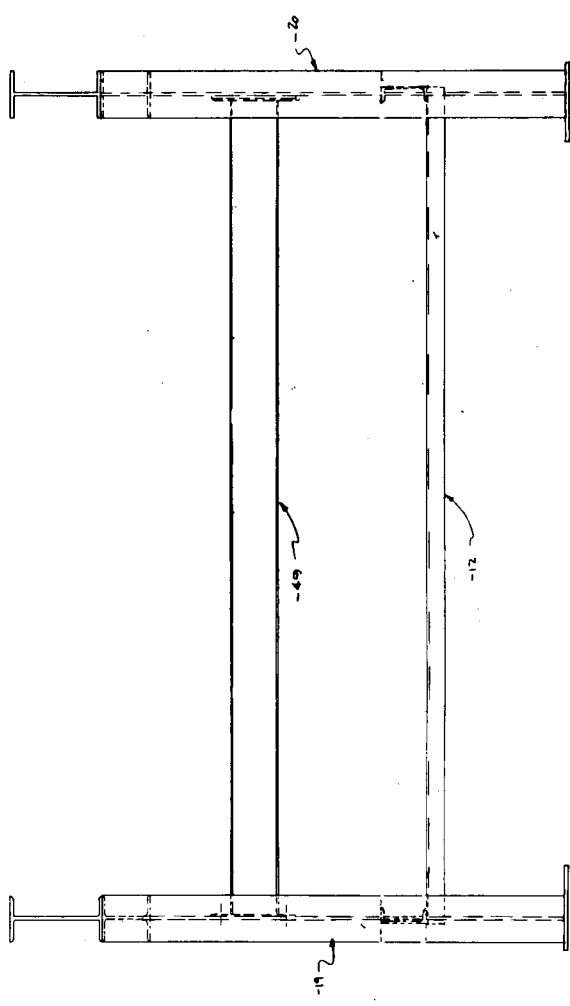


PLAN VIEW



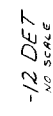
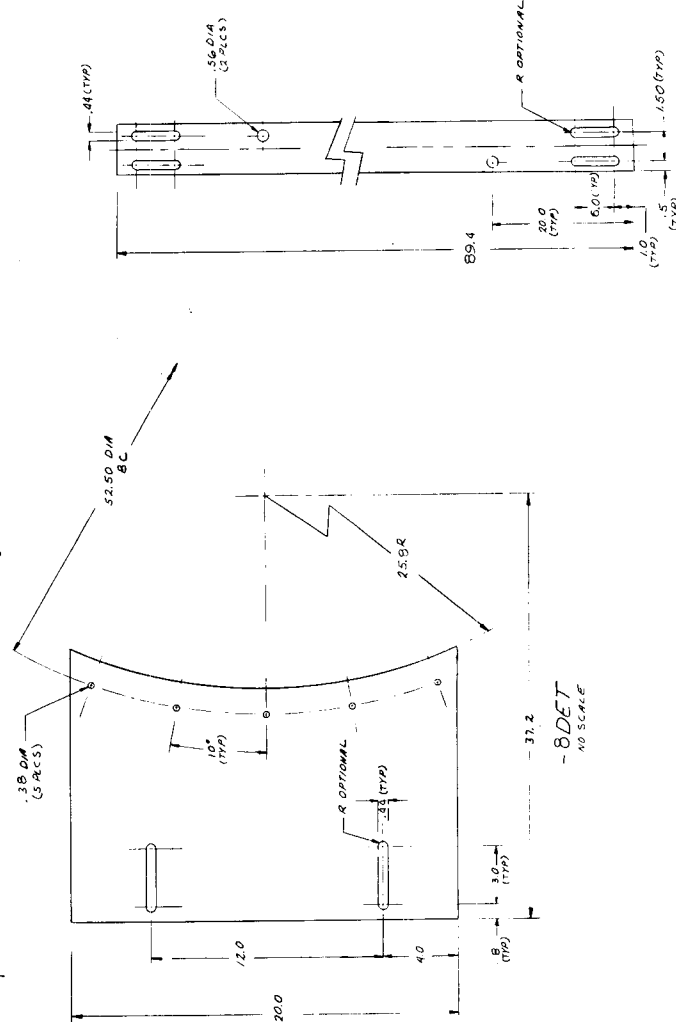
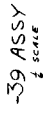
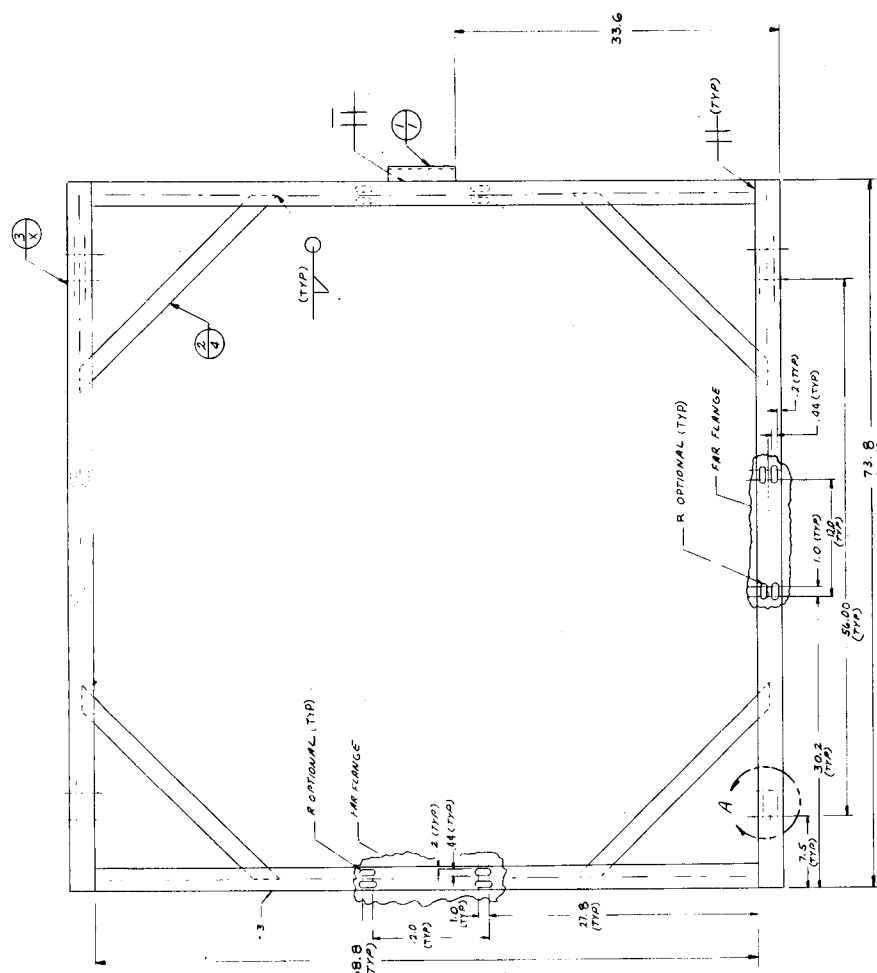
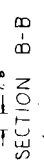
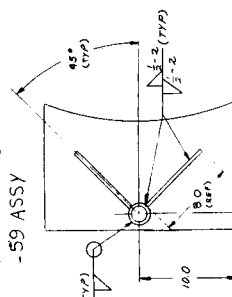
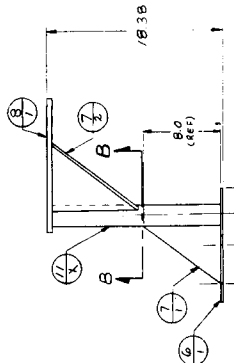
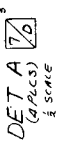
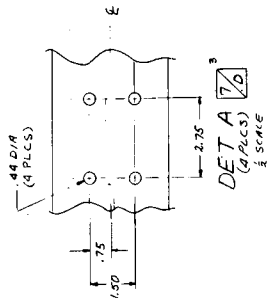
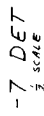
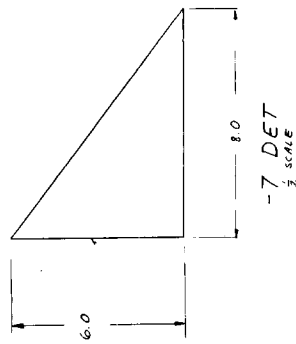
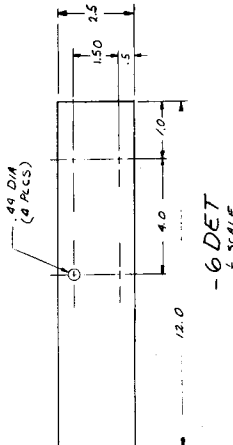
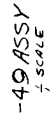
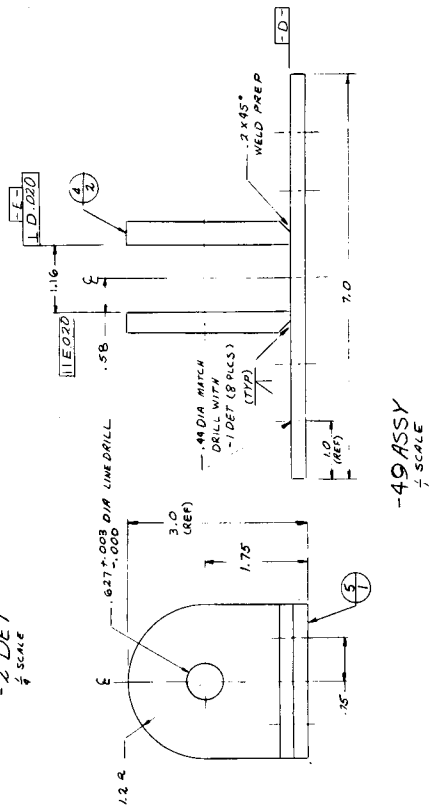
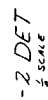
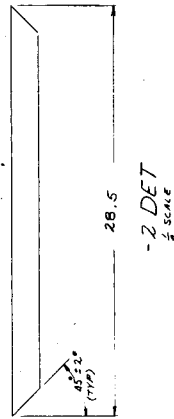
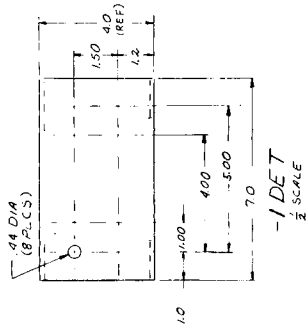
FRONT ELEVATION

- 9 ASSY

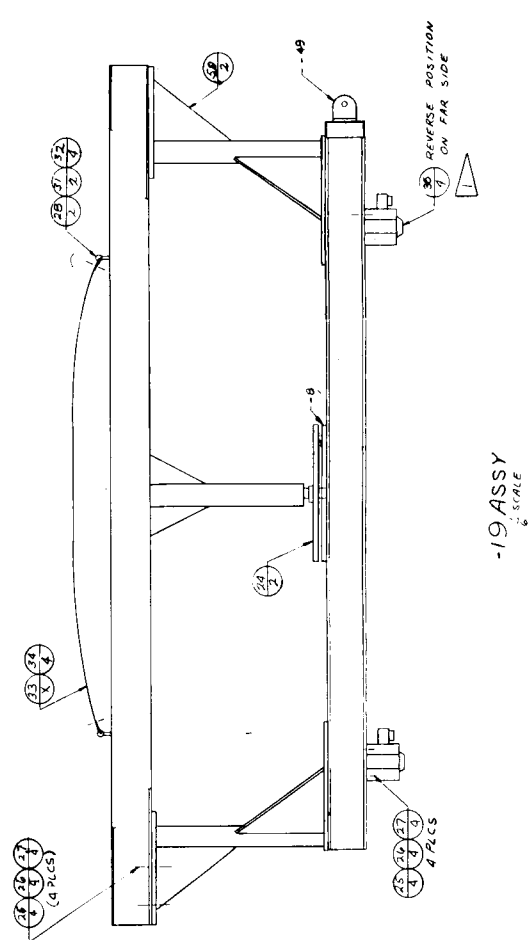
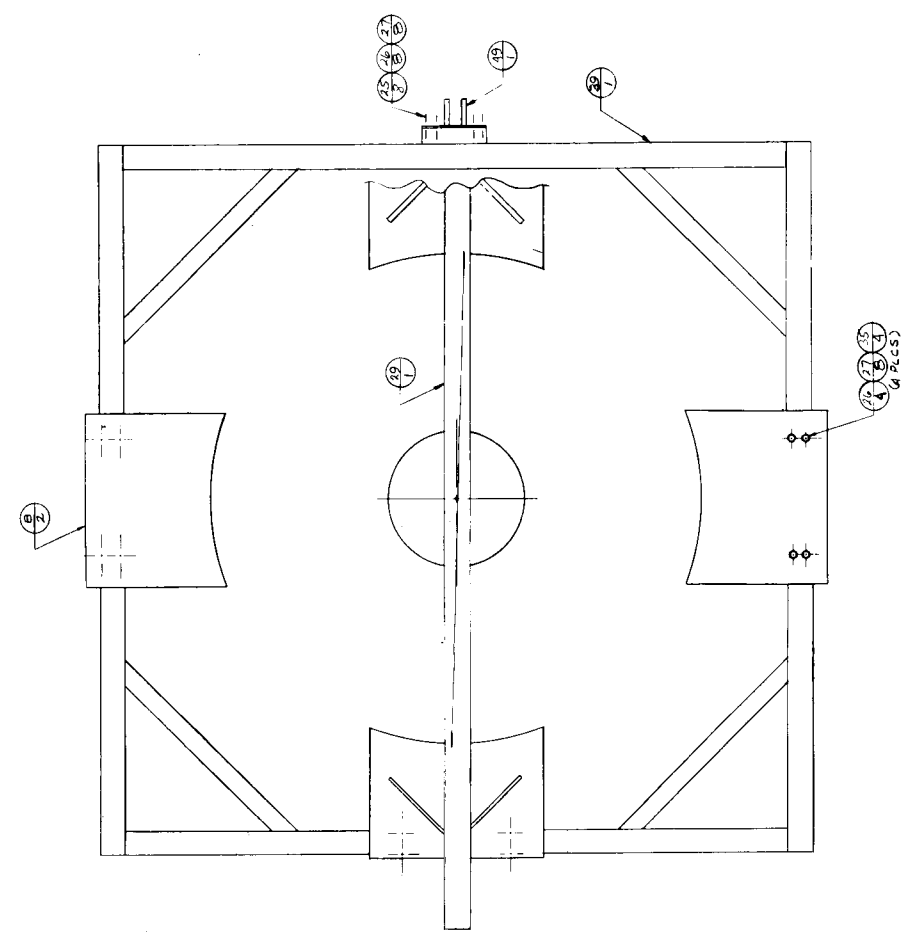
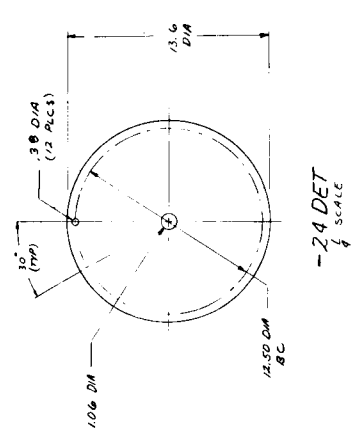
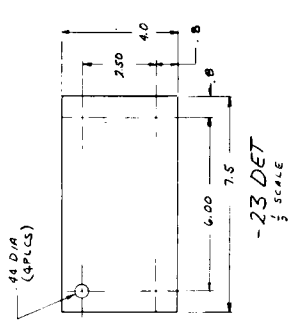
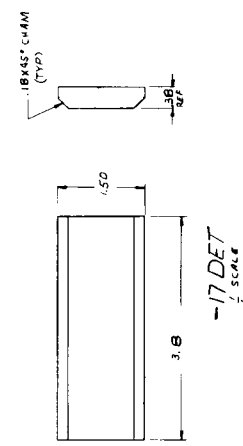
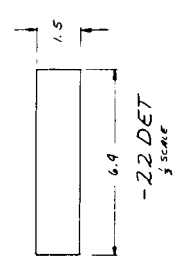
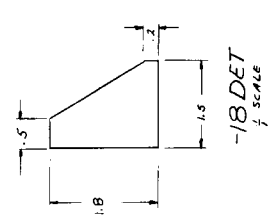
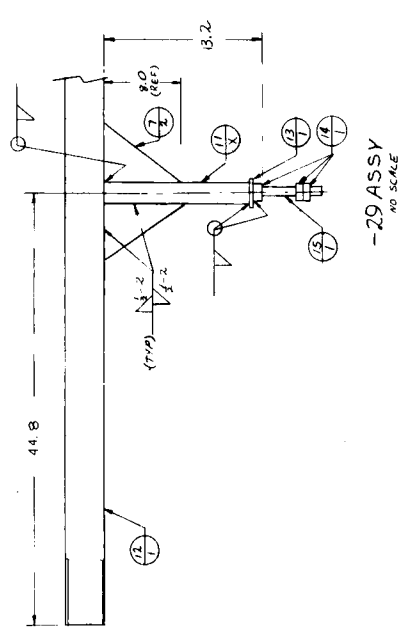


SIDE ELEVATION


REVISION		DATE	APPROVED
REV	DESCRIPTION	DATE	APPROVED

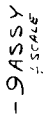


COORDINANT NO.	DATE	
38597	E	CF 6100594
SEAL	APPROVED	SHEET 3 OF 3
H 4003246 L		



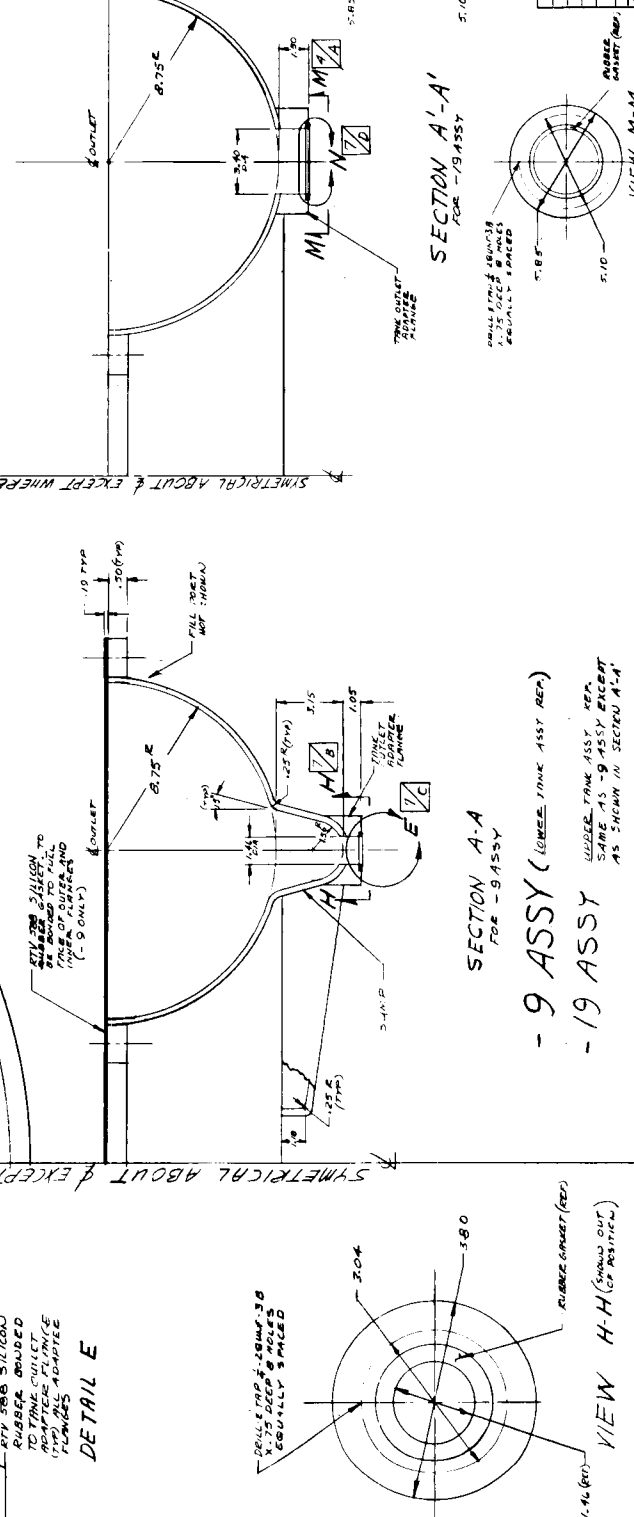
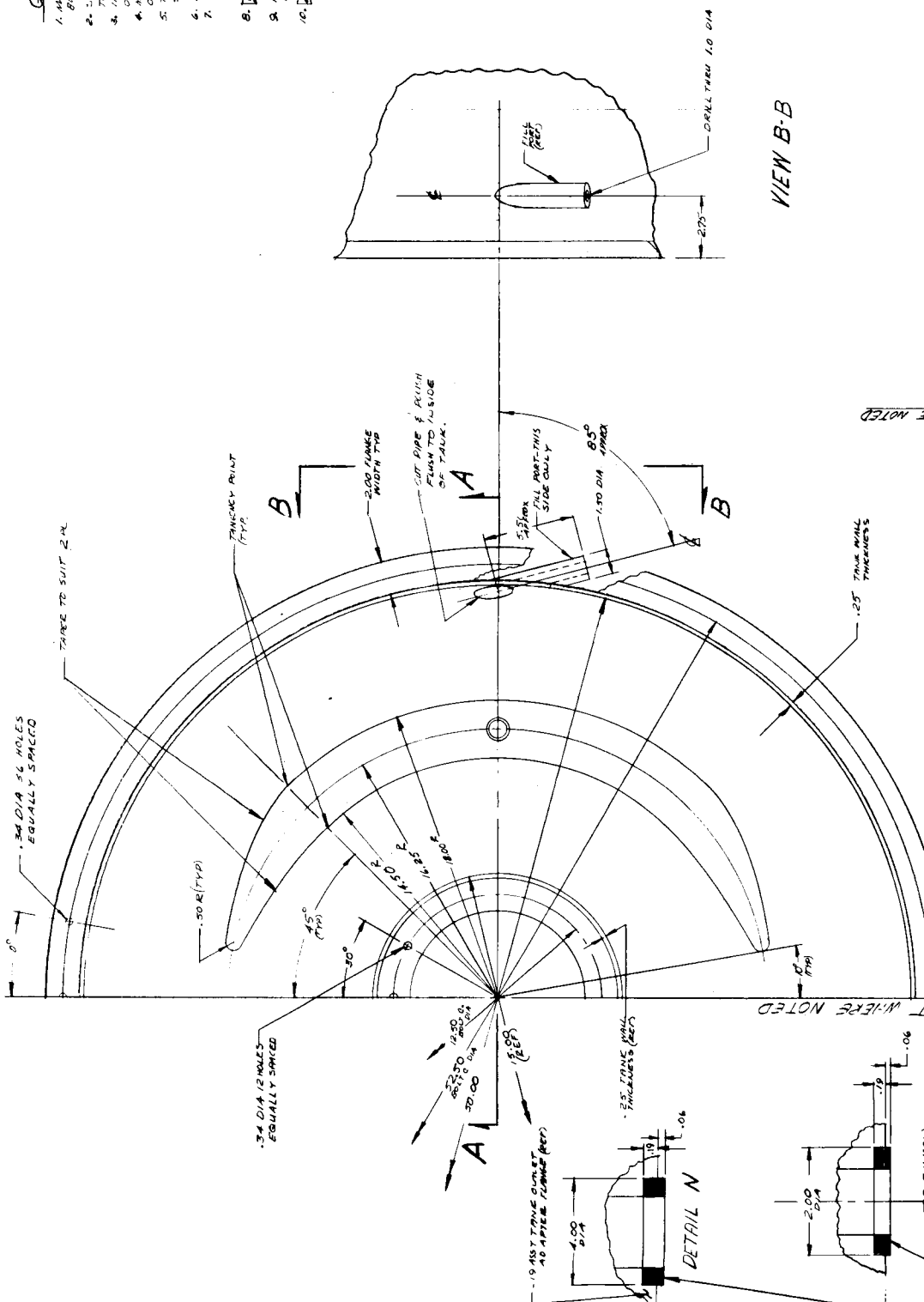
GENERAL NOTES

1. DESIGN LOAD OF 7.5 LBS FOR -19
2. FACTOR OF SAFETY EXCEEDS 2.
3.  PROTECT BEARING SURFACES OF -9

[illegible]

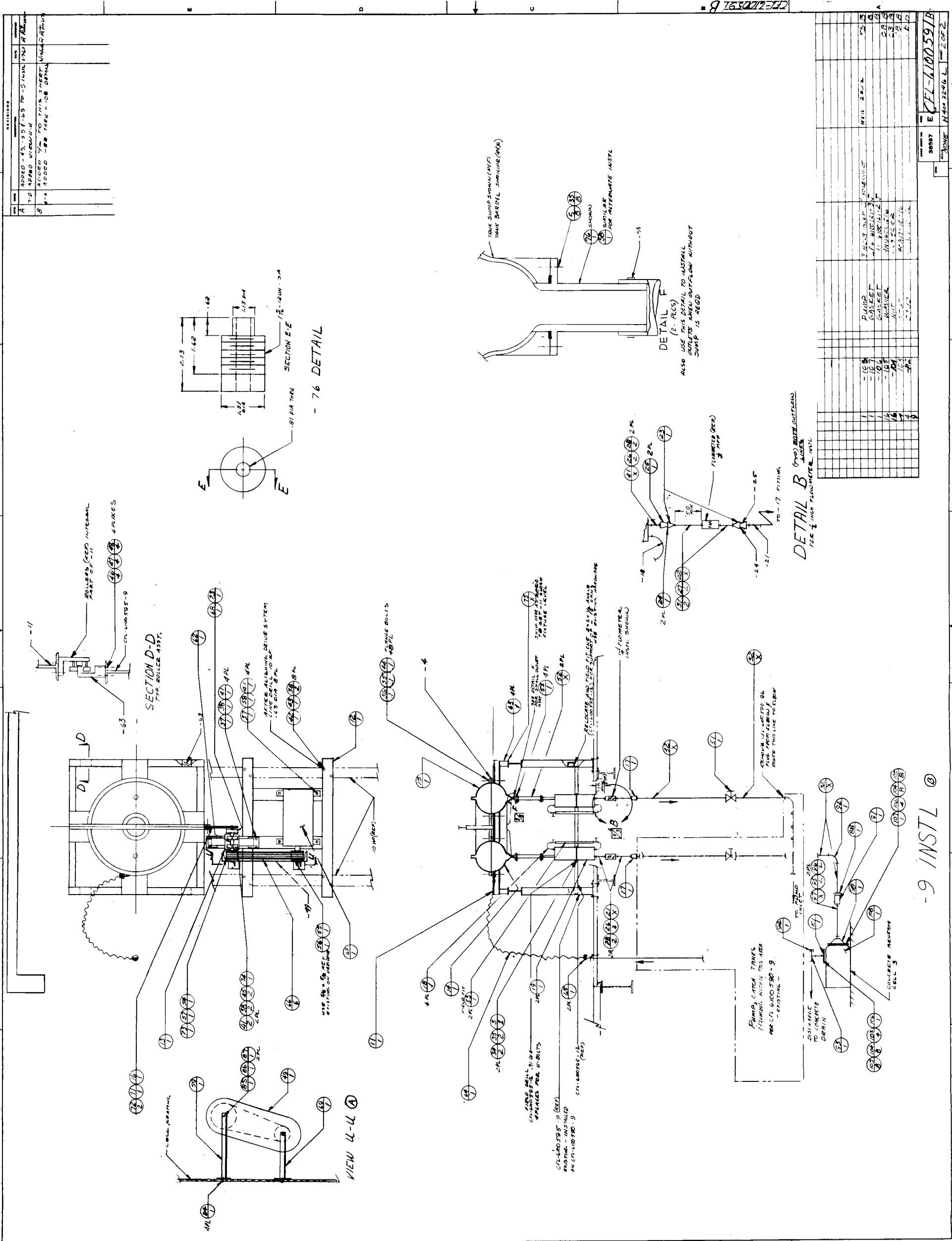
GENERAL NOTES

1. MATERIAL TO BE TYPICALLY FLEXIBLES G" RIE OF CARBON, BUBBLES AND FLAMES.
2. SECURELY BOND ALL PARTS ALONG CEMENT II (FOR REGULANT).
3. TO FORM WATER TIGHT UNITS.
4. INSIDE SURFACES OF TANK MUST BE SMOOTH & CONTINUOUS FREE OF ANY PROTRUSIONS EXCEPT WHERE NOTED.
5. MINIMUM STICK THICKNESS SHALL BE .125 INCHES FOR ALL SECTIONS.
6. TANKS MUST BE FILLED WITH WATER TO BE TESTED TO 150 PSI.
7. SECTION AND FILMING.
8. REMOVE ALL SHARP EDGES & BURRS.
9. FOR TECHNICAL DRAWING (OUTLET MATERIALS - COLD FLOW DESIGN UNIT, DICE PETERSON OR DICE ANDERSON).
10. MAKE TWO - OUTLETS ARE TO BE INTERCHANGEABLE AT 80% - 85% TANK OUTLET ADAPTER FLANGES.
11. FINAL ASSEMBLY OF TANKS TO BE COMPLETED AT MARTIN CO. COLD FLOW LAB.
12. MAKE TWO - OUTLETS ARE TO BE INTERCHANGEABLE AT BOTH - 85% TANK OUTLET ADAPTER FLANGES.



SECTION A-A FOR -9 ASSY	
-9 ASSY (LOWER TANK ASSY REP.)	
-19 ASSY (UPPER TANK ASSY REP.)	
SAME AS -9 ASSY EXCEPT AS SHOWN IN SECTION A-A	
VIEW H-H (SYMMETRICAL)	
VIEW M-M (SYMMETRICAL)	
VIEW B-B (SYMMETRICAL)	
VIEW A-A (SYMMETRICAL)	
VIEW F-F (SYMMETRICAL)	
VIEW G-G (SYMMETRICAL)	
VIEW K-K (SYMMETRICAL)	
VIEW J-J (SYMMETRICAL)	
VIEW I-I (SYMMETRICAL)	
VIEW D-D (SYMMETRICAL)	
VIEW C-C (SYMMETRICAL)	
VIEW E-E (SYMMETRICAL)	
VIEW F-F (SYMMETRICAL)	
VIEW G-G (SYMMETRICAL)	
VIEW H-H (SYMMETRICAL)	
VIEW I-I (SYMMETRICAL)	
VIEW J-J (SYMMETRICAL)	
VIEW K-K (SYMMETRICAL)	
VIEW L-L (SYMMETRICAL)	
VIEW M-M (SYMMETRICAL)	
VIEW N-N (SYMMETRICAL)	
VIEW O-O (SYMMETRICAL)	
VIEW P-P (SYMMETRICAL)	
VIEW Q-Q (SYMMETRICAL)	
VIEW R-R (SYMMETRICAL)	
VIEW S-S (SYMMETRICAL)	
VIEW T-T (SYMMETRICAL)	
VIEW U-U (SYMMETRICAL)	
VIEW V-V (SYMMETRICAL)	
VIEW W-W (SYMMETRICAL)	
VIEW X-X (SYMMETRICAL)	
VIEW Y-Y (SYMMETRICAL)	
VIEW Z-Z (SYMMETRICAL)	

MARTIN COMPANY
TANK PLASTIC
TOROIDAL
COLD FLOW LAB
38507 E
EFL-6100593
DATE 3-1-67
1071



-9 INSTL ③

DETAIL B (TYP) BOLT OUTLINE
FOR 1/2 INCH FLANGE, INSTL

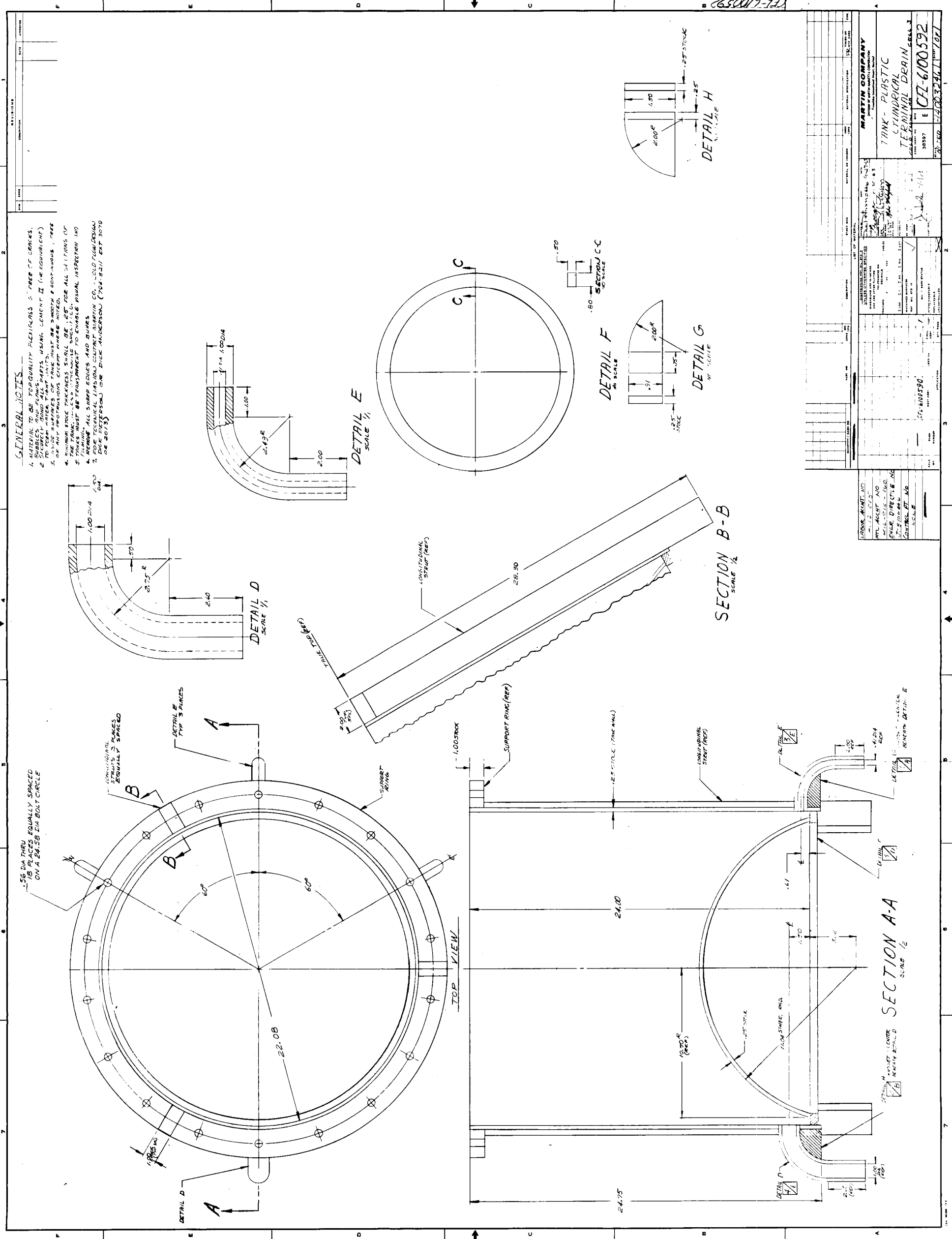
DETAIL F
(2 PLCS)
ALSO USE THIS DETAIL TO INSTALL
BOLTS WHEN OUTFLOW WITHOUT
SUMP IS REQD

- 76 DETAIL

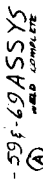
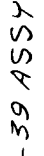
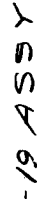
SECTION D-D
TYP. ROLLER ASST.

VIEW LL-11 A

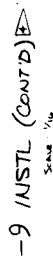
ITEM	DESCRIPTION	QTY	UNIT	REMARKS
1	PUMP	1	EA	CTI-100550-9
2	GASKET	1	EA	CTI-100550-12
3	BOLT	16	EA	CTI-100550-12
4	FLANGE	1	EA	CTI-100550-12
5	ROLLER	4	EA	CTI-100550-9
6	DRIVE SYSTEM	1	EA	CTI-100550-12
7	PIPE DETAIL TO PUMP	1	EA	CTI-100550-12
8	PIPE DETAIL TO PUMP	1	EA	CTI-100550-12
9	PIPE DETAIL TO PUMP	1	EA	CTI-100550-12
10	PIPE DETAIL TO PUMP	1	EA	CTI-100550-12
11	PIPE DETAIL TO PUMP	1	EA	CTI-100550-12
12	PIPE DETAIL TO PUMP	1	EA	CTI-100550-12
13	PIPE DETAIL TO PUMP	1	EA	CTI-100550-12
14	PIPE DETAIL TO PUMP	1	EA	CTI-100550-12
15	PIPE DETAIL TO PUMP	1	EA	CTI-100550-12
16	PIPE DETAIL TO PUMP	1	EA	CTI-100550-12
17	PIPE DETAIL TO PUMP	1	EA	CTI-100550-12
18	PIPE DETAIL TO PUMP	1	EA	CTI-100550-12
19	PIPE DETAIL TO PUMP	1	EA	CTI-100550-12
20	PIPE DETAIL TO PUMP	1	EA	CTI-100550-12
21	PIPE DETAIL TO PUMP	1	EA	CTI-100550-12
22	PIPE DETAIL TO PUMP	1	EA	CTI-100550-12
23	PIPE DETAIL TO PUMP	1	EA	CTI-100550-12
24	PIPE DETAIL TO PUMP	1	EA	CTI-100550-12
25	PIPE DETAIL TO PUMP	1	EA	CTI-100550-12
26	PIPE DETAIL TO PUMP	1	EA	CTI-100550-12
27	PIPE DETAIL TO PUMP	1	EA	CTI-100550-12
28	PIPE DETAIL TO PUMP	1	EA	CTI-100550-12
29	PIPE DETAIL TO PUMP	1	EA	CTI-100550-12
30	PIPE DETAIL TO PUMP	1	EA	CTI-100550-12
31	PIPE DETAIL TO PUMP	1	EA	CTI-100550-12
32	PIPE DETAIL TO PUMP	1	EA	CTI-100550-12
33	PIPE DETAIL TO PUMP	1	EA	CTI-100550-12
34	PIPE DETAIL TO PUMP	1	EA	CTI-100550-12
35	PIPE DETAIL TO PUMP	1	EA	CTI-100550-12
36	PIPE DETAIL TO PUMP	1	EA	CTI-100550-12
37	PIPE DETAIL TO PUMP	1	EA	CTI-100550-12
38	PIPE DETAIL TO PUMP	1	EA	CTI-100550-12
39	PIPE DETAIL TO PUMP	1	EA	CTI-100550-12
40	PIPE DETAIL TO PUMP	1	EA	CTI-100550-12
41	PIPE DETAIL TO PUMP	1	EA	CTI-100550-12
42	PIPE DETAIL TO PUMP	1	EA	CTI-100550-12
43	PIPE DETAIL TO PUMP	1	EA	CTI-100550-12
44	PIPE DETAIL TO PUMP	1	EA	CTI-100550-12
45	PIPE DETAIL TO PUMP	1	EA	CTI-100550-12
46	PIPE DETAIL TO PUMP	1	EA	CTI-100550-12
47	PIPE DETAIL TO PUMP	1	EA	CTI-100550-12
48	PIPE DETAIL TO PUMP	1	EA	CTI-100550-12
49	PIPE DETAIL TO PUMP	1	EA	CTI-100550-12
50	PIPE DETAIL TO PUMP	1	EA	CTI-100550-12
51	PIPE DETAIL TO PUMP	1	EA	CTI-100550-12
52	PIPE DETAIL TO PUMP	1	EA	CTI-100550-12
53	PIPE DETAIL TO PUMP	1	EA	CTI-100550-12
54	PIPE DETAIL TO PUMP	1	EA	CTI-100550-12
55	PIPE DETAIL TO PUMP	1	EA	CTI-100550-12
56	PIPE DETAIL TO PUMP	1	EA	CTI-100550-12
57	PIPE DETAIL TO PUMP	1	EA	CTI-100550-12
58	PIPE DETAIL TO PUMP	1	EA	CTI-100550-12
59	PIPE DETAIL TO PUMP	1	EA	CTI-100550-12
60	PIPE DETAIL TO PUMP	1	EA	CTI-100550-12
61	PIPE DETAIL TO PUMP	1	EA	CTI-100550-12
62	PIPE DETAIL TO PUMP	1	EA	CTI-100550-12
63	PIPE DETAIL TO PUMP	1	EA	CTI-100550-12
64	PIPE DETAIL TO PUMP	1	EA	CTI-100550-12
65	PIPE DETAIL TO PUMP	1	EA	CTI-100550-12
66	PIPE DETAIL TO PUMP	1	EA	CTI-100550-12
67	PIPE DETAIL TO PUMP	1	EA	CTI-100550-12
68	PIPE DETAIL TO PUMP	1	EA	CTI-100550-12
69	PIPE DETAIL TO PUMP	1	EA	CTI-100550-12
70	PIPE DETAIL TO PUMP	1	EA	CTI-100550-12
71	PIPE DETAIL TO PUMP	1	EA	CTI-100550-12
72	PIPE DETAIL TO PUMP	1	EA	CTI-100550-12
73	PIPE DETAIL TO PUMP	1	EA	CTI-100550-12
74	PIPE DETAIL TO PUMP	1	EA	CTI-100550-12
75	PIPE DETAIL TO PUMP	1	EA	CTI-100550-12
76	PIPE DETAIL TO PUMP	1	EA	CTI-100550-12
77	PIPE DETAIL TO PUMP	1	EA	CTI-100550-12
78	PIPE DETAIL TO PUMP	1	EA	CTI-100550-12
79	PIPE DETAIL TO PUMP	1	EA	CTI-100550-12
80	PIPE DETAIL TO PUMP	1	EA	CTI-100550-12
81	PIPE DETAIL TO PUMP	1	EA	CTI-100550-12
82	PIPE DETAIL TO PUMP	1	EA	CTI-100550-12
83	PIPE DETAIL TO PUMP	1	EA	CTI-100550-12
84	PIPE DETAIL TO PUMP	1	EA	CTI-100550-12
85	PIPE DETAIL TO PUMP	1	EA	CTI-100550-12
86	PIPE DETAIL TO PUMP	1	EA	CTI-100550-12
87	PIPE DETAIL TO PUMP	1	EA	CTI-100550-12
88	PIPE DETAIL TO PUMP	1	EA	CTI-100550-12
89	PIPE DETAIL TO PUMP	1	EA	CTI-100550-12
90	PIPE DETAIL TO PUMP	1	EA	CTI-100550-12
91	PIPE DETAIL TO PUMP	1	EA	CTI-100550-12
92	PIPE DETAIL TO PUMP	1	EA	CTI-100550-12
93	PIPE DETAIL TO PUMP	1	EA	CTI-100550-12
94	PIPE DETAIL TO PUMP	1	EA	CTI-100550-12
95	PIPE DETAIL TO PUMP	1	EA	CTI-100550-12
96	PIPE DETAIL TO PUMP	1	EA	CTI-100550-12
97	PIPE DETAIL TO PUMP	1	EA	CTI-100550-12
98	PIPE DETAIL TO PUMP	1	EA	CTI-100550-12
99	PIPE DETAIL TO PUMP	1	EA	CTI-100550-12
100	PIPE DETAIL TO PUMP	1	EA	CTI-100550-12



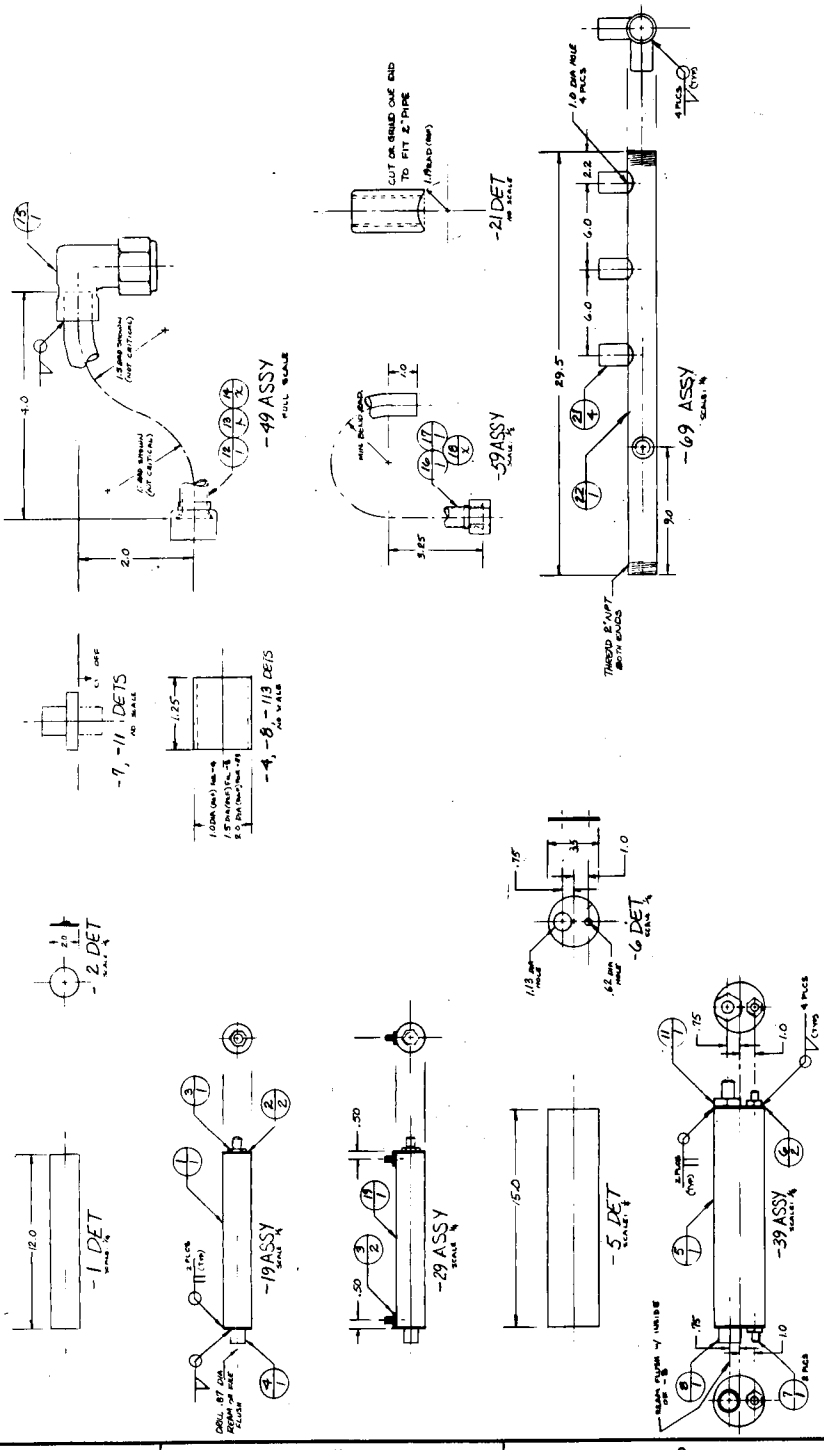
1. MAKE ALL ASSTS; MAKE DETAILS AS NEEDED
2. 1. USE PARTS FROM CPL-600500-9 AFTER COMPLETION OF TEST PHASE USING CYLINDRICAL PANE.
3. 2. ORDERED FOR CPL-600500, USE REMAINING STOCK AFTER COMPLETION OF THAT DMR.

[illegible]

1700 ACNT NO
4012-018
MTZ ACNT NO
4012-015-160
ENSE DISTINE NO
J20100446
CNTL PT NO
0000

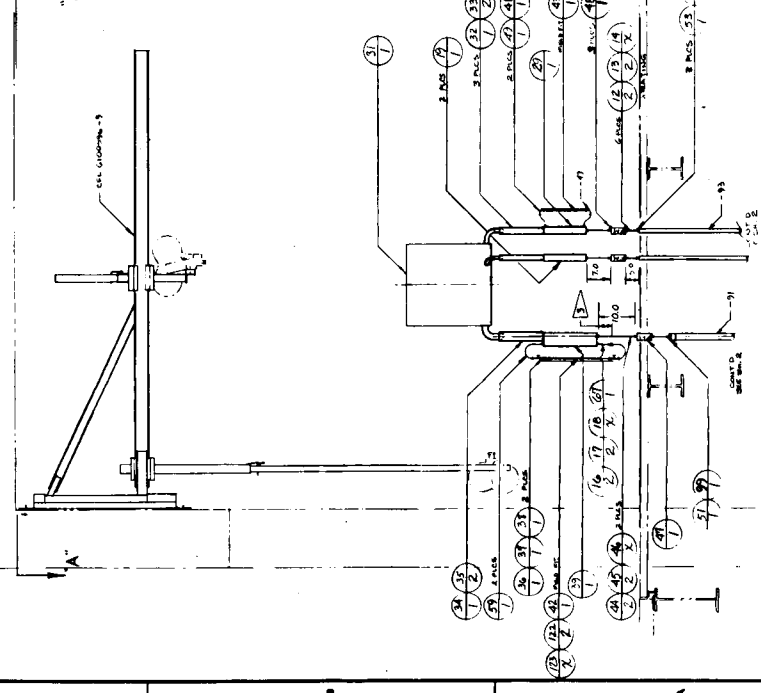
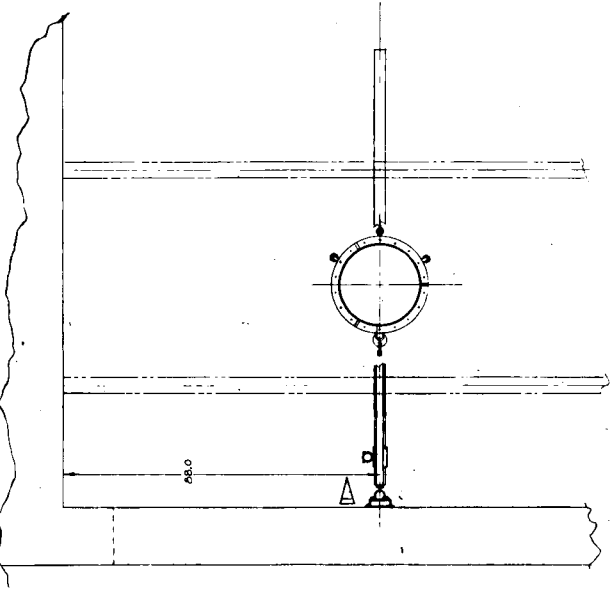


GENERAL NOTES:
1. MARK ALL ASSYS, DETS AND WELDS.
2. POSITION AS SHOWN, UNLESS OTHERWISE SPECIFIED.
3. THIS SPECIAL PILE ARM, INCLUDING -87, IS NOT REMAINING -50.
4. FIELD FIT ALL PIPE UNLESS NOT SPECIFIED.
5. SPACES - USE AS WELD, BUT DO NOT USE UNLESS ABSOLUTELY NECESSARY.




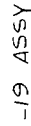
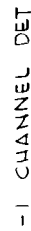
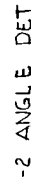
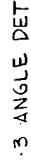
L/M CONT'D ON SH 2

ITEM NO.	DESCRIPTION	QTY	UNIT	REMARKS
1	FLANGE	1	EA	
2	FLANGE	1	EA	
3	FLANGE	1	EA	
4	FLANGE	1	EA	
5	FLANGE	1	EA	
6	FLANGE	1	EA	
7	FLANGE	1	EA	
8	FLANGE	1	EA	
9	FLANGE	1	EA	
10	FLANGE	1	EA	
11	FLANGE	1	EA	
12	FLANGE	1	EA	
13	FLANGE	1	EA	
14	FLANGE	1	EA	
15	FLANGE	1	EA	
16	FLANGE	1	EA	
17	FLANGE	1	EA	
18	FLANGE	1	EA	
19	FLANGE	1	EA	
20	FLANGE	1	EA	
21	FLANGE	1	EA	
22	FLANGE	1	EA	
23	FLANGE	1	EA	
24	FLANGE	1	EA	
25	FLANGE	1	EA	
26	FLANGE	1	EA	
27	FLANGE	1	EA	
28	FLANGE	1	EA	
29	FLANGE	1	EA	
30	FLANGE	1	EA	
31	FLANGE	1	EA	
32	FLANGE	1	EA	
33	FLANGE	1	EA	
34	FLANGE	1	EA	
35	FLANGE	1	EA	
36	FLANGE	1	EA	
37	FLANGE	1	EA	
38	FLANGE	1	EA	
39	FLANGE	1	EA	
40	FLANGE	1	EA	
41	FLANGE	1	EA	
42	FLANGE	1	EA	
43	FLANGE	1	EA	
44	FLANGE	1	EA	
45	FLANGE	1	EA	
46	FLANGE	1	EA	
47	FLANGE	1	EA	
48	FLANGE	1	EA	
49	FLANGE	1	EA	
50	FLANGE	1	EA	
51	FLANGE	1	EA	
52	FLANGE	1	EA	
53	FLANGE	1	EA	
54	FLANGE	1	EA	
55	FLANGE	1	EA	
56	FLANGE	1	EA	
57	FLANGE	1	EA	
58	FLANGE	1	EA	
59	FLANGE	1	EA	
60	FLANGE	1	EA	
61	FLANGE	1	EA	
62	FLANGE	1	EA	
63	FLANGE	1	EA	
64	FLANGE	1	EA	
65	FLANGE	1	EA	
66	FLANGE	1	EA	
67	FLANGE	1	EA	
68	FLANGE	1	EA	
69	FLANGE	1	EA	
70	FLANGE	1	EA	
71	FLANGE	1	EA	
72	FLANGE	1	EA	
73	FLANGE	1	EA	
74	FLANGE	1	EA	
75	FLANGE	1	EA	
76	FLANGE	1	EA	
77	FLANGE	1	EA	
78	FLANGE	1	EA	
79	FLANGE	1	EA	
80	FLANGE	1	EA	
81	FLANGE	1	EA	
82	FLANGE	1	EA	
83	FLANGE	1	EA	
84	FLANGE	1	EA	
85	FLANGE	1	EA	
86	FLANGE	1	EA	
87	FLANGE	1	EA	
88	FLANGE	1	EA	
89	FLANGE	1	EA	
90	FLANGE	1	EA	
91	FLANGE	1	EA	
92	FLANGE	1	EA	
93	FLANGE	1	EA	
94	FLANGE	1	EA	
95	FLANGE	1	EA	
96	FLANGE	1	EA	
97	FLANGE	1	EA	
98	FLANGE	1	EA	
99	FLANGE	1	EA	
100	FLANGE	1	EA	



MARTIN COMPANY
Cylindrical Tank Instl
Terminal Drain Study
CELL 3
CFL 6100590
DATE: 10/13/50
BY: [Signature]
CHECKED: [Signature]
APPROVED: [Signature]

1. MAKE ALL ASSYS. DETAILS AS READ
2.  ASSEMBLE IN CELL 3
3. DESIGNED WITH A SAFETY FACTOR OF 4 OR MORE
4. MAX LOAD CAP 1000 #

[illegible]

APPENDIX D

FIGURES AND TABLES

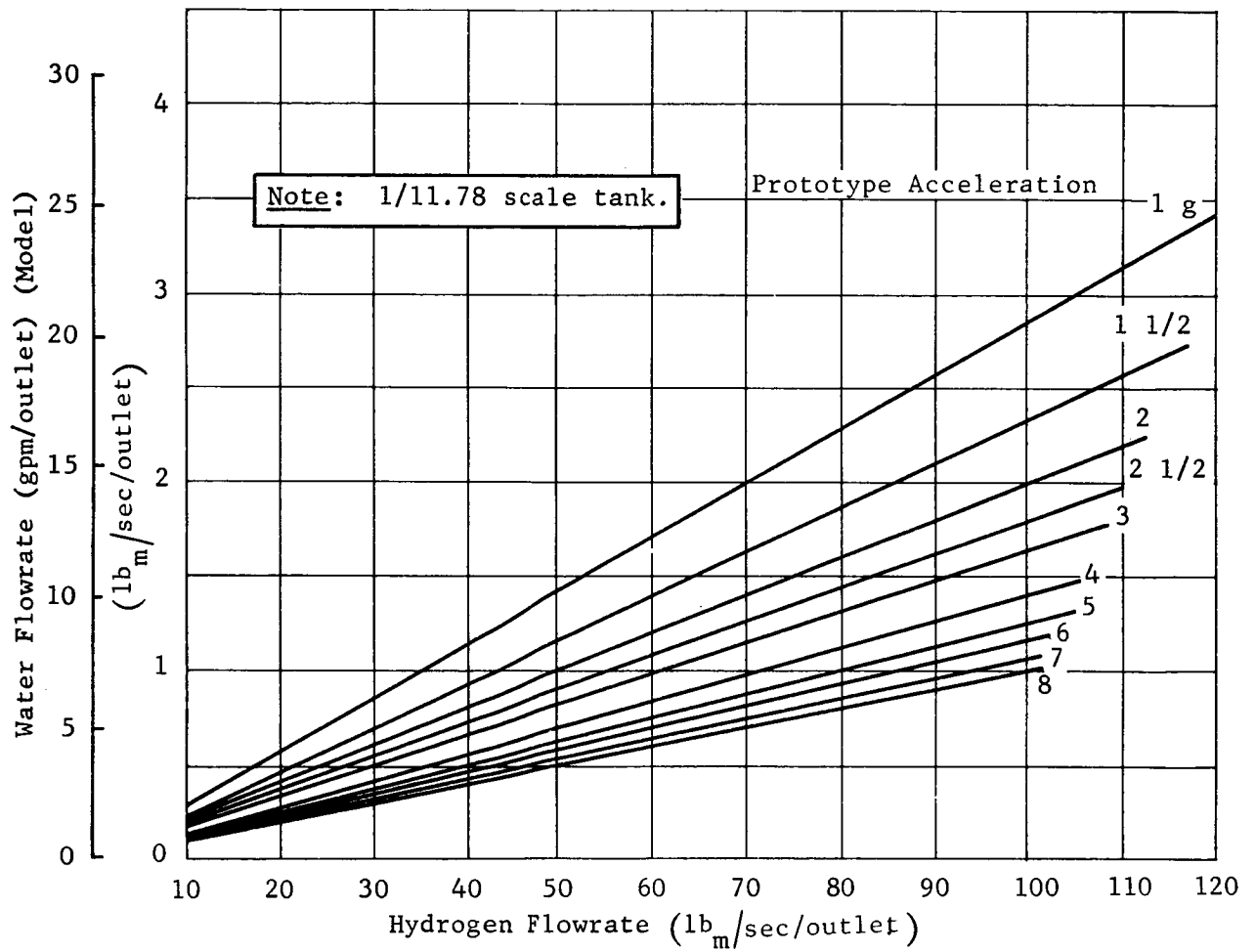


Fig. 1 Simulation Parameters, Cylindrical Tank

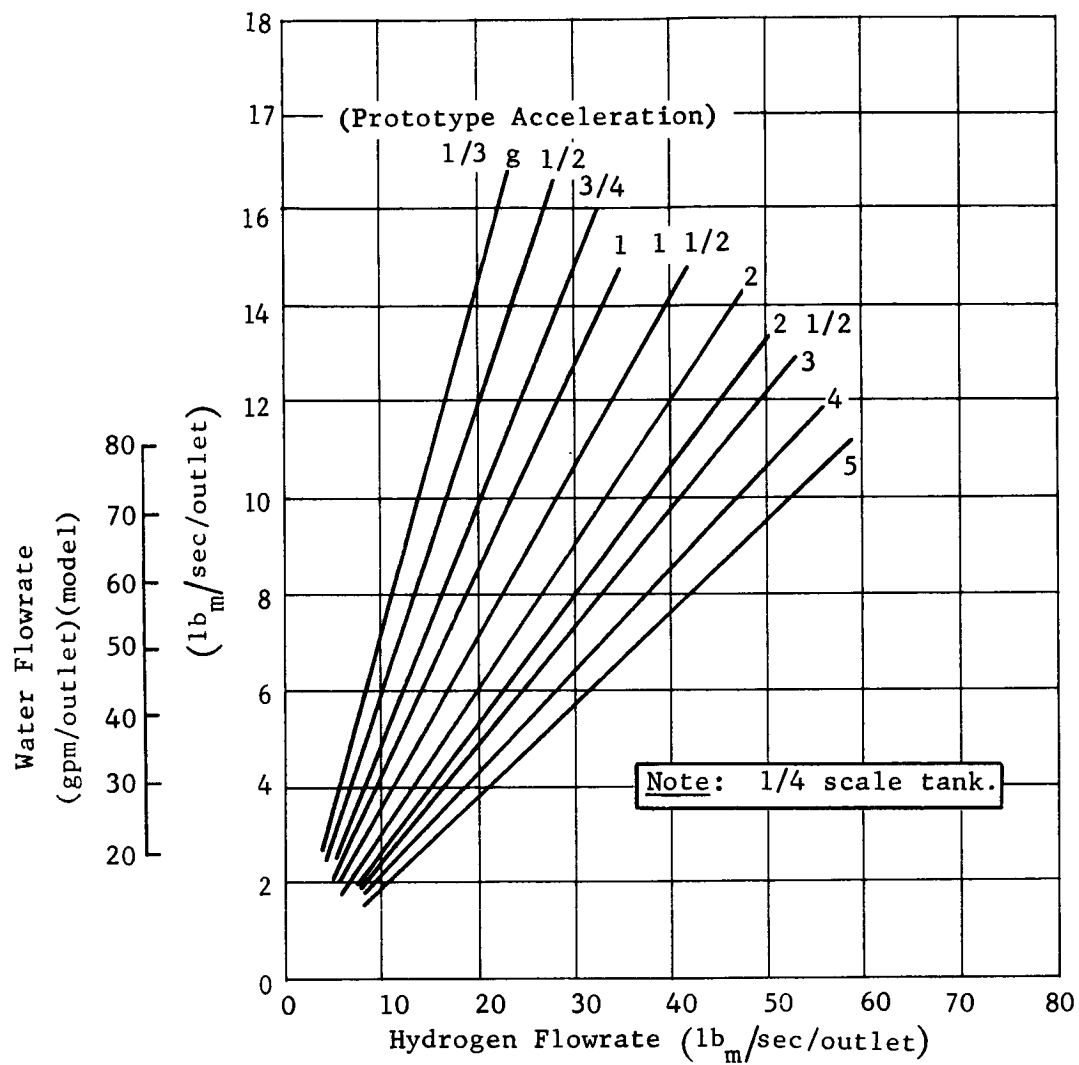
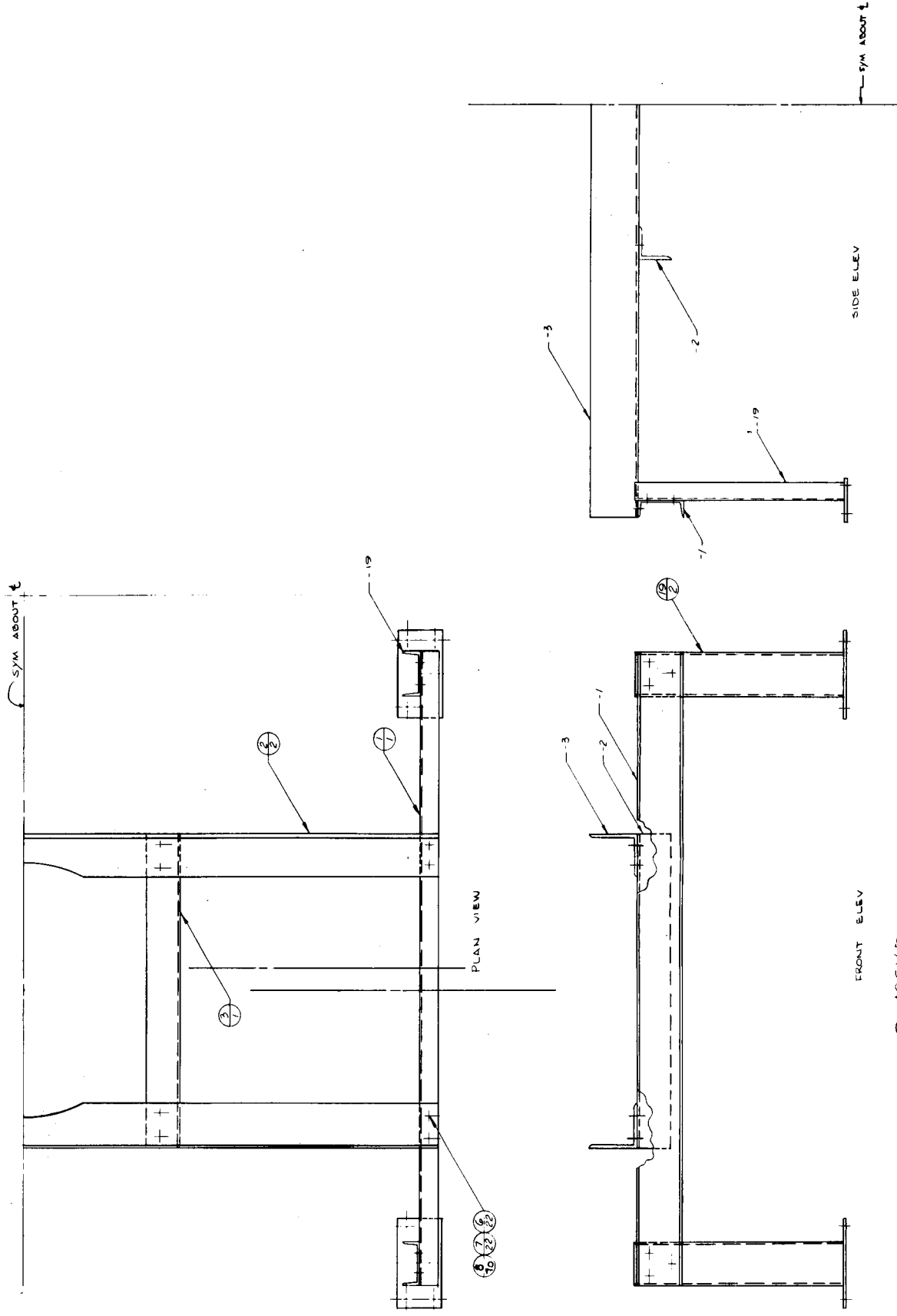
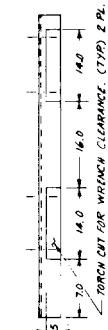
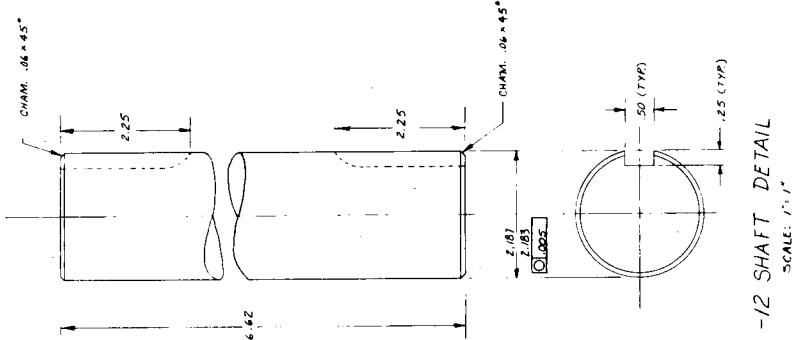


Fig. 2 Simulation Parameters, Toroidal Tank, Hydrogen



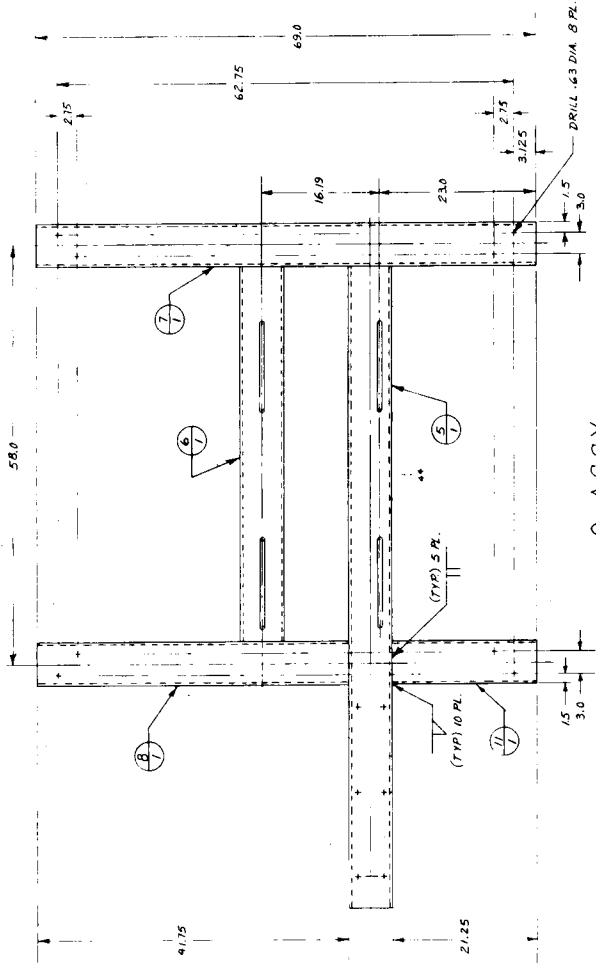
-9 ASSY [11]

REVISIONS		DATE	BY	APP'D

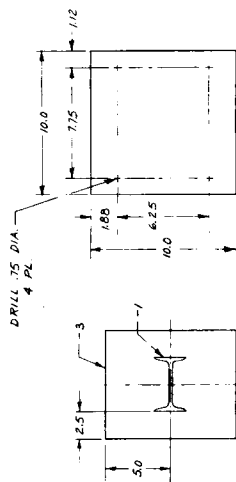


SEC. C-C
SCALE: NONE

SEC. D-D
ROTATED 180°
SCALE: NONE

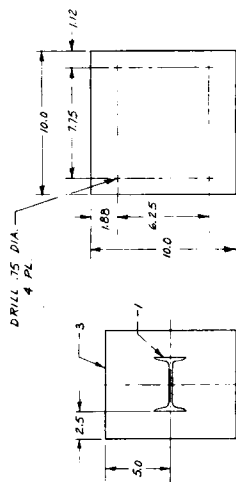


-9 ASSY
SCALE: 1/8" = 1"



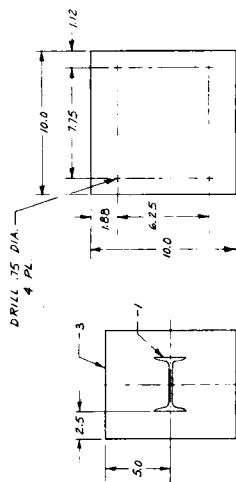
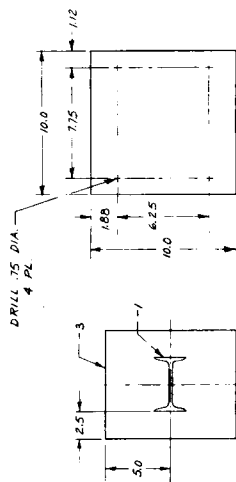
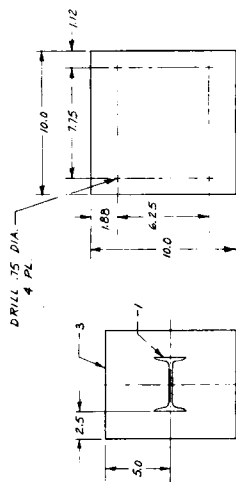
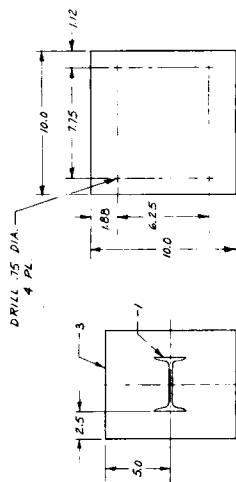
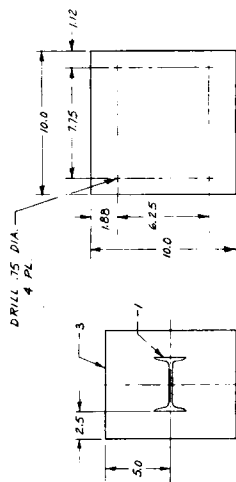
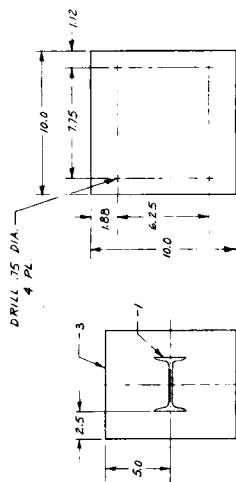
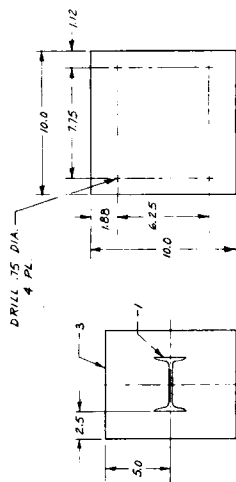
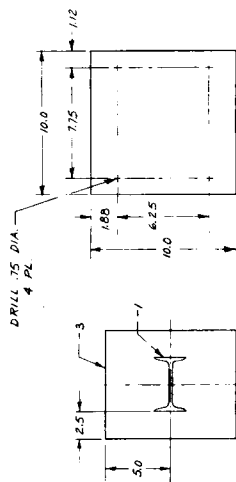
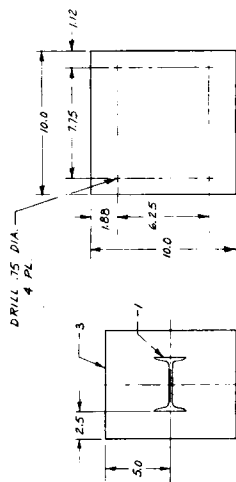
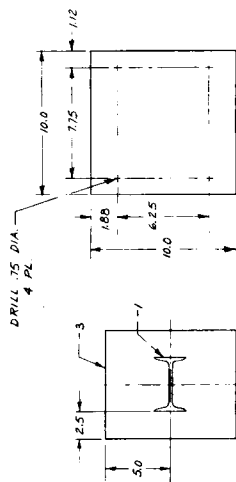
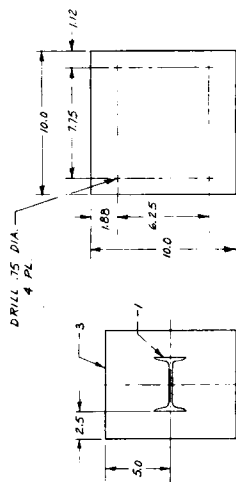
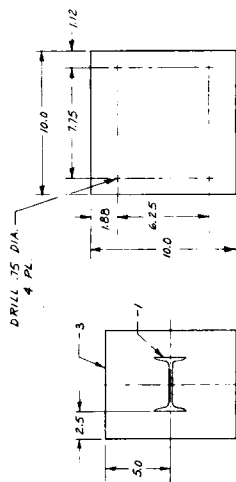
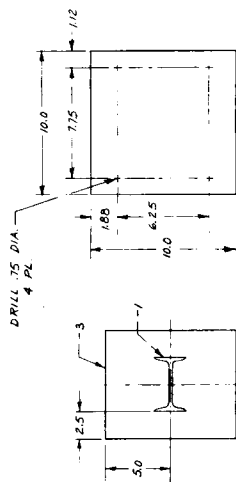
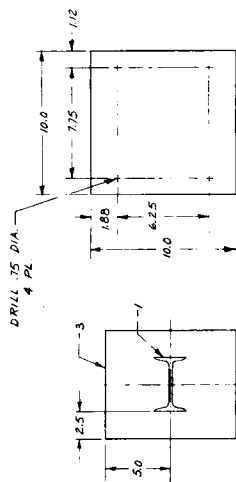
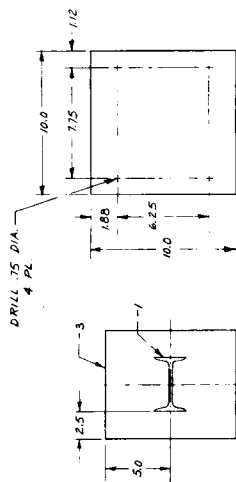
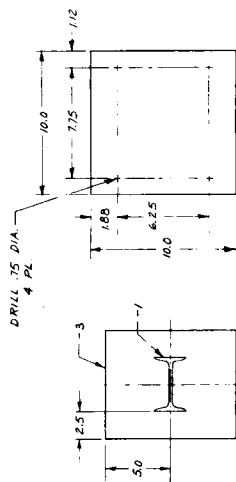
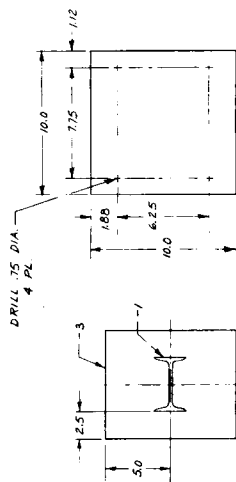
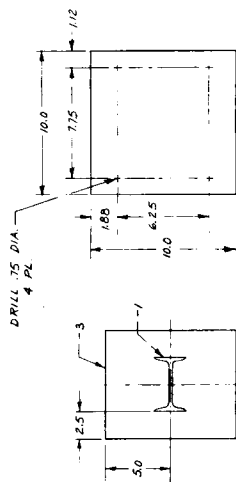
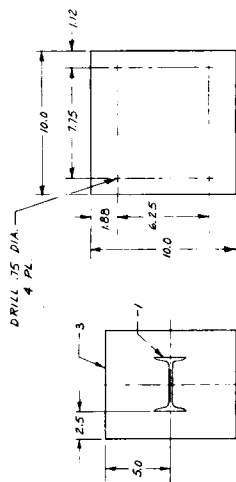
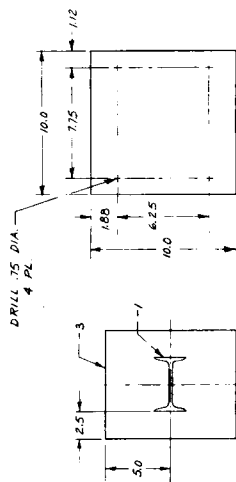
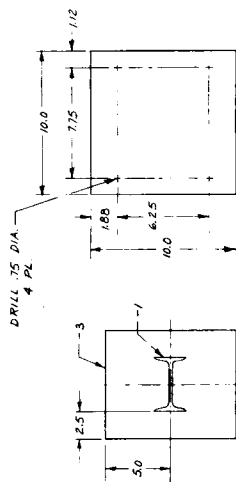
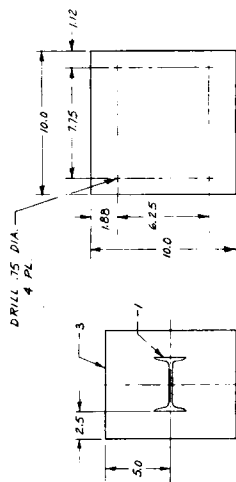
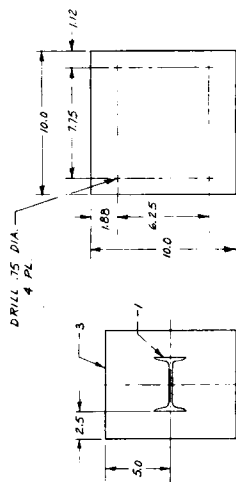
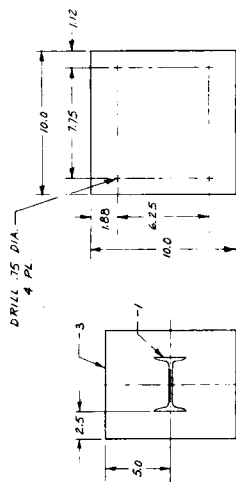
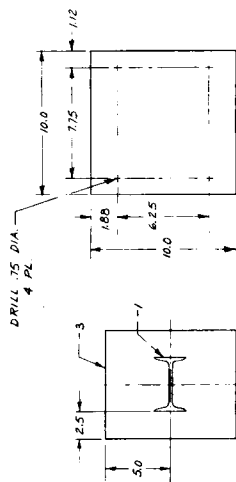
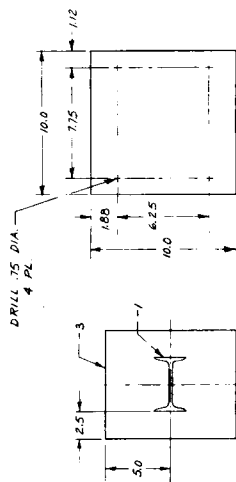
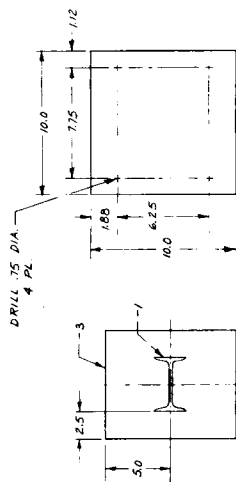
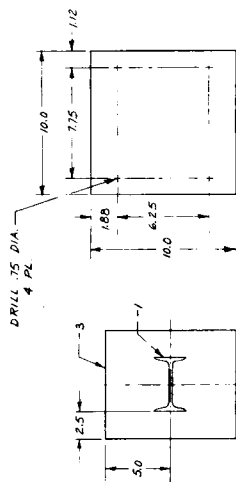
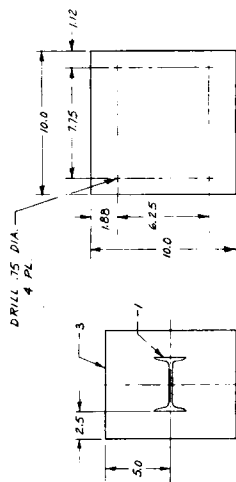
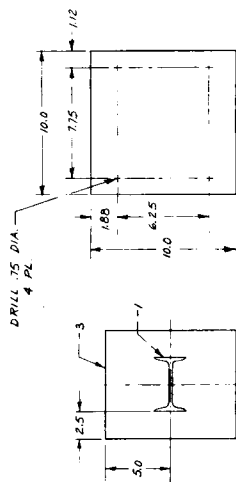
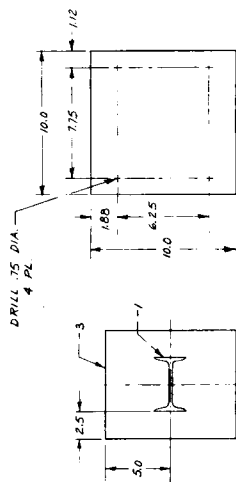
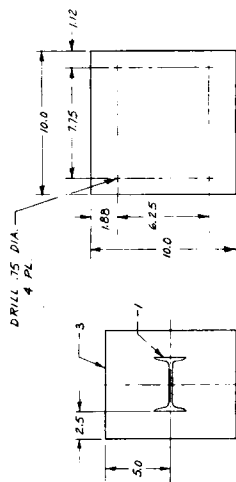
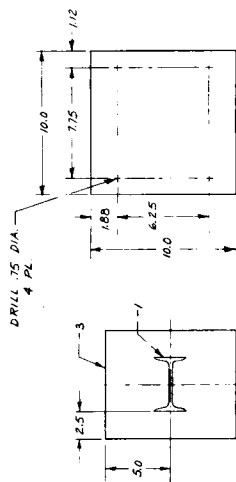
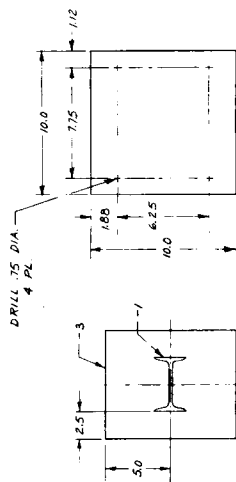
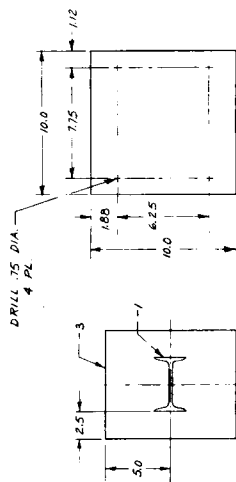
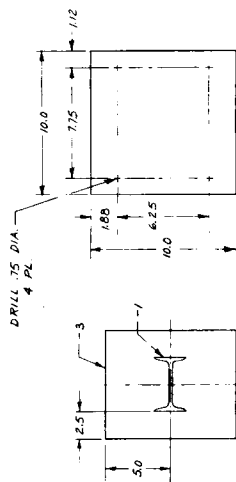
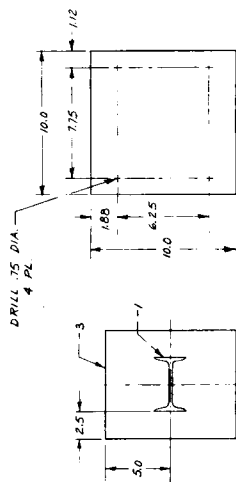
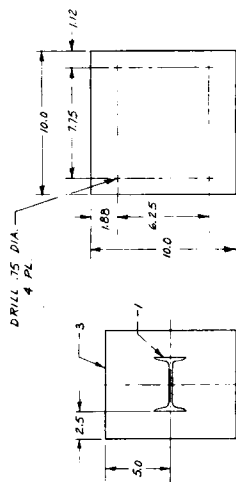
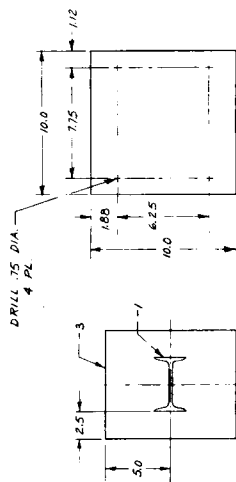
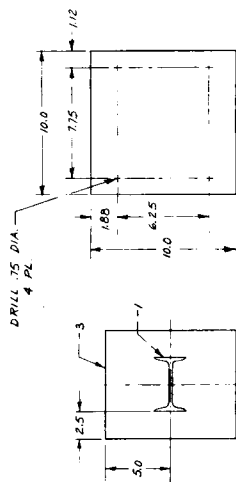
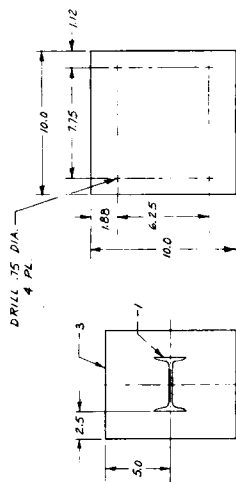
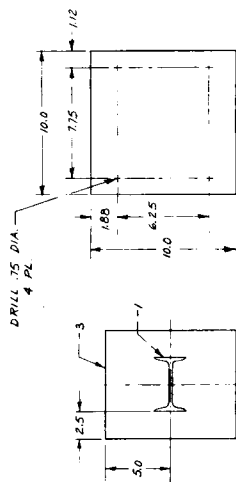
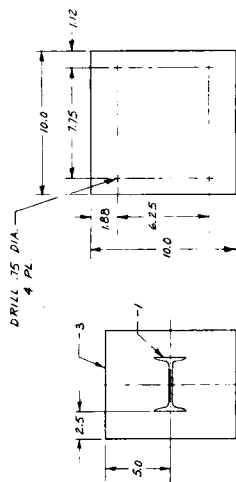
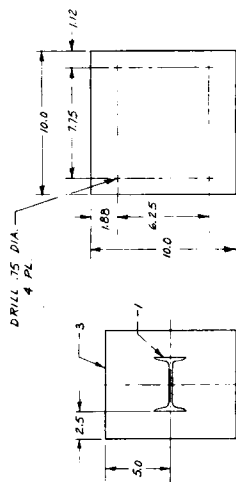
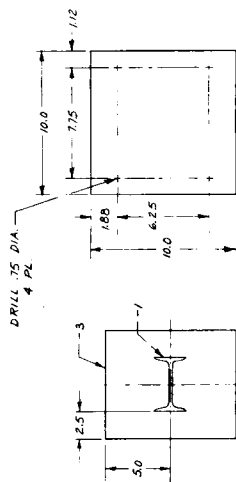
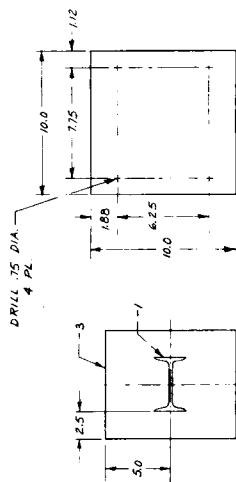
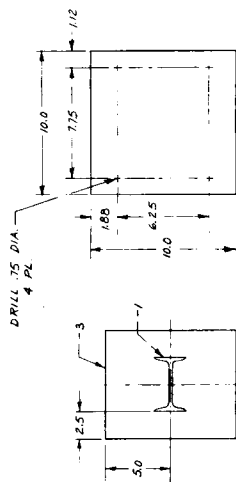
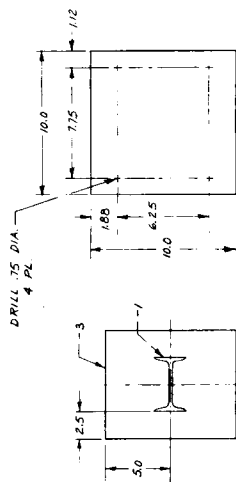
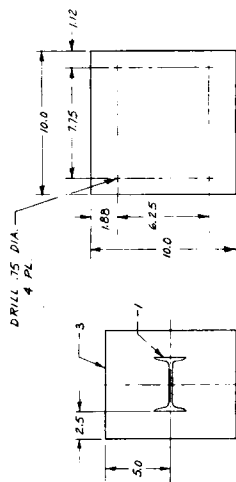
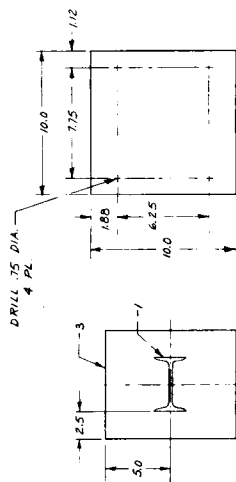
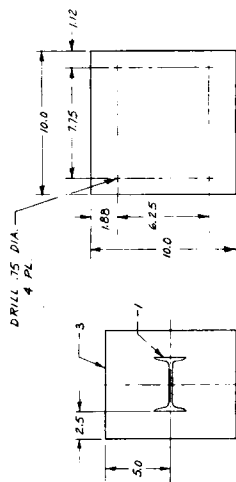
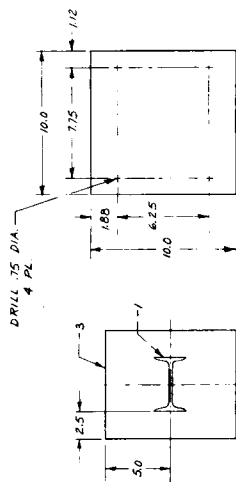
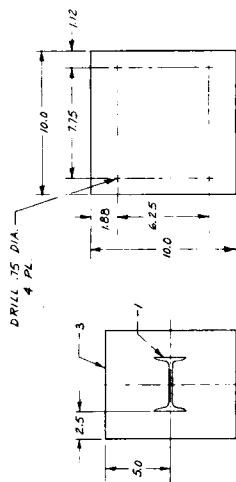
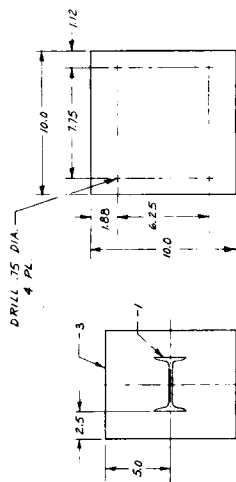
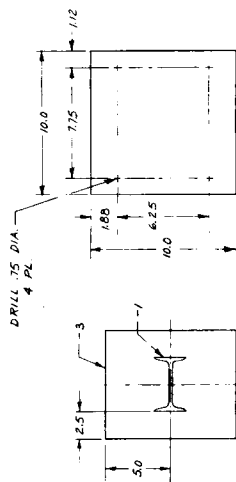
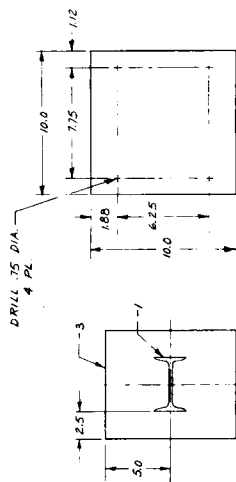
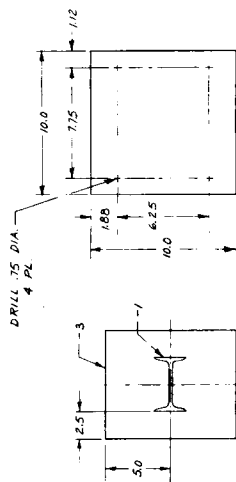
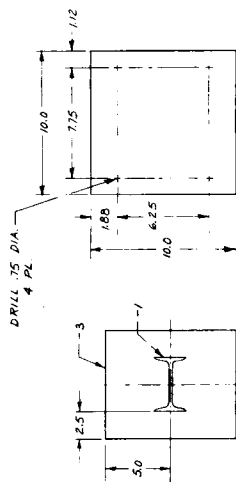
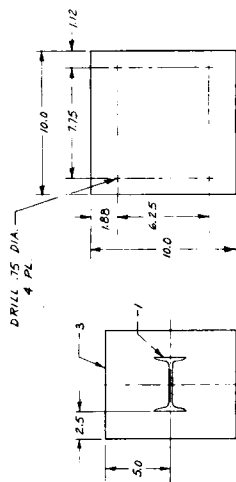
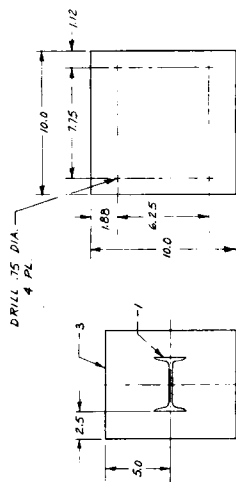
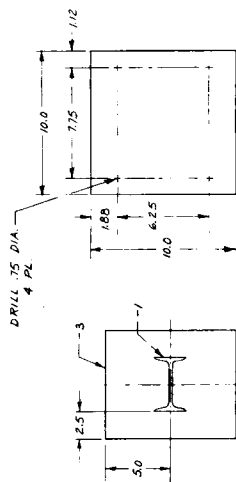
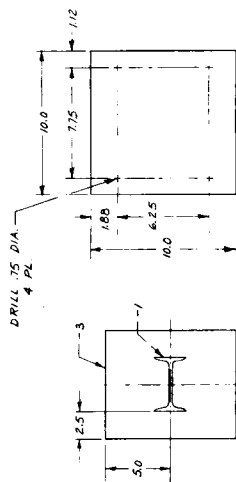
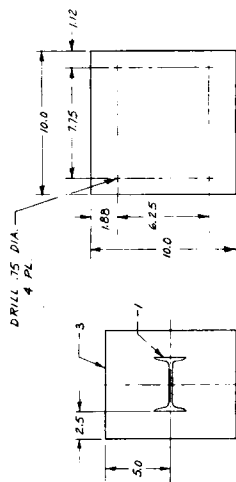
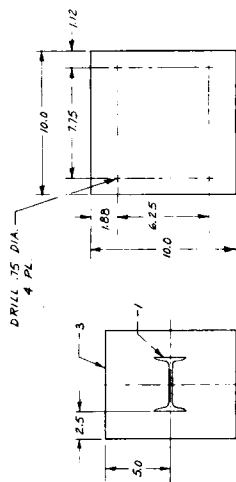
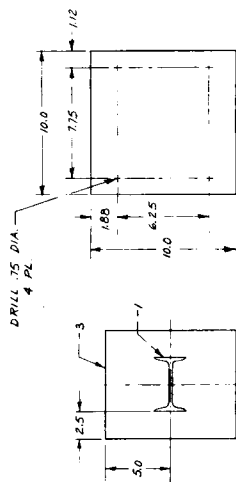
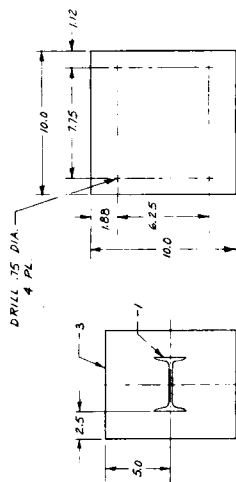
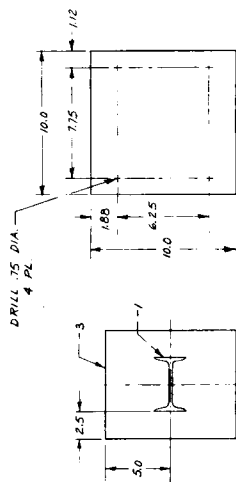
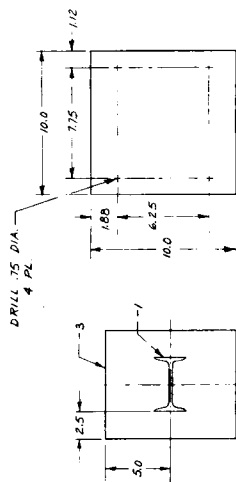
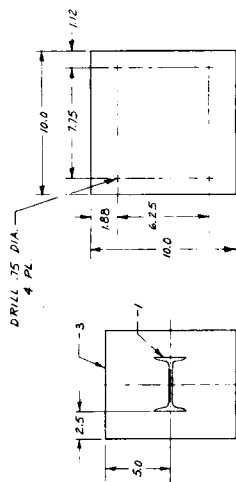
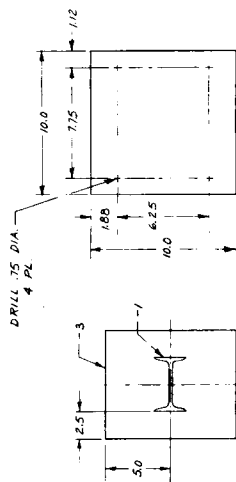
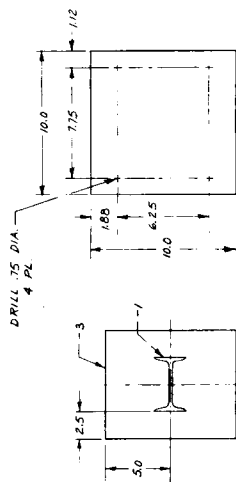
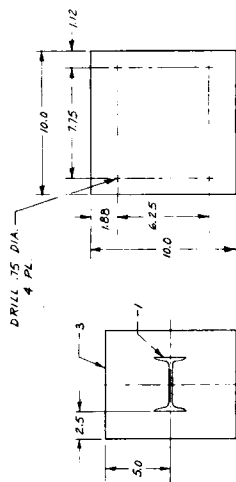
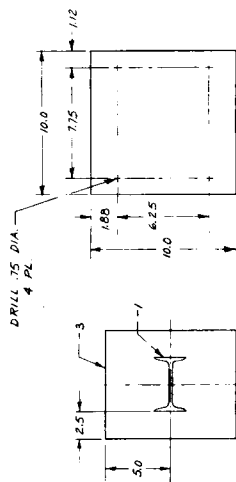
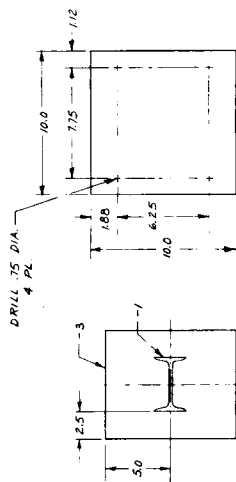
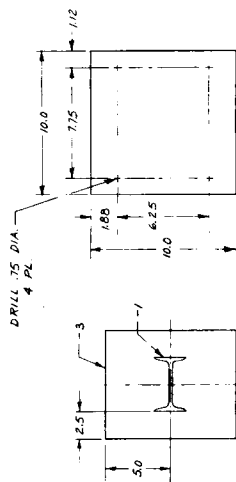
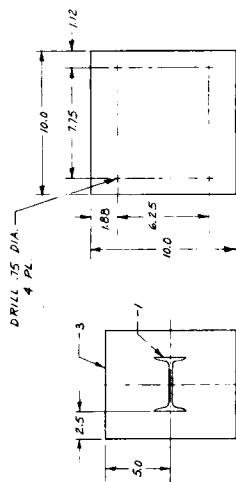
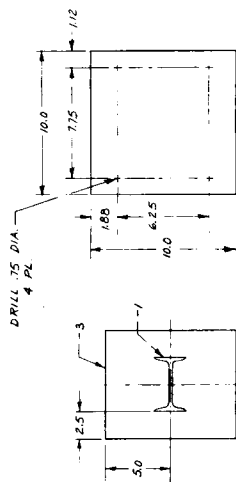
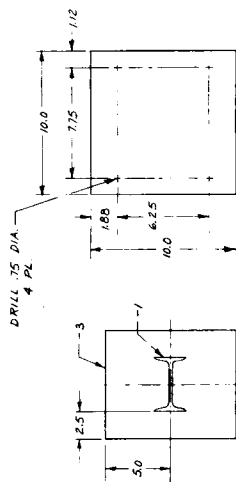
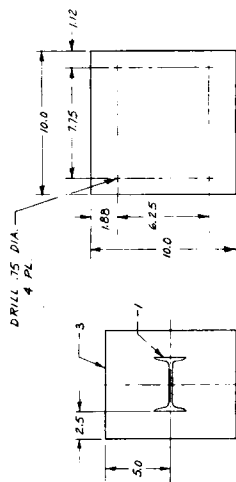
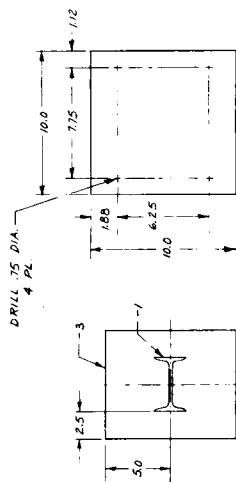
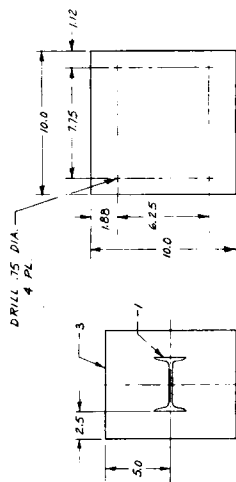
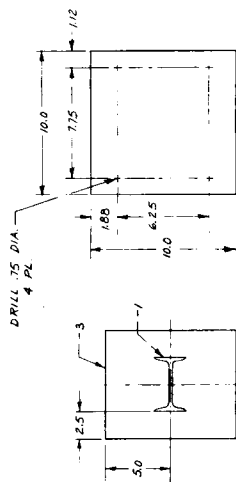
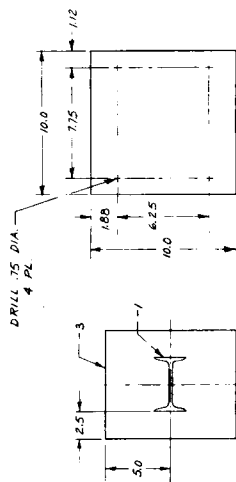
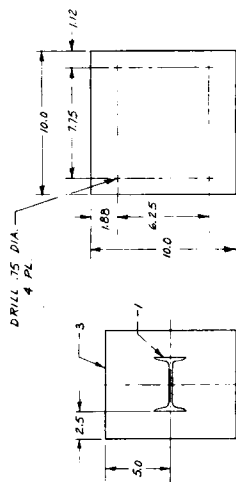
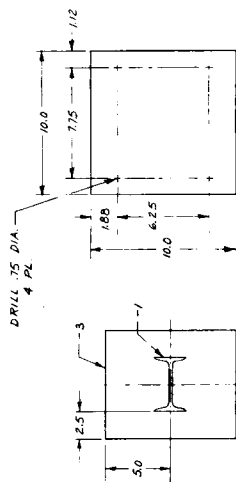
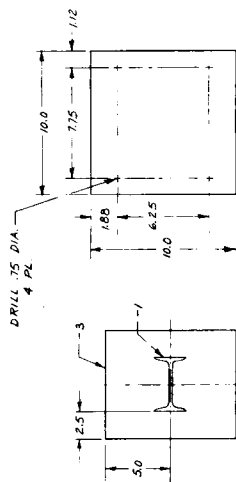
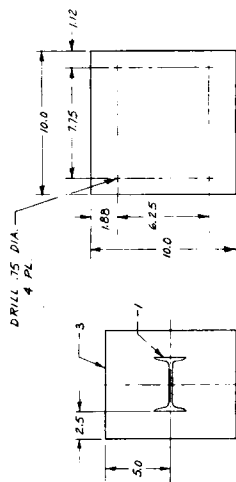
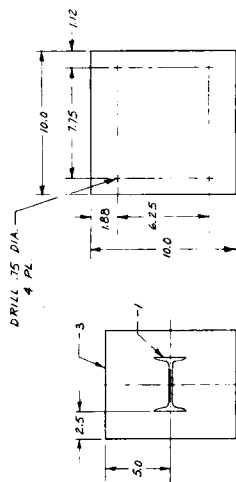
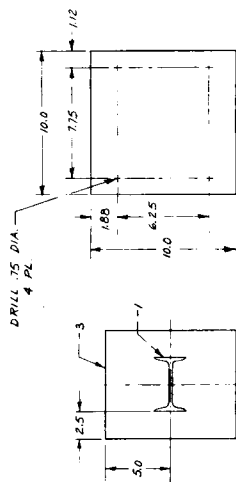
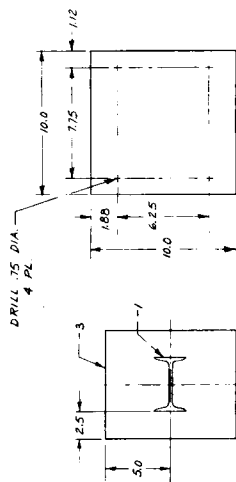
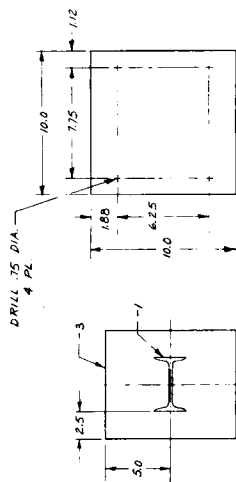
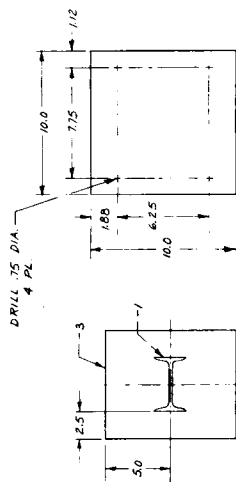
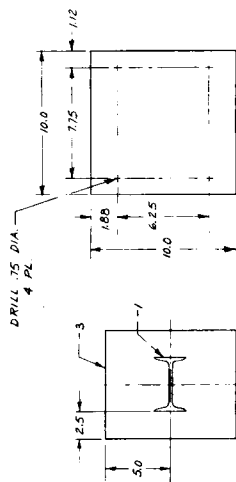
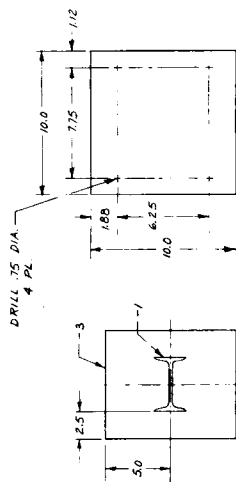
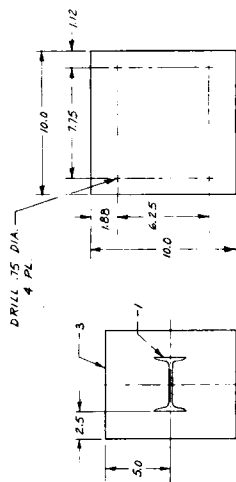
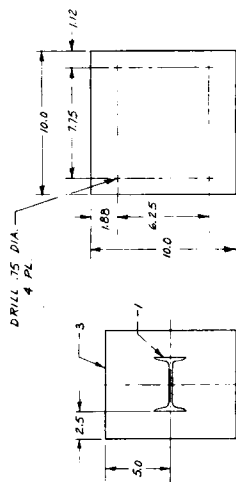
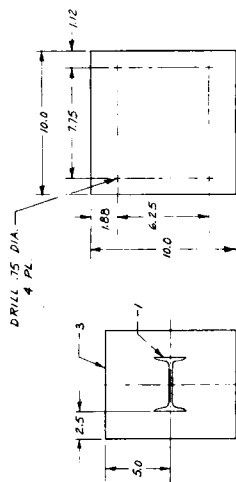
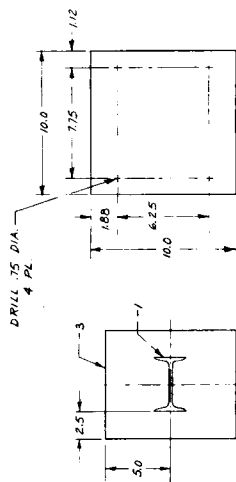
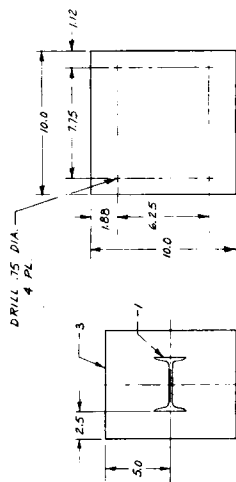
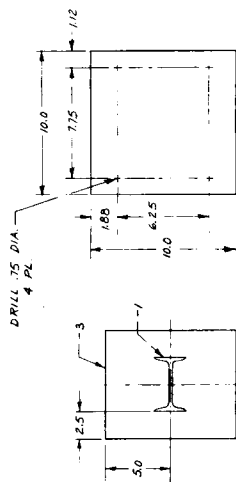
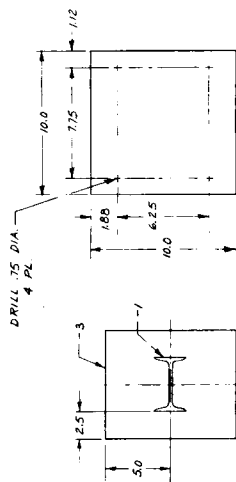
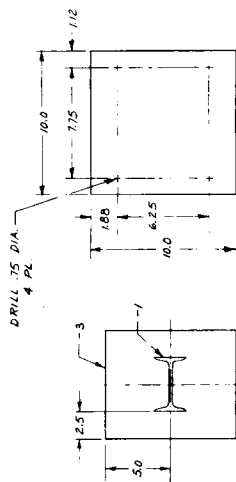
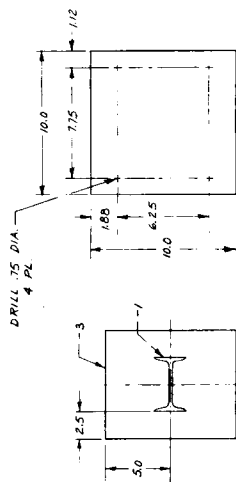
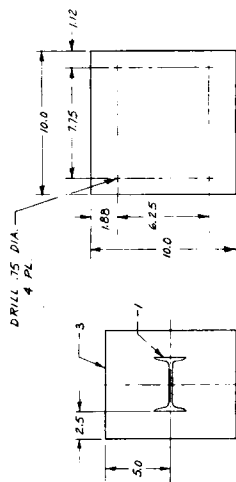
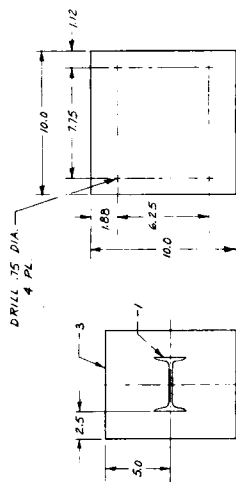
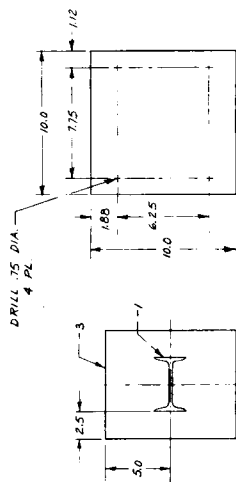
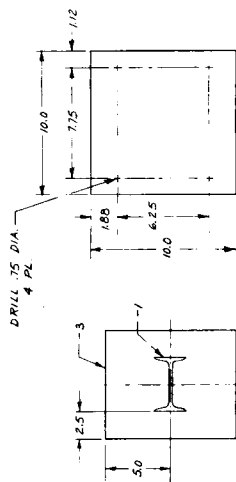
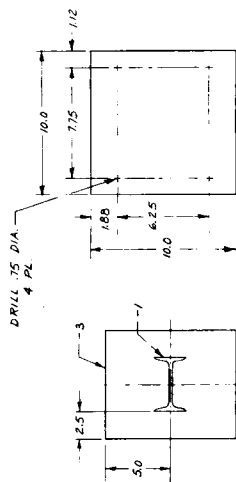
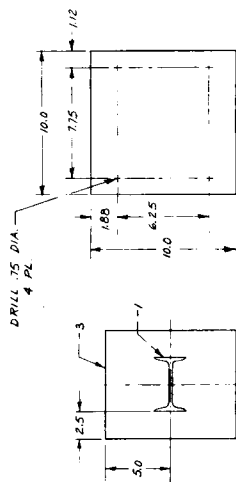
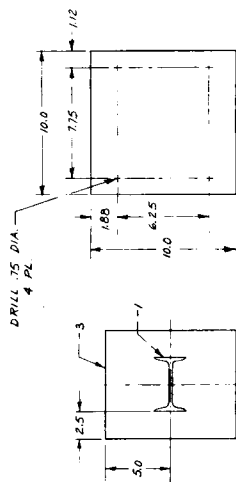
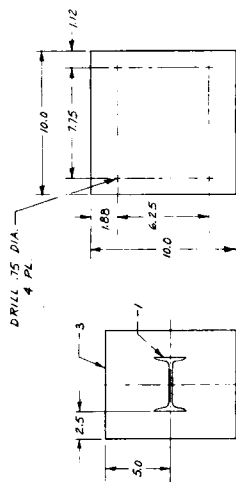
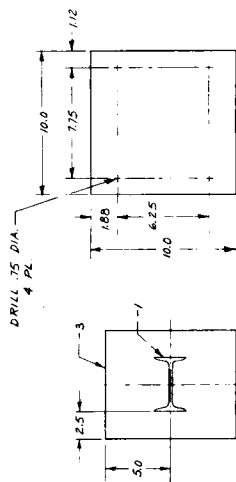
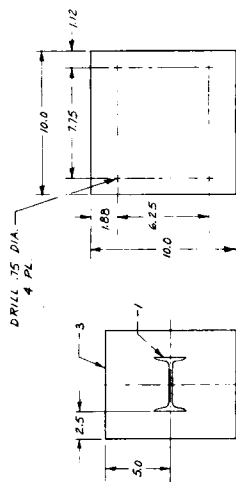
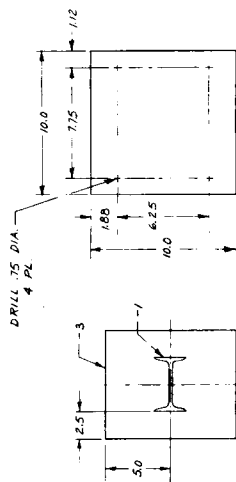
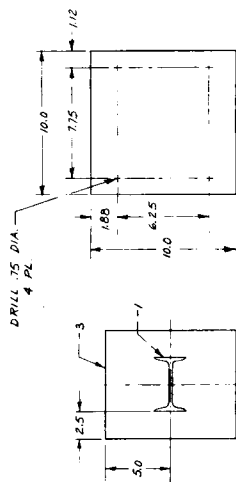
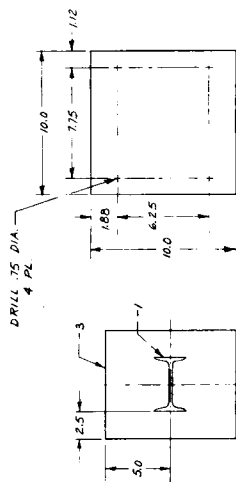
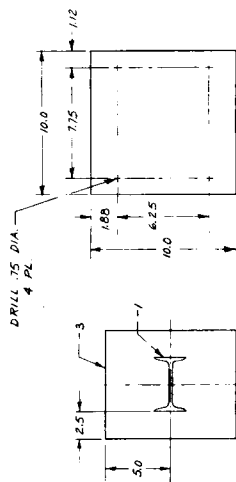
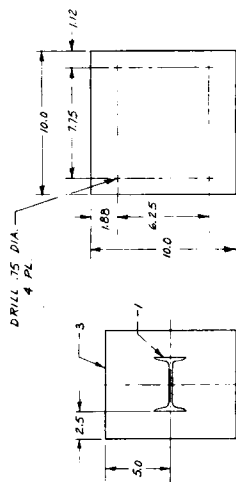
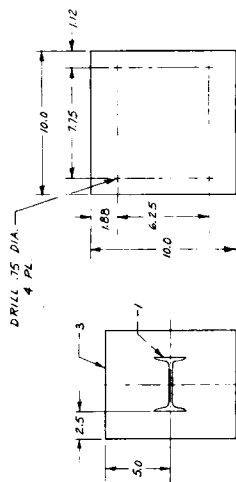
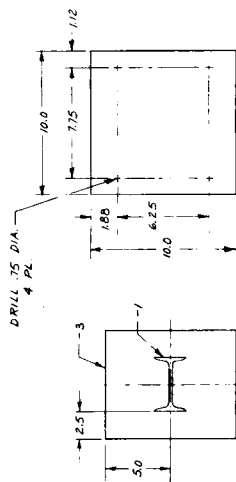
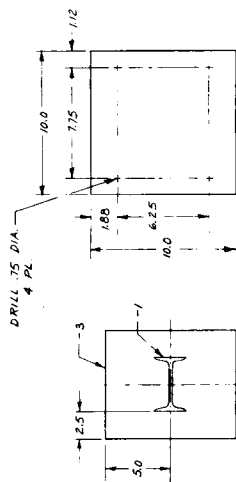
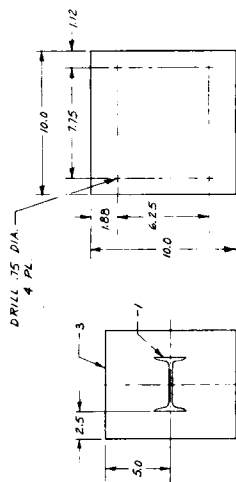
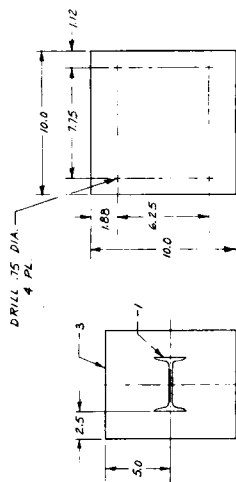
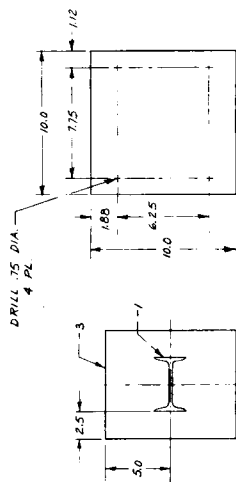
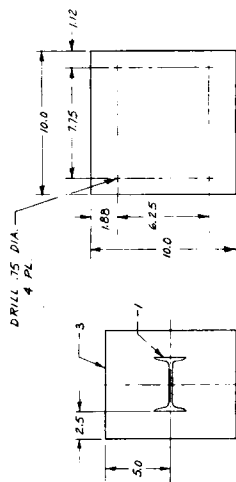
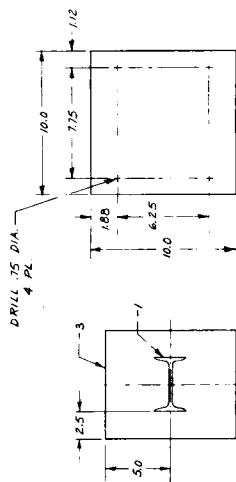
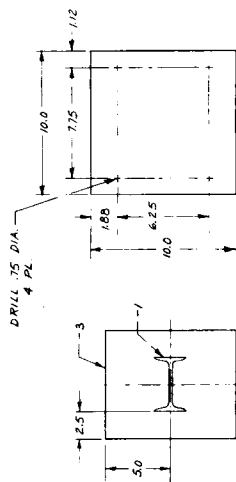
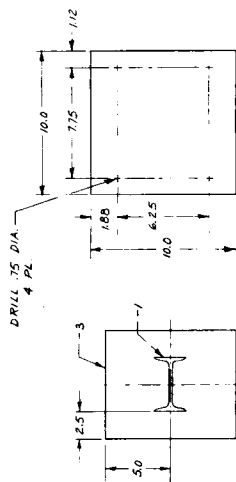
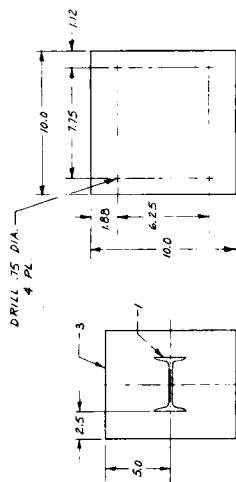
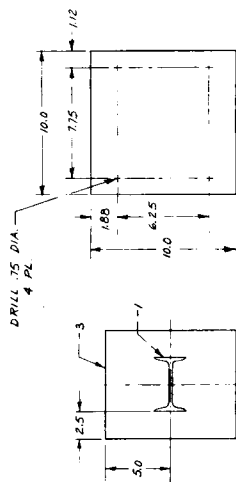
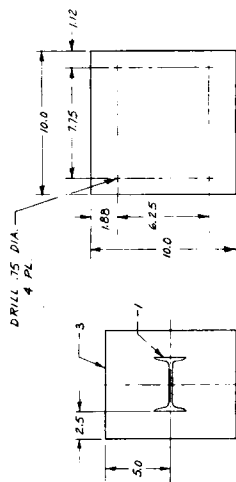
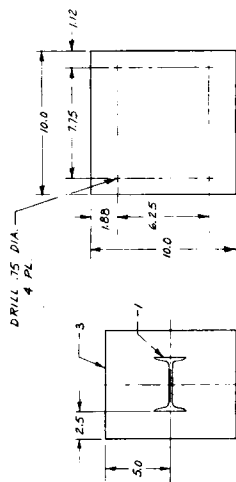
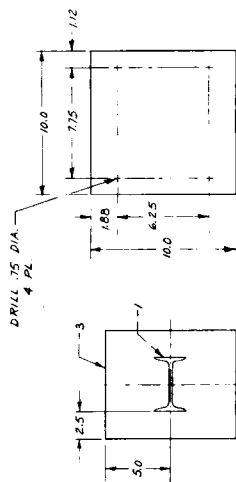
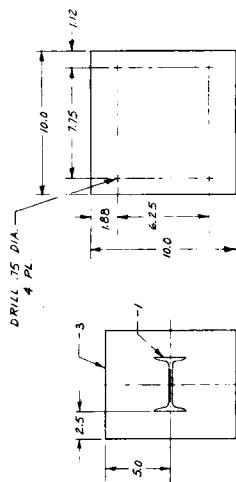
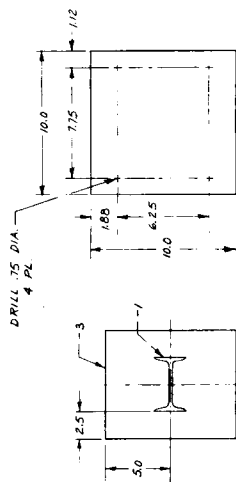
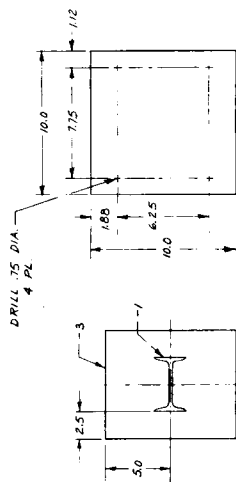
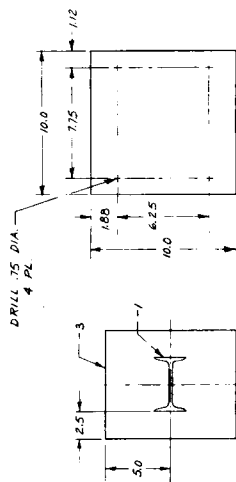
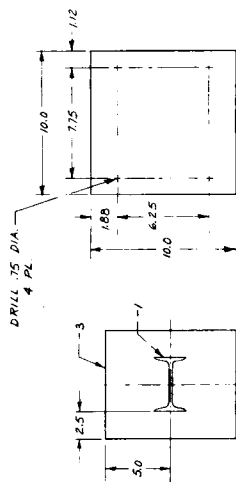
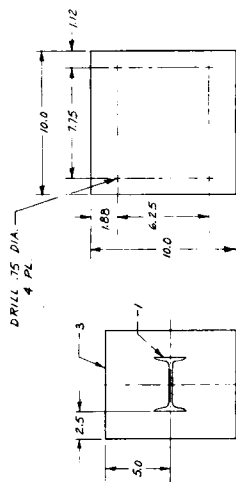
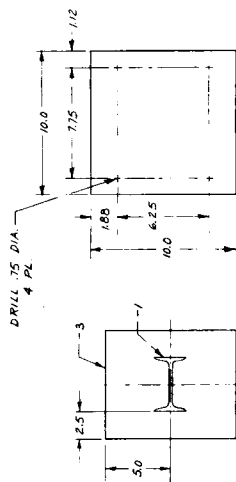
-3 DETAIL
SCALE: 3/4" = 1"

SEC. A-A
SCALE: 3/4" = 1"



-4 DETAIL
SCALE: 3/4" = 1"

SEC. B-B
SCALE: 3/4" = 1"



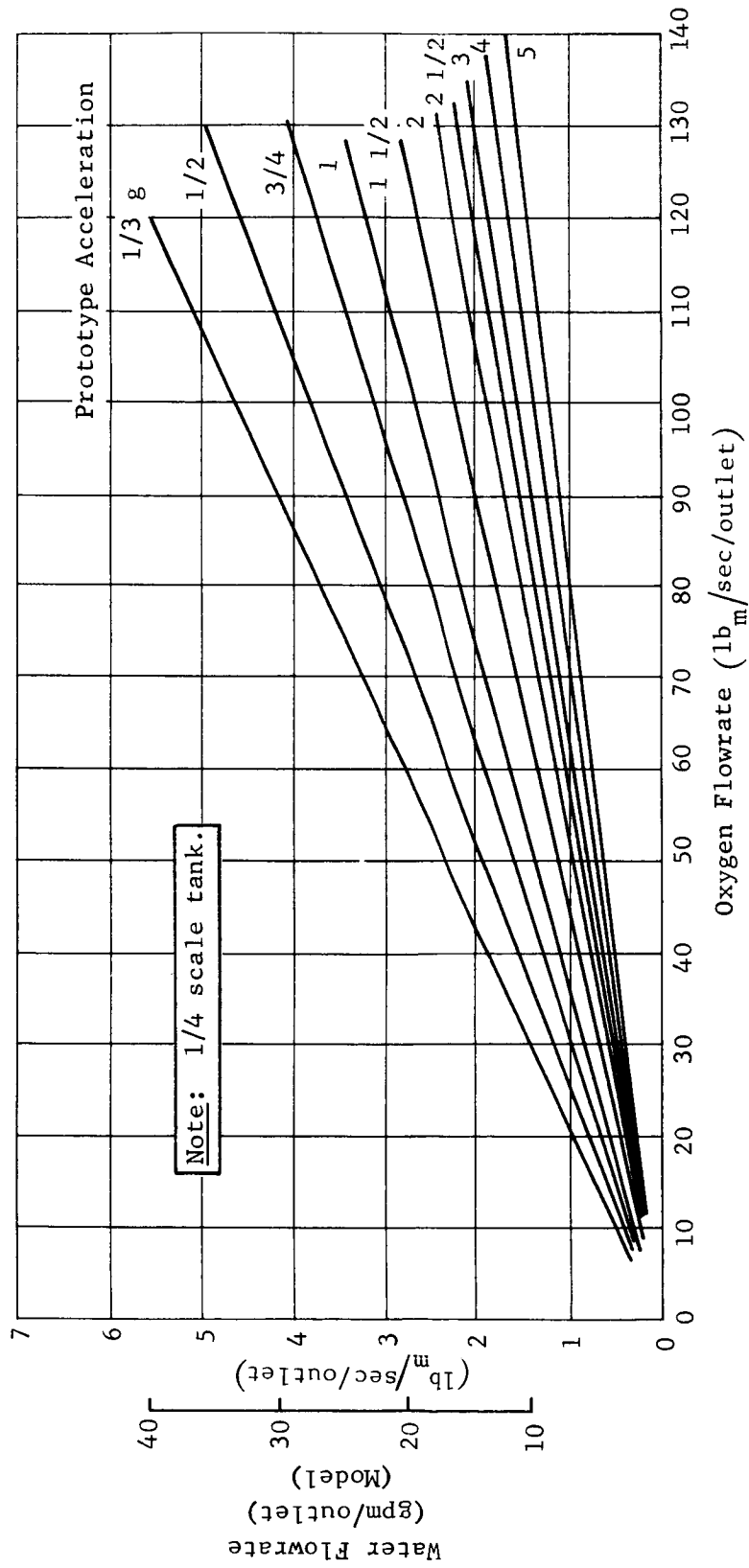


Fig. 3 Simulation Parameters, Toroidal Tank, Oxygen

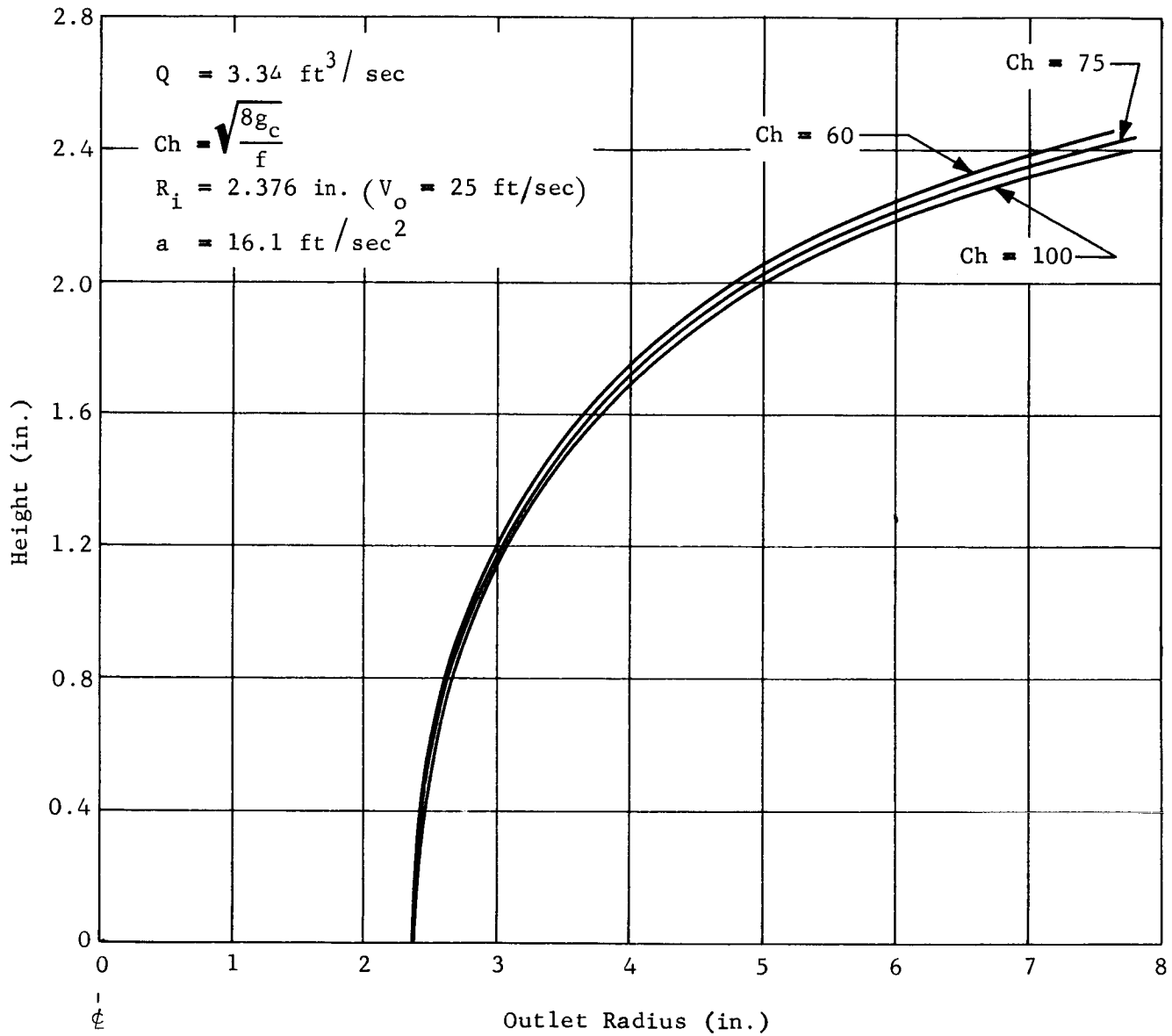


Fig. 4 Influence of Friction on Nondropout Outlet Contour, Hydrogen

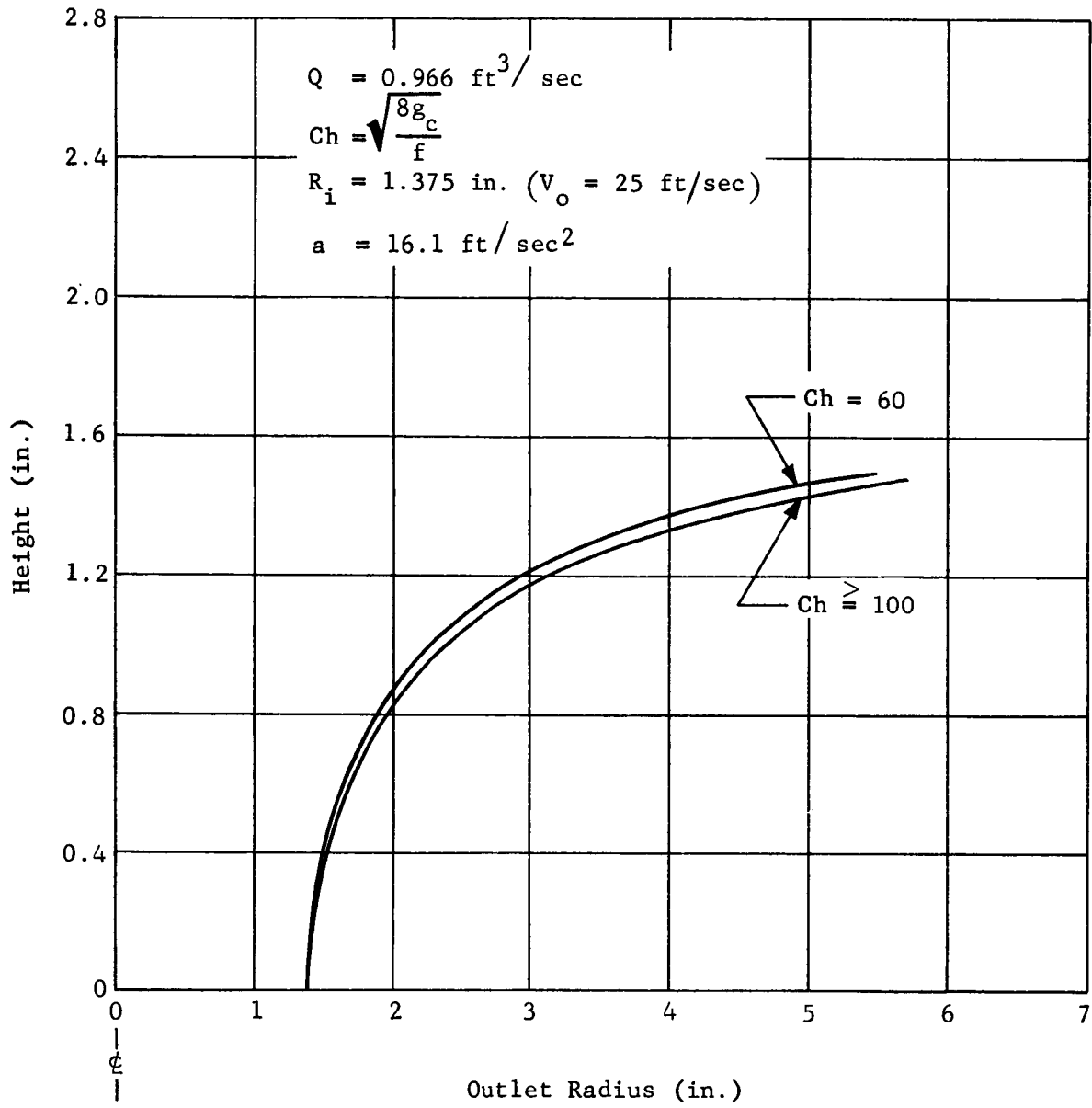


Fig. 5 Influence of Friction on Nondropout Outlet Contour, Oxygen

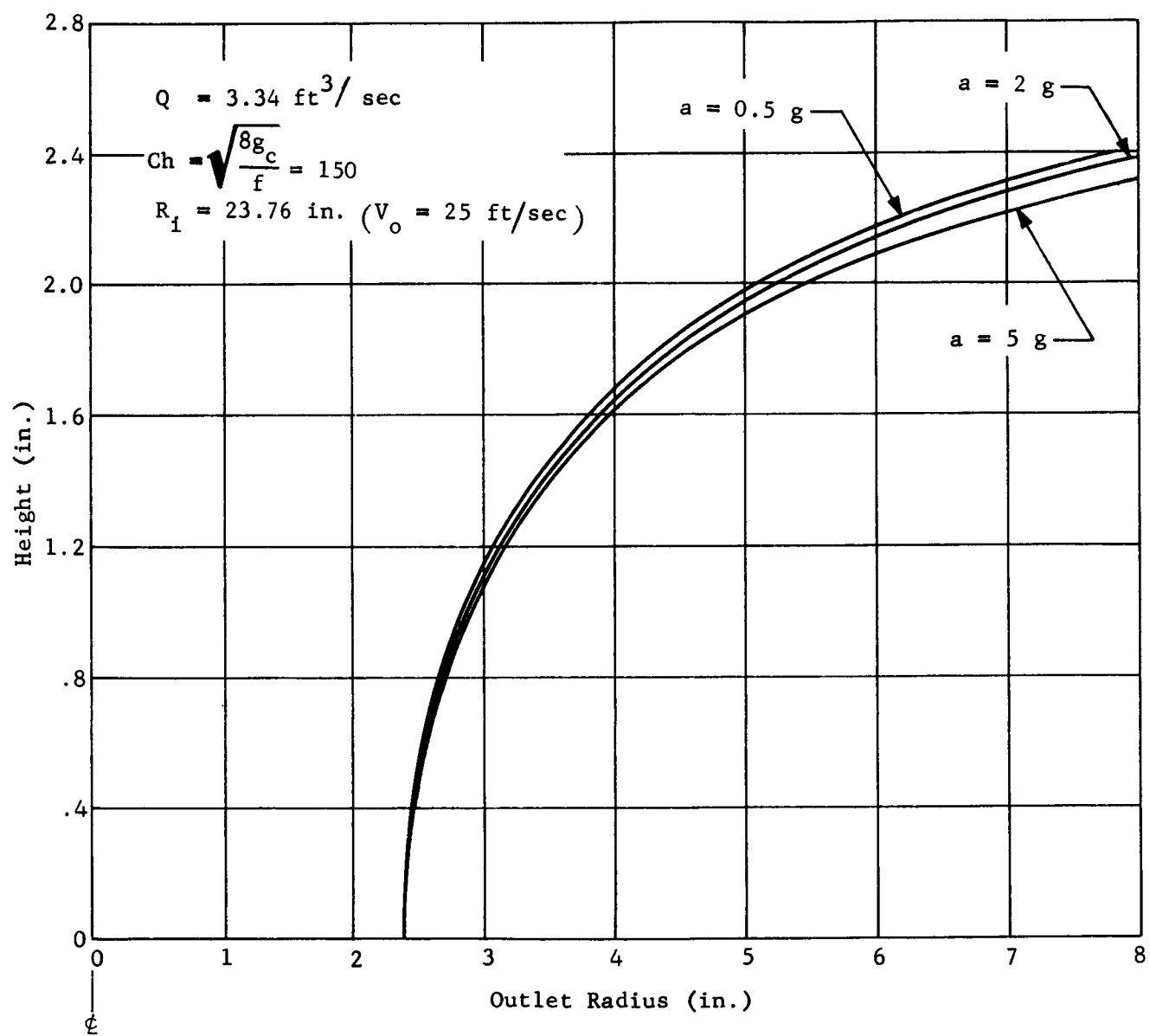


Fig. 6 Influence of Acceleration on Nondropout Outlet Contour, Hydrogen

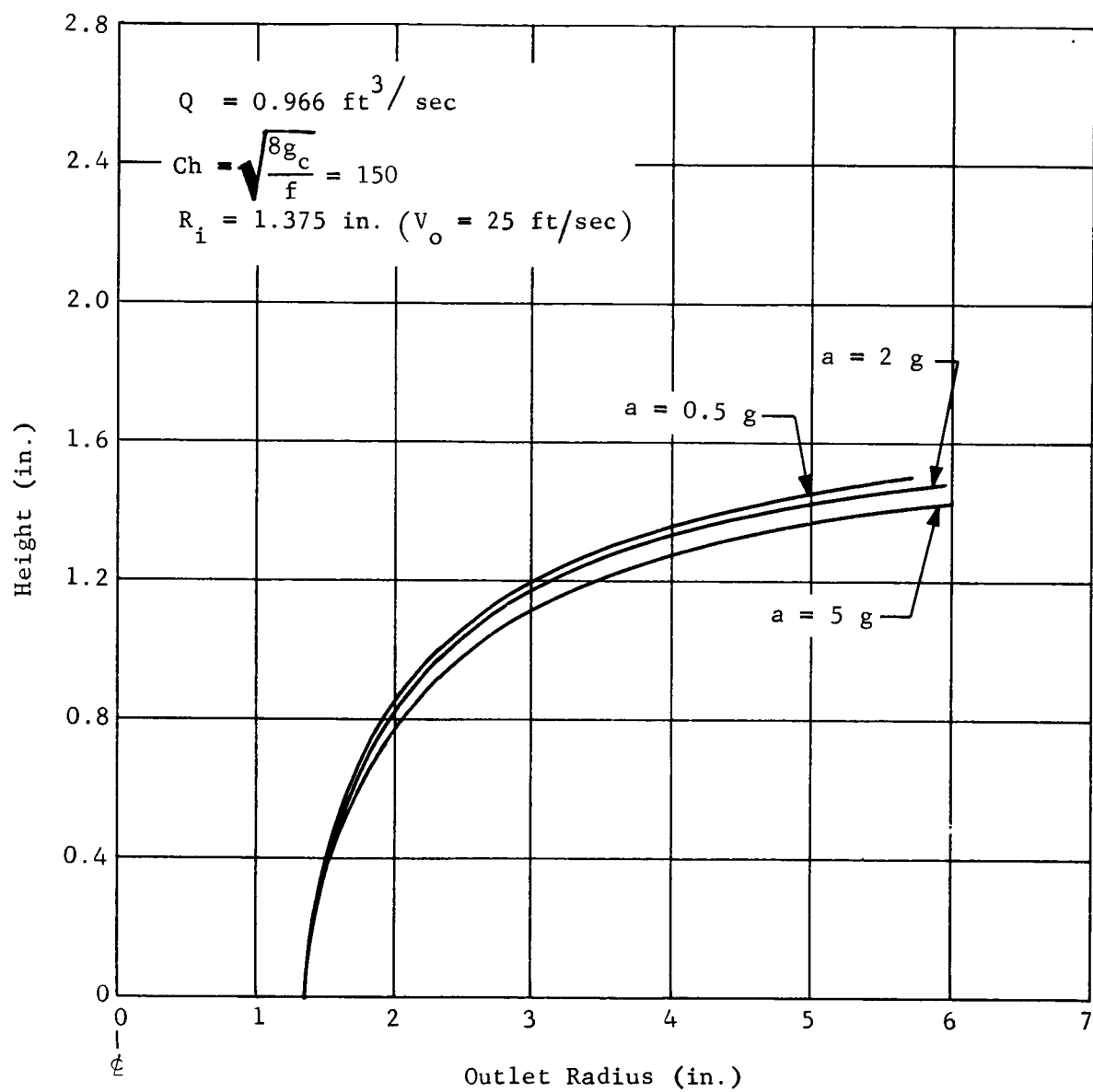


Fig. 7 Influence of Acceleration on Nondropout Outlet Contour, Oxygen

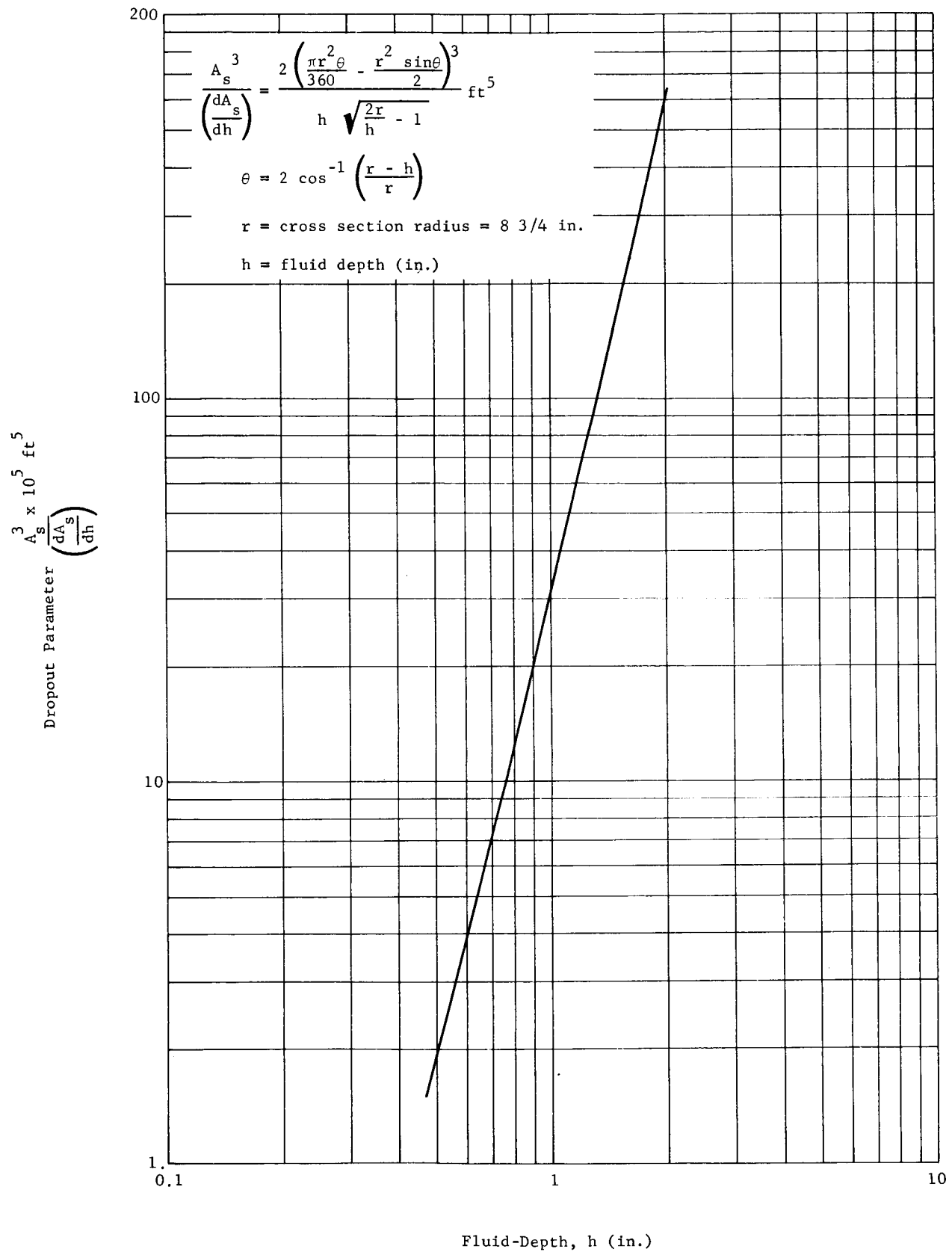


Fig. 8 Dropout Parameter, Toroidal Tank, Nonsump Bottom

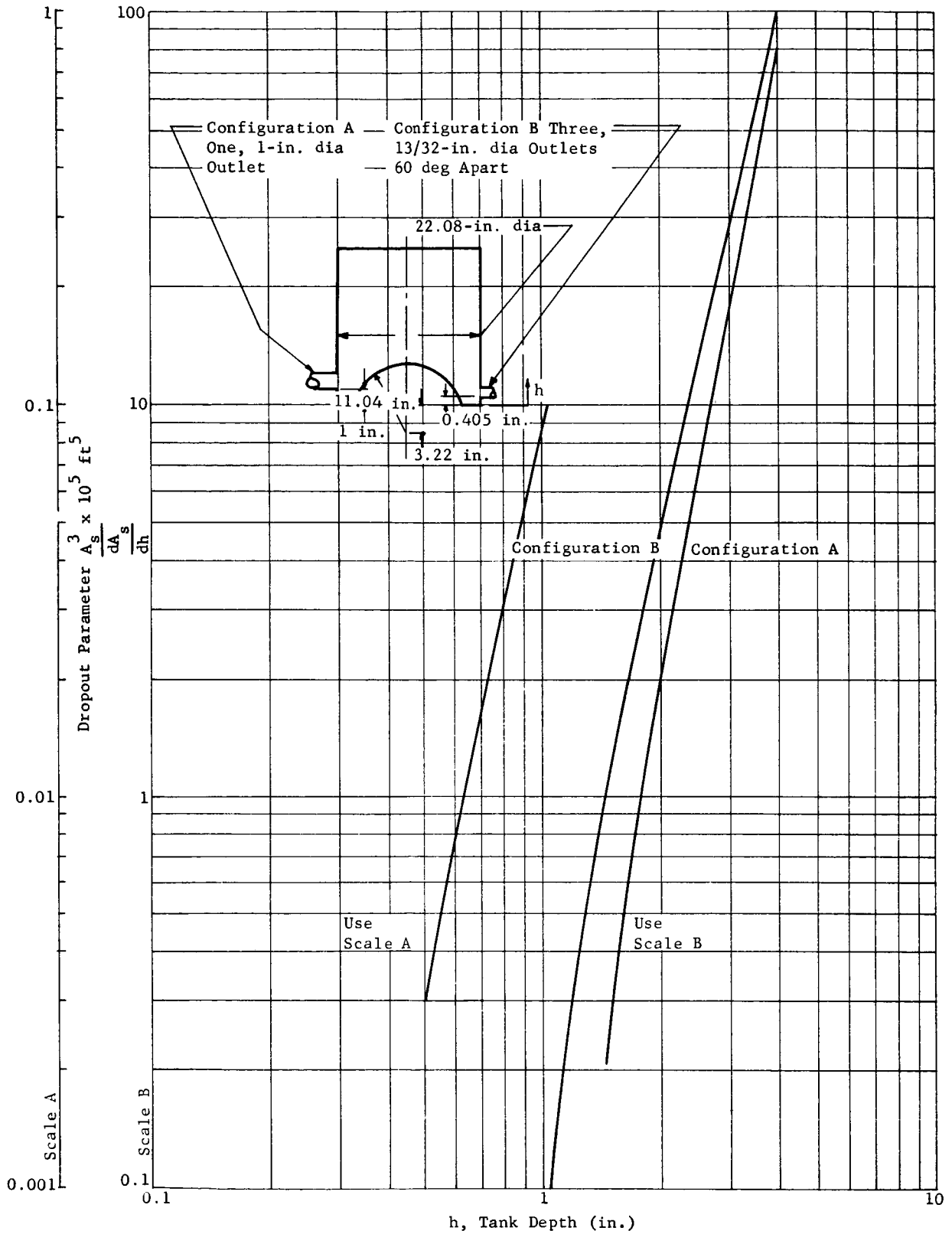


Fig. 9 Dropout Parameter, Cylindrical Tank with Concave Lower Dome and Side Outlets

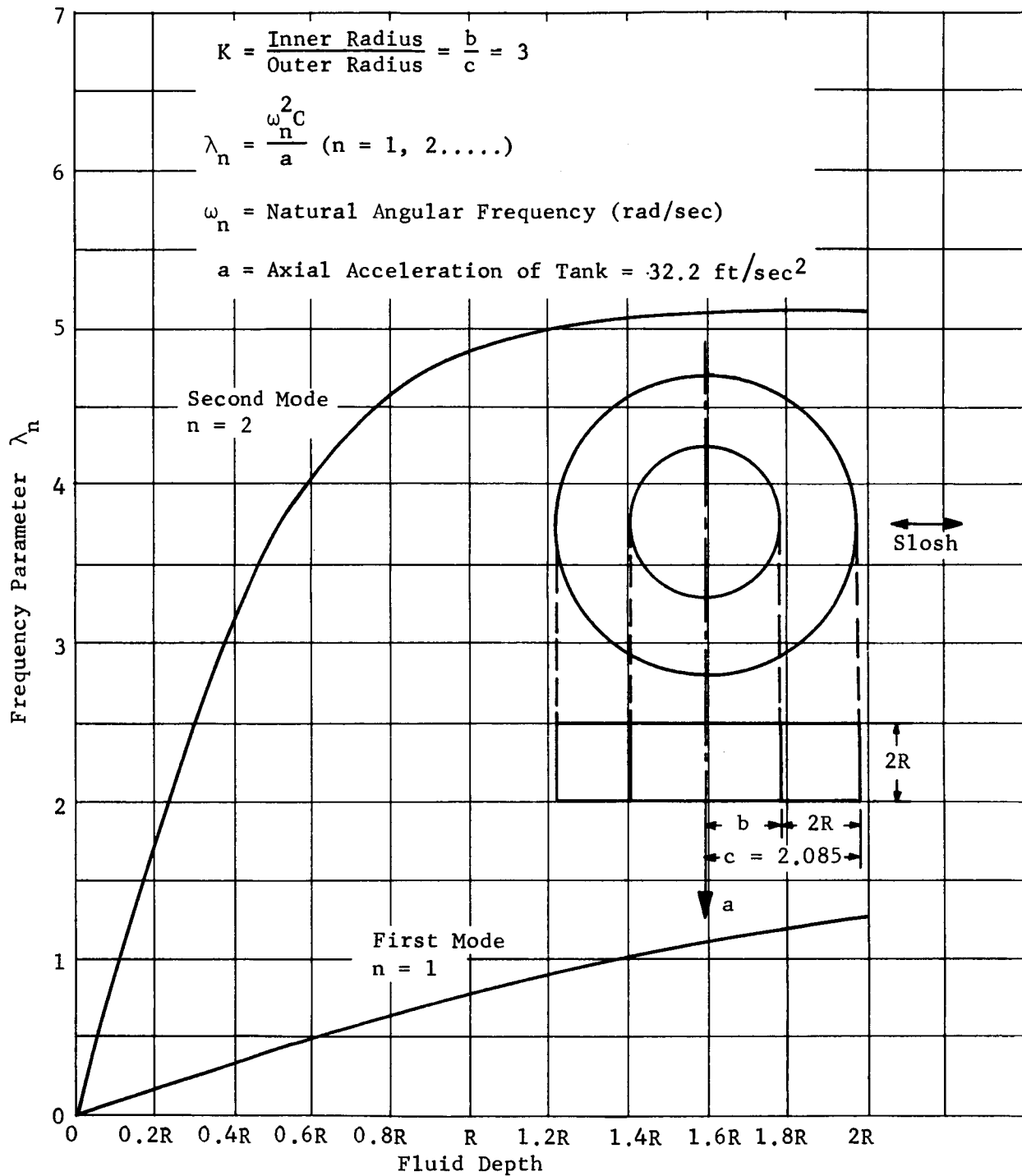


Fig. 10 Toroidal Tank Sloshing Natural Frequency, Cylindrical Ring Tank

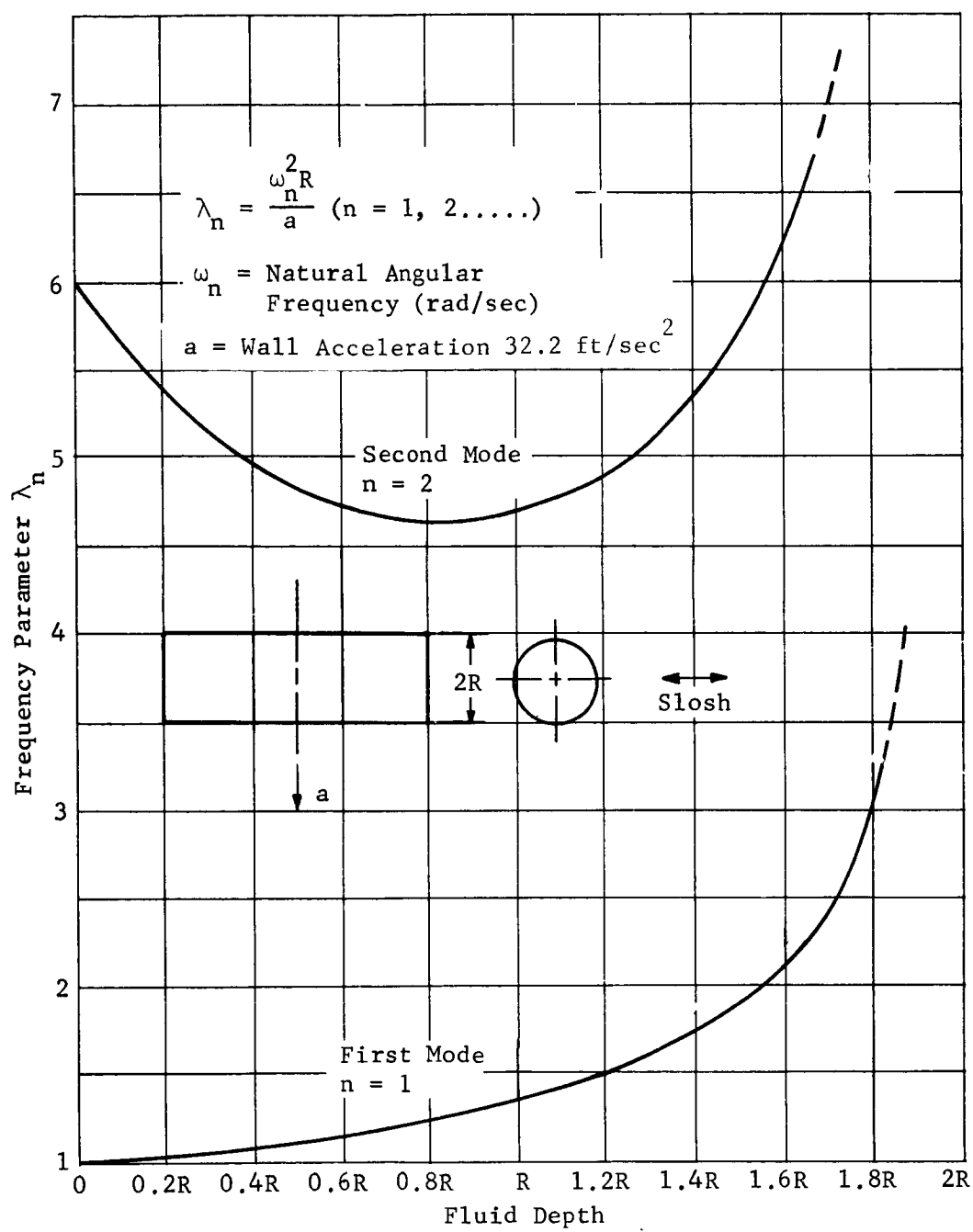


Fig. 11 Toroidal Tank Sloshing Natural Frequency, Circular Canal

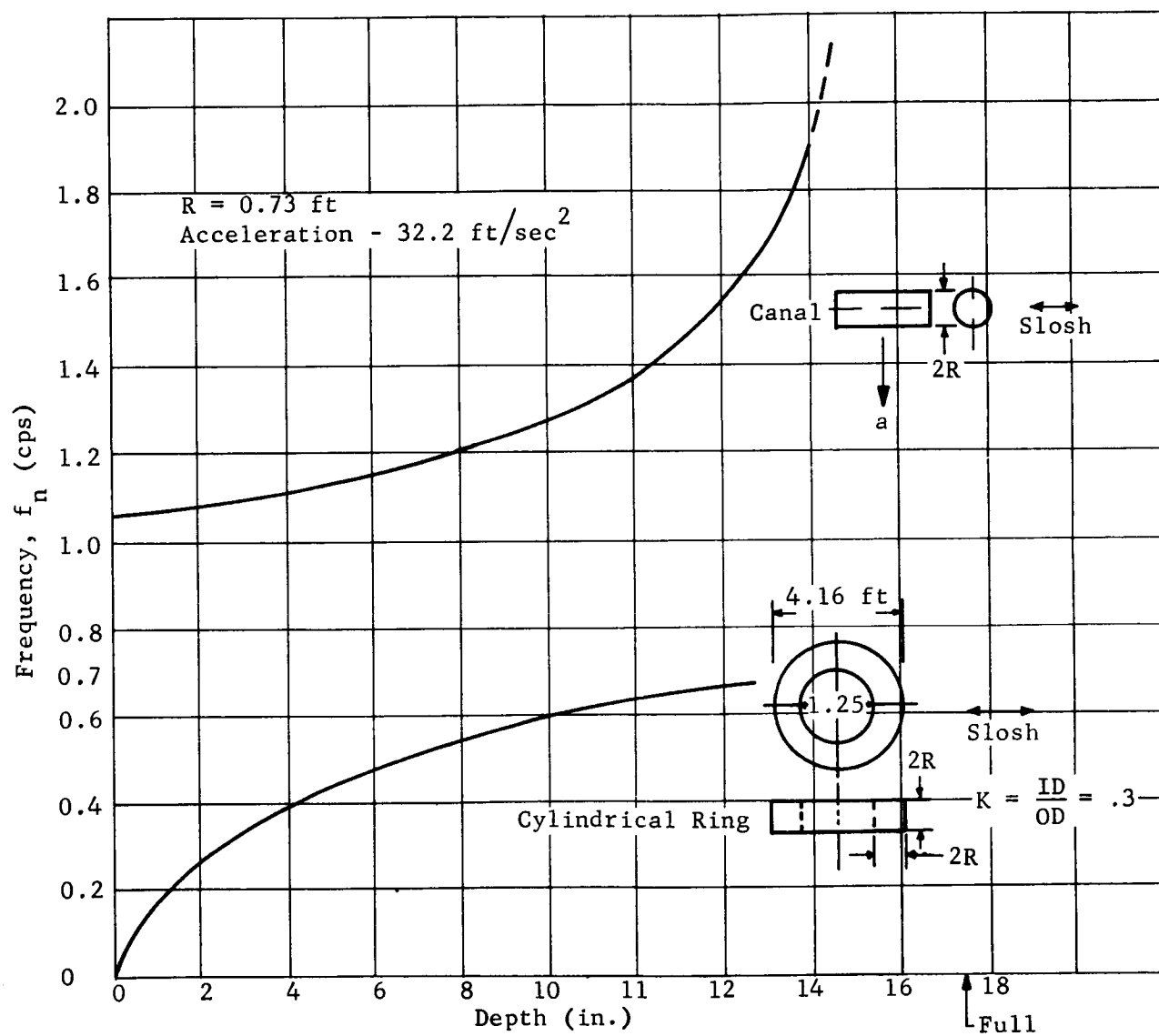


Fig. 12 Predicted Dominant Modes, Toroidal Model Tank

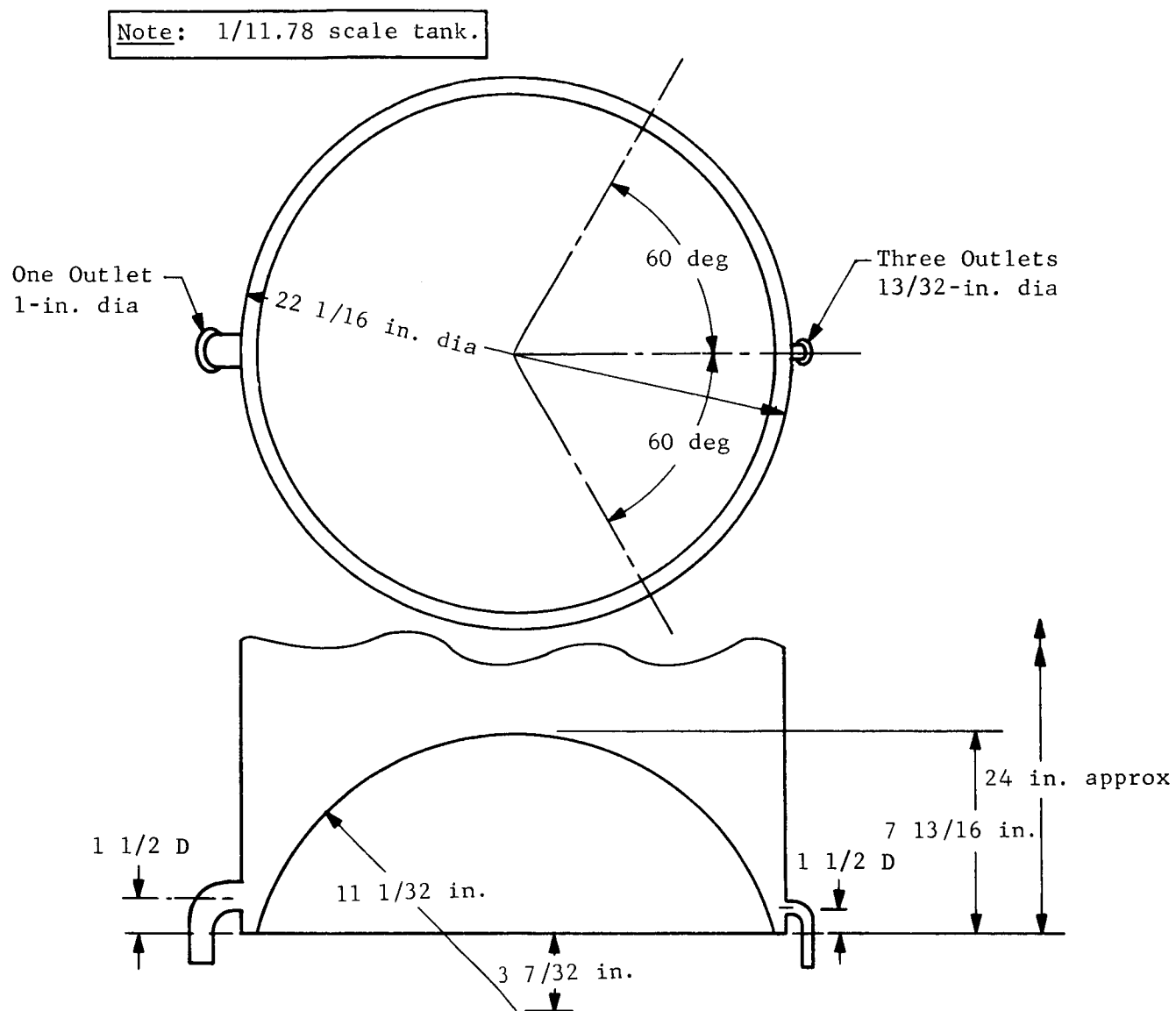


Fig. 13 Model Cylindrical Tank, Concave Lower Dome

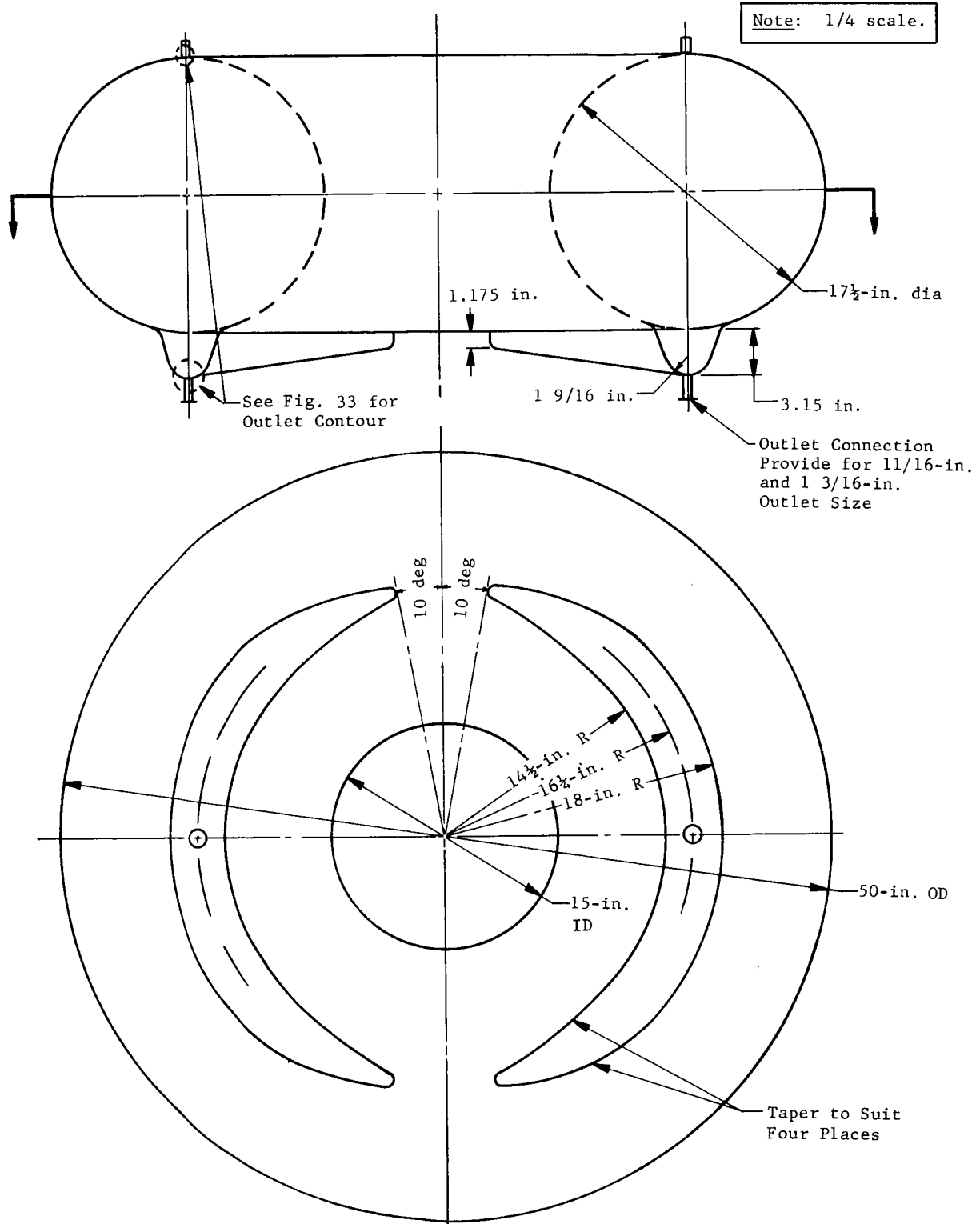


Fig. 14 Model Toroidal Tank

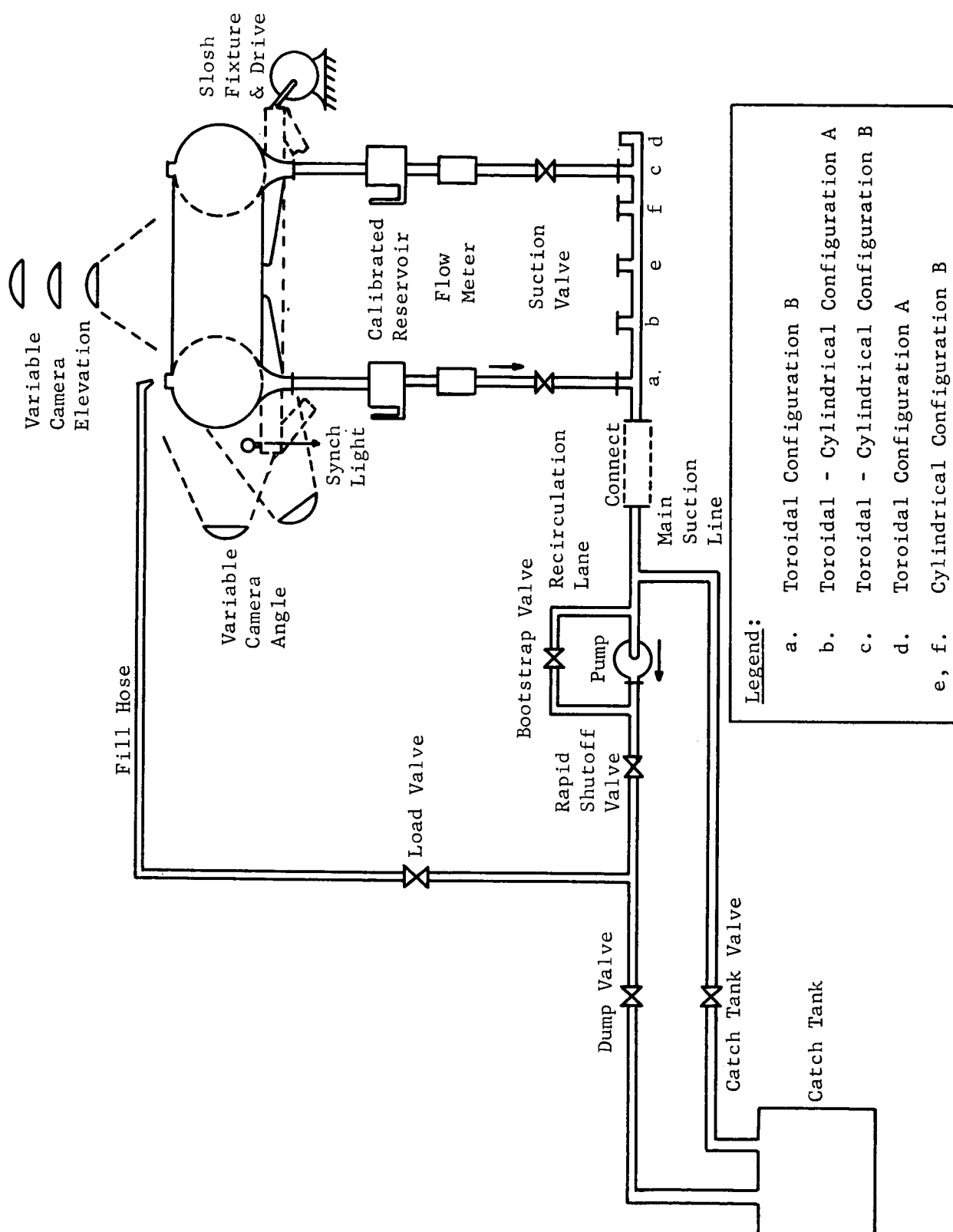


Fig. 15 Test System Schematic

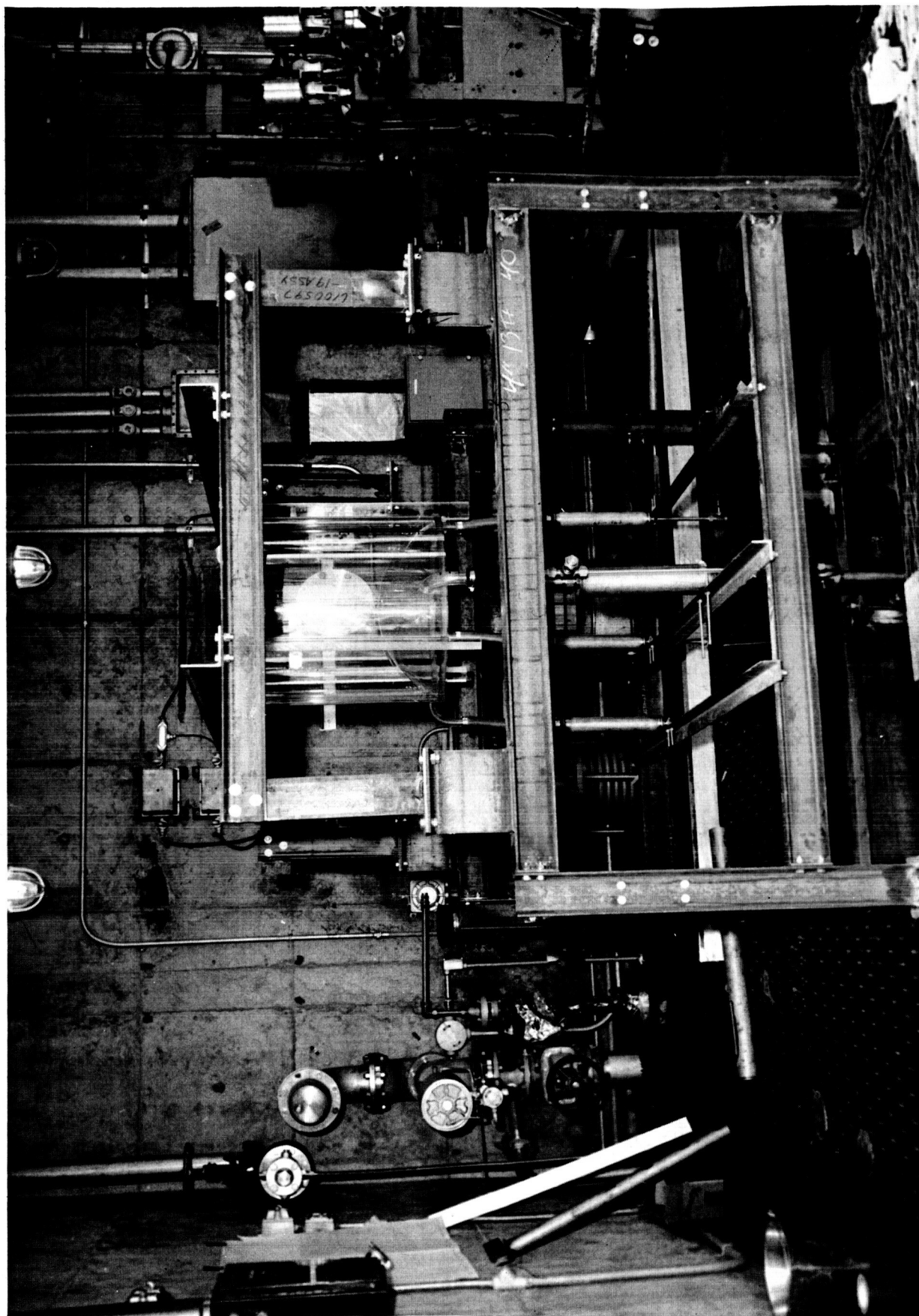


Fig. 16 Terminal Draining Study Test Setup, Cylindrical Tank Installed

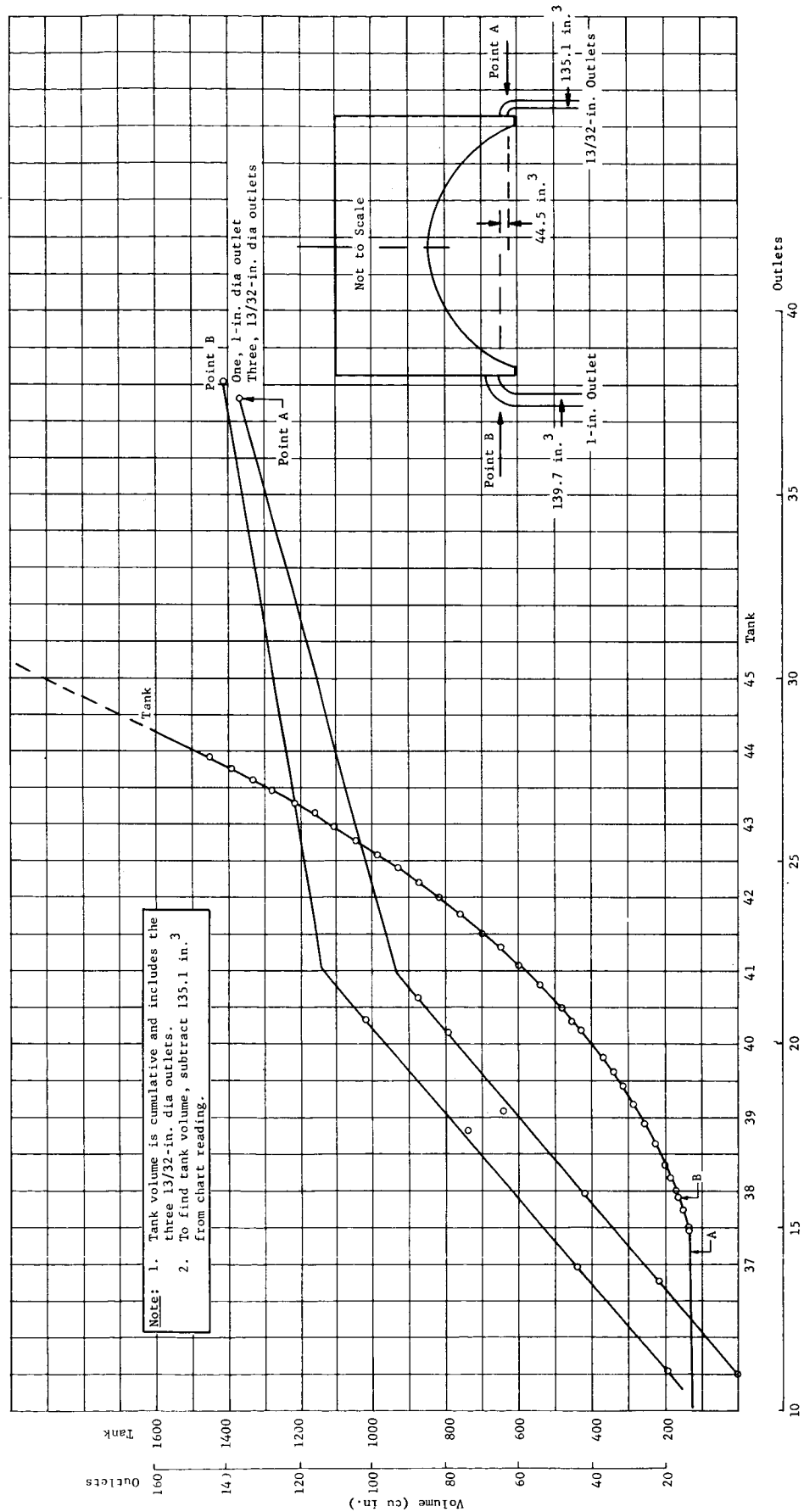


Fig. 17 Calibration Chart, Cylindrical Tank, Concave Lower Dome

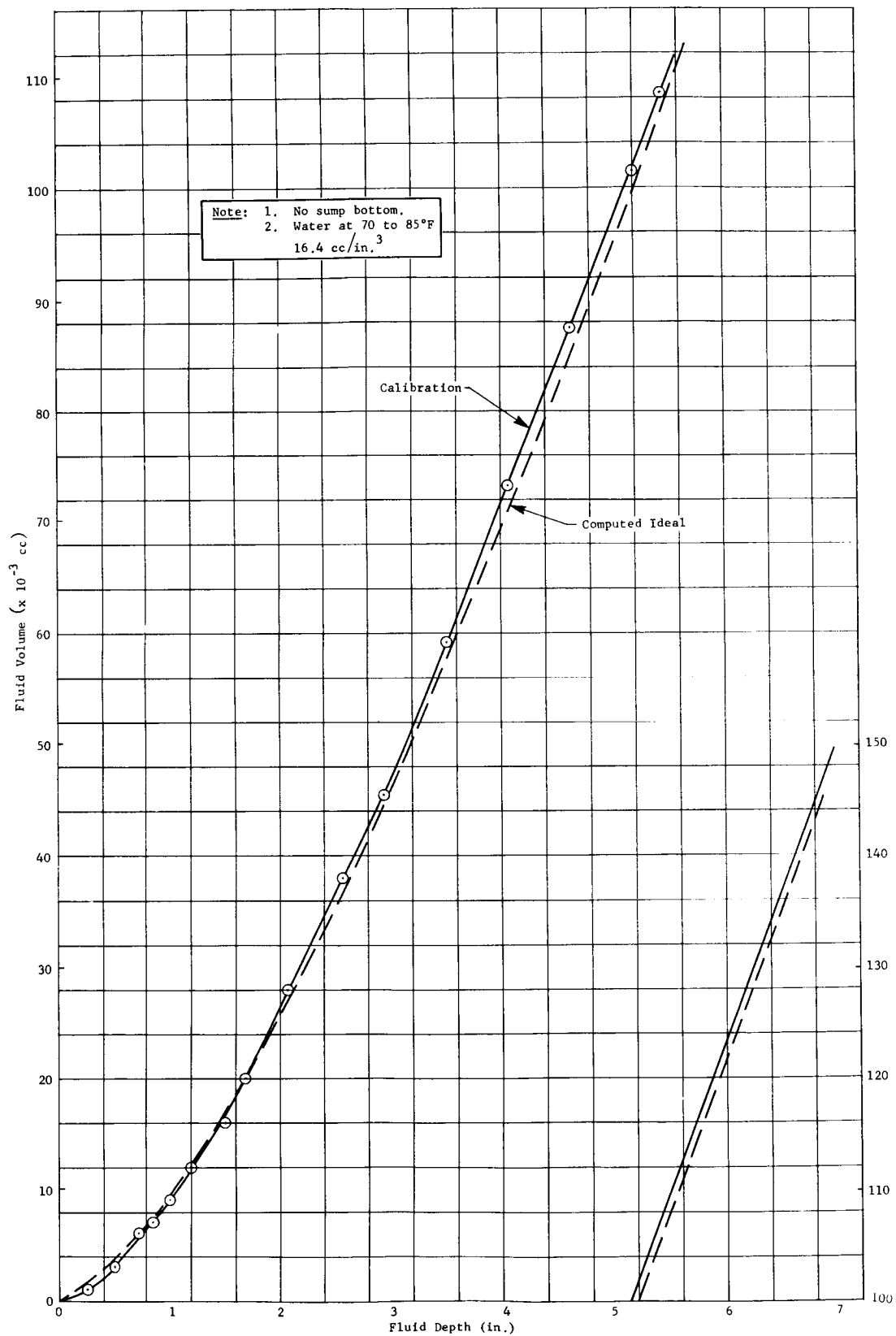


Fig. 18 Calibration Chart, Toroidal Tank

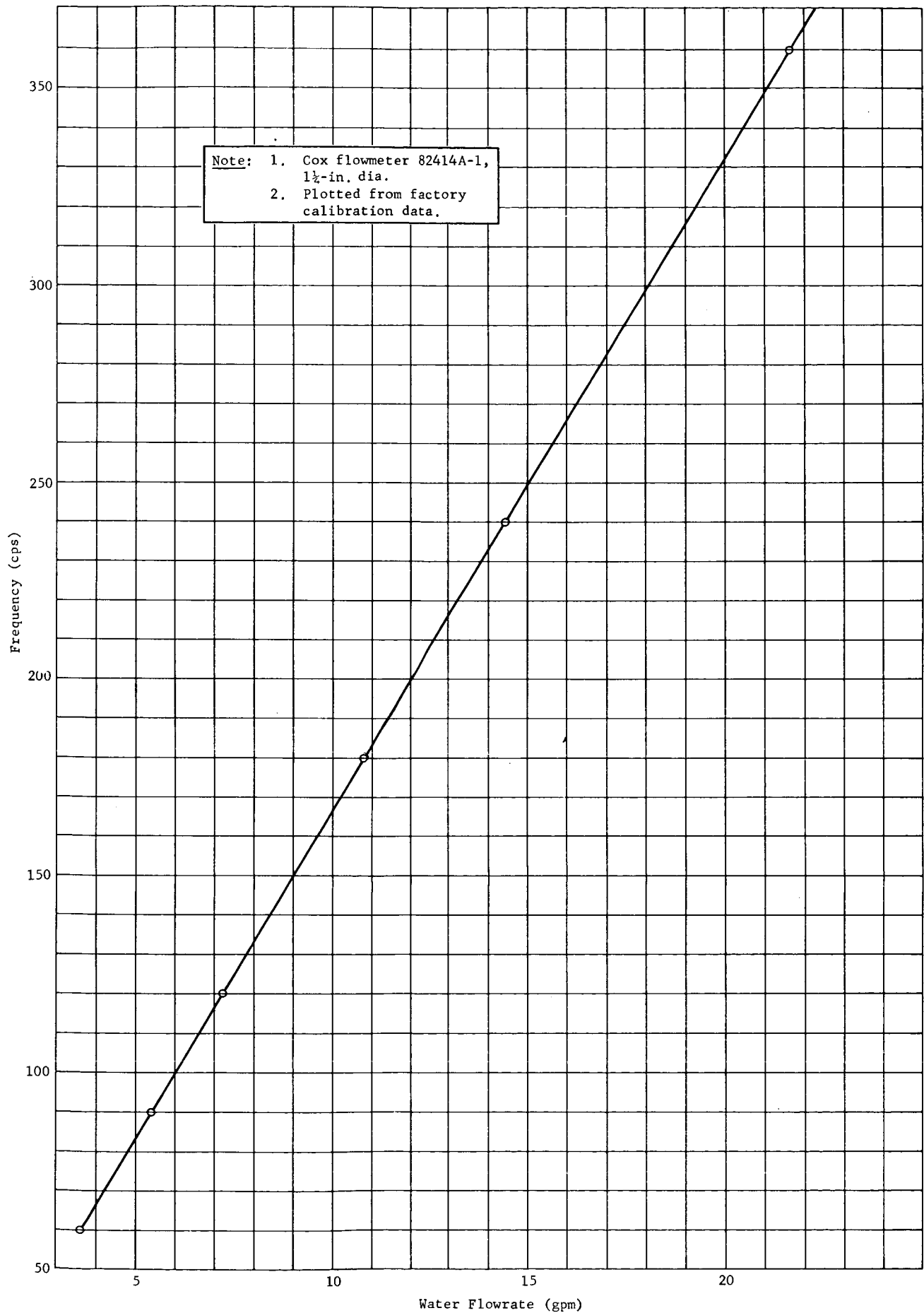


Fig. 19 Calibration Part 1, 1 1/4-in. Flowmeter

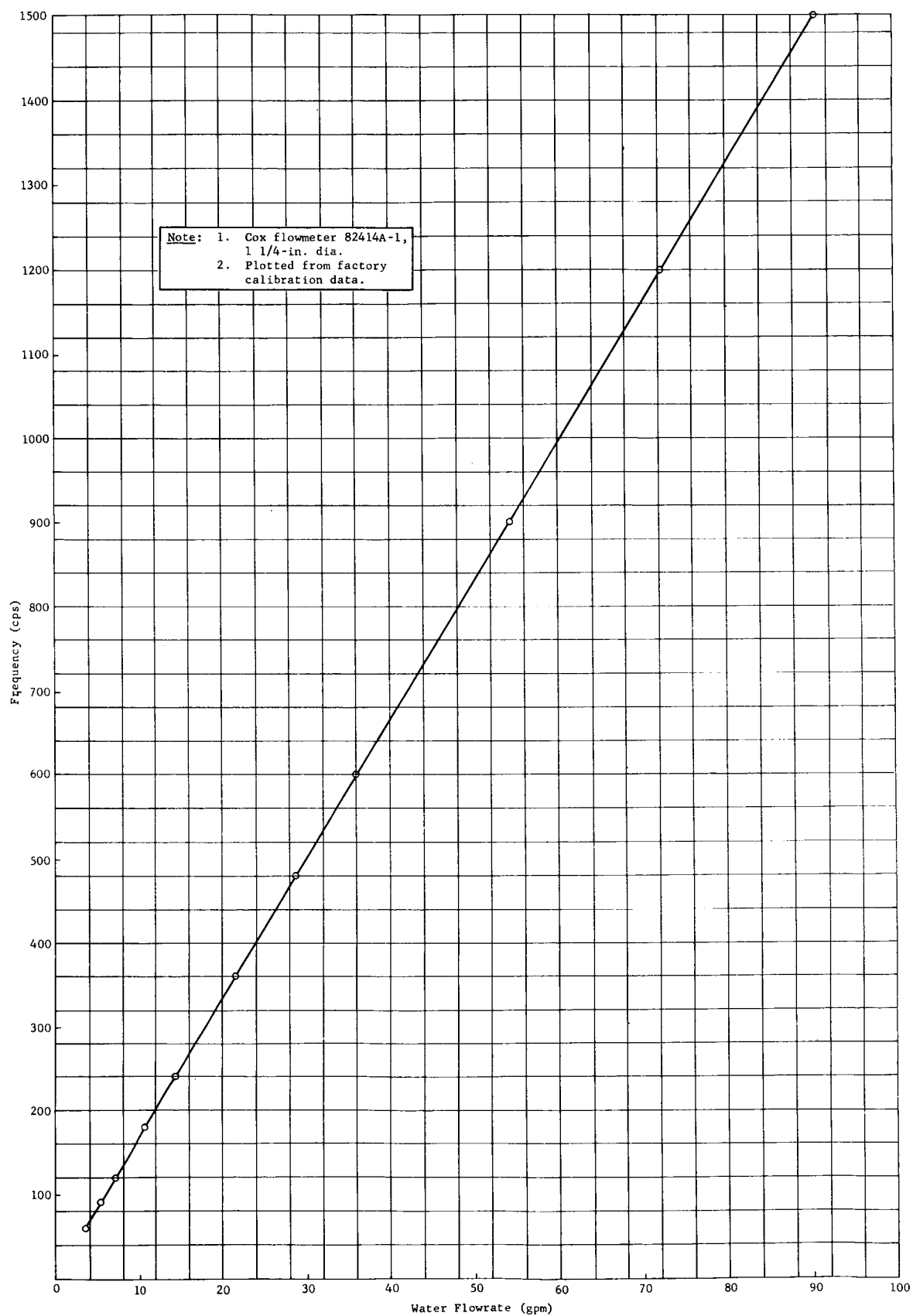


Fig. 20 Calibration Part 2, 1 1/4-in. Flowmeter

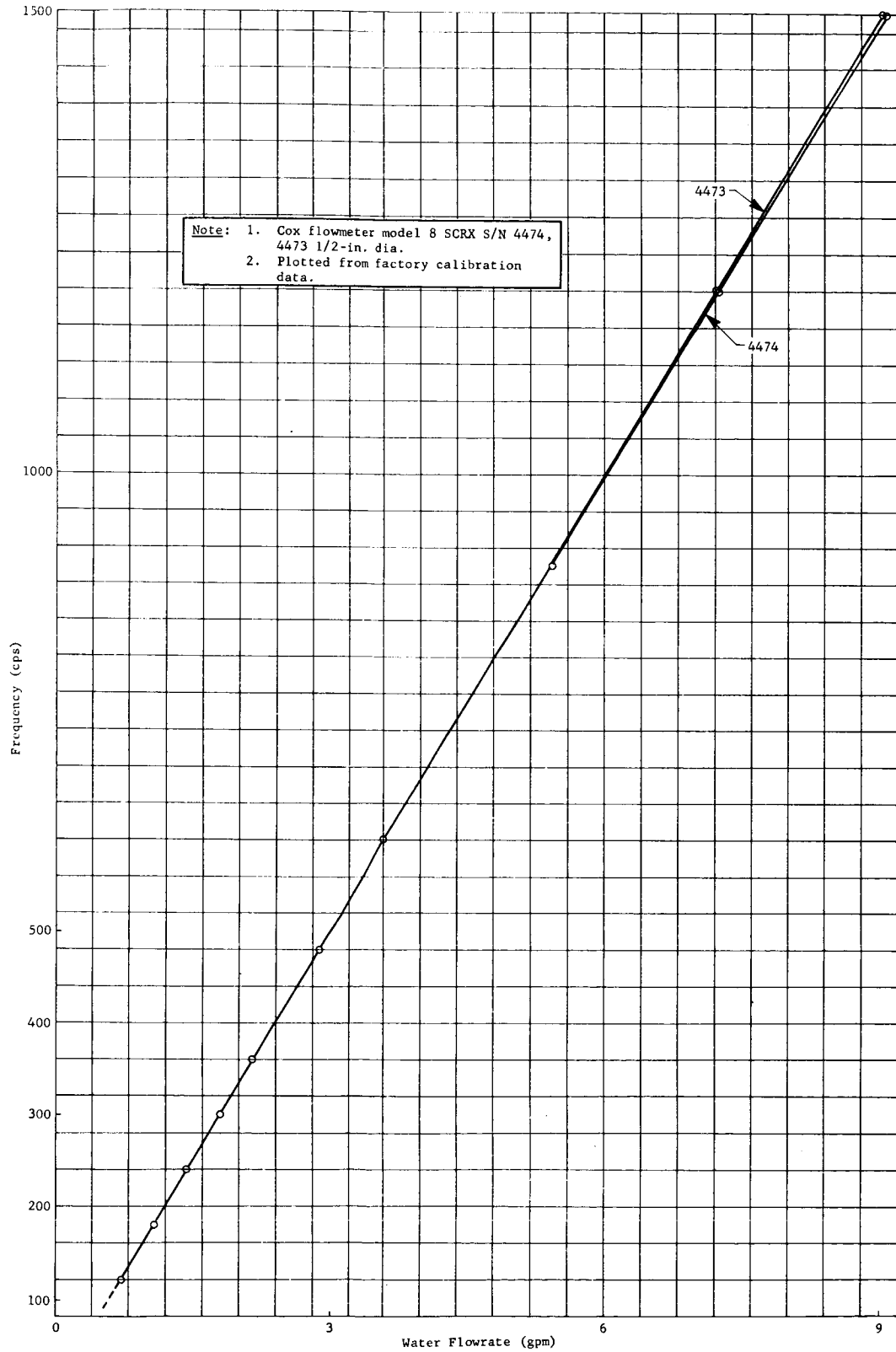


Fig. 21 Calibration, 1/2-in. Flowmeter

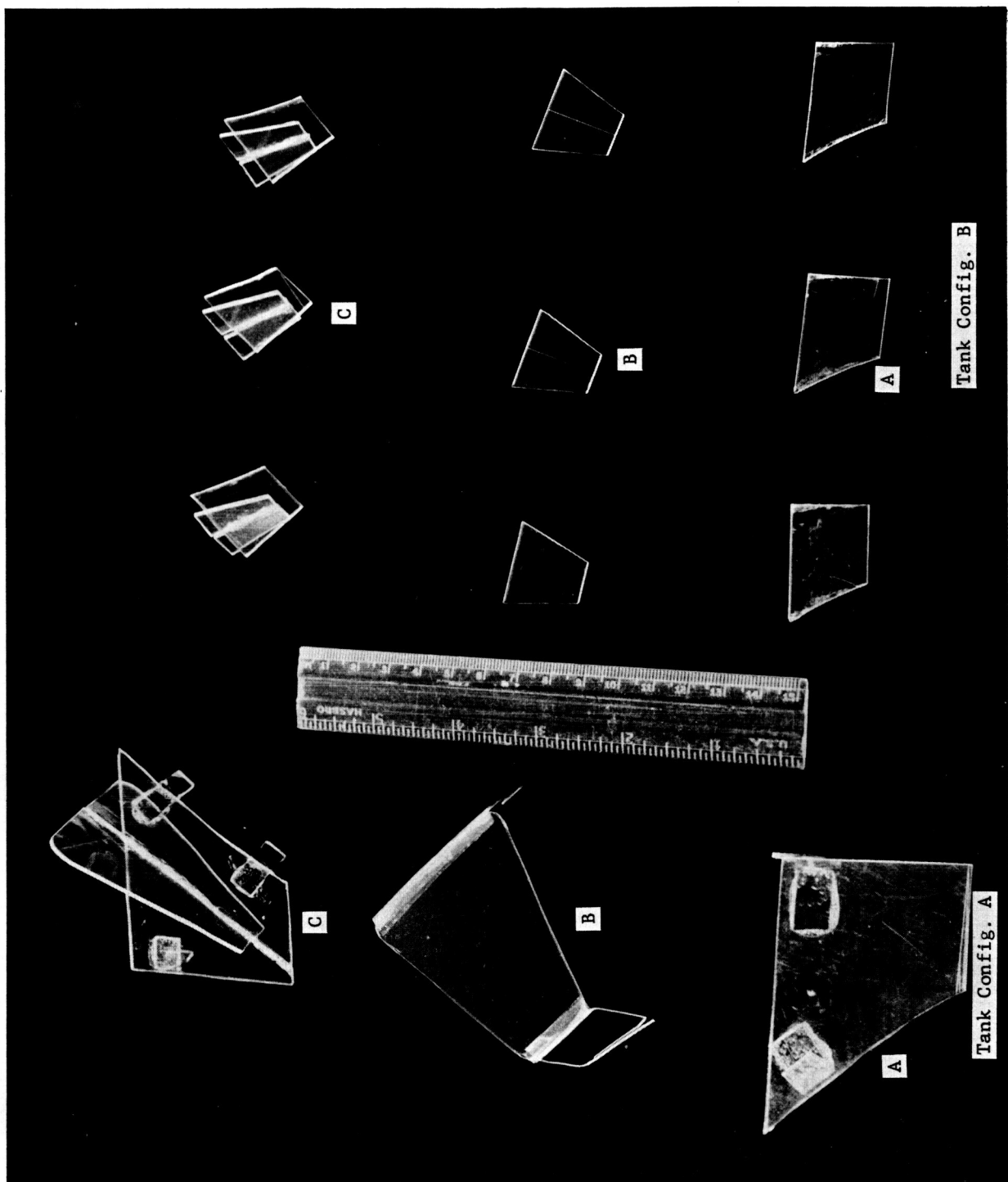


Fig. 22 Cylindrical Tank Baffle Configurations

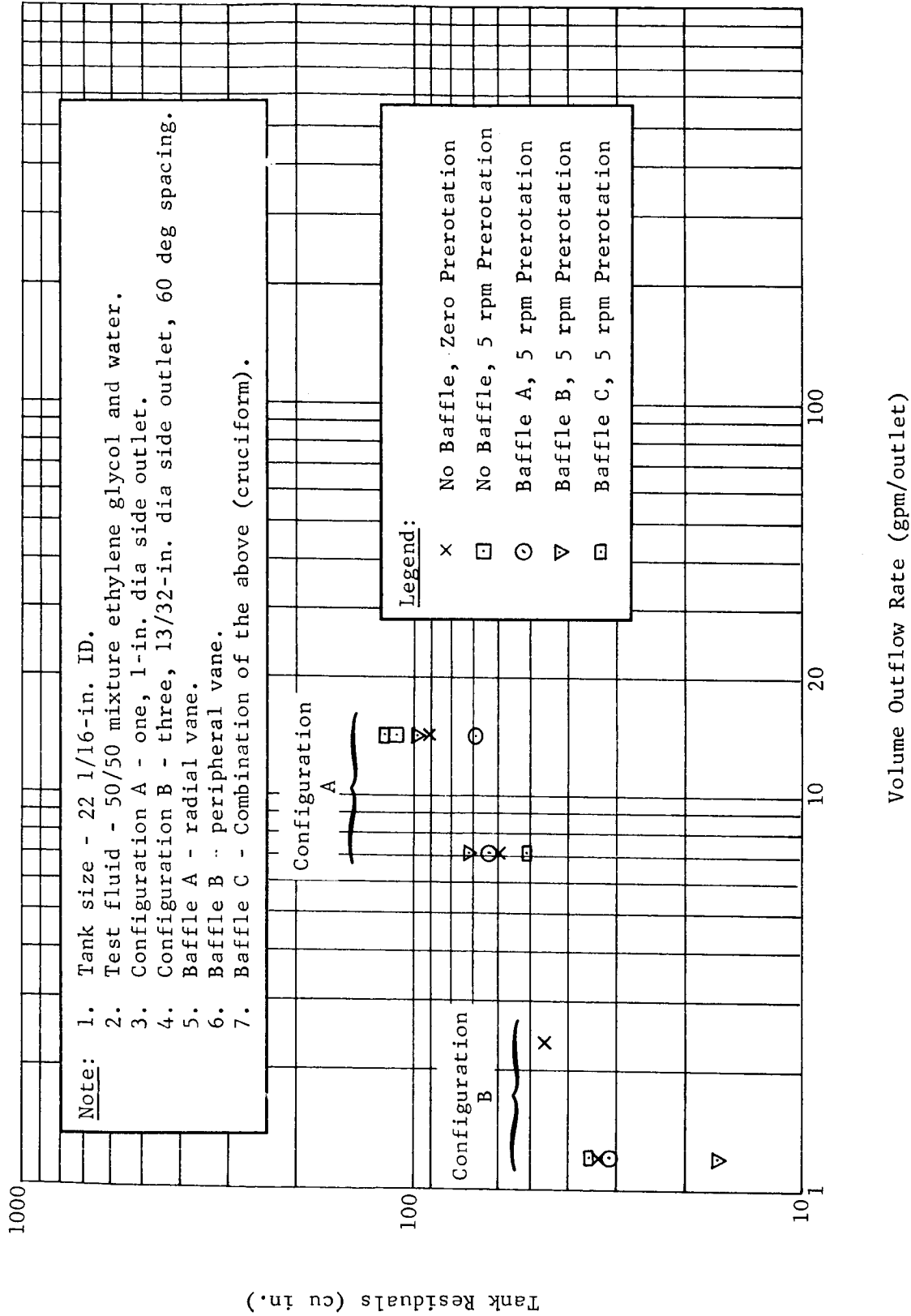


Fig. 23 Cylindrical Tank, Concave Lower Dome - Influences of Flowrate, Outlet Configuration, and Baffle Design on Residuals

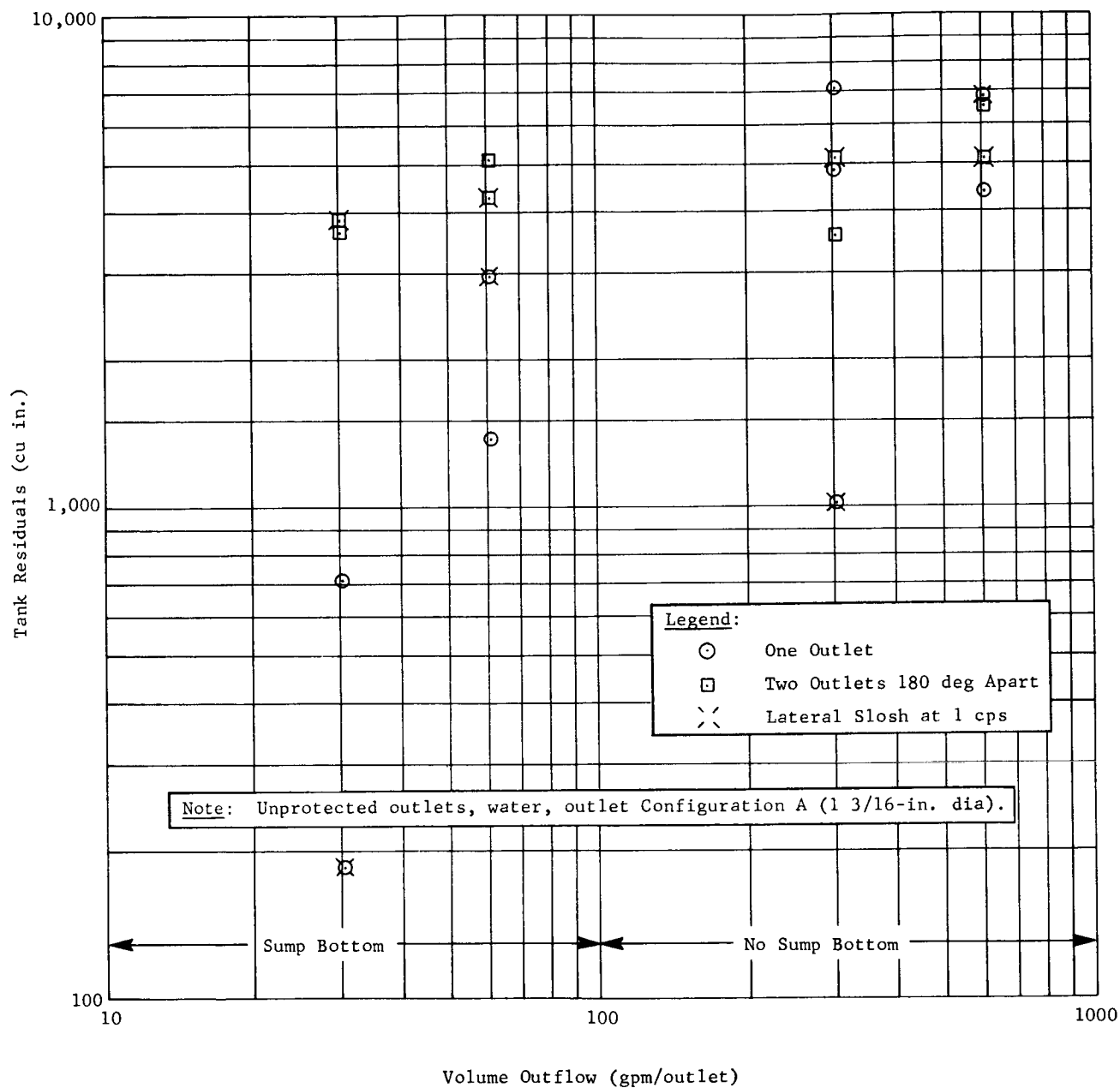


Fig. 24 Influence of Slosh and Number of Outlets on Toroidal Tank Residuals

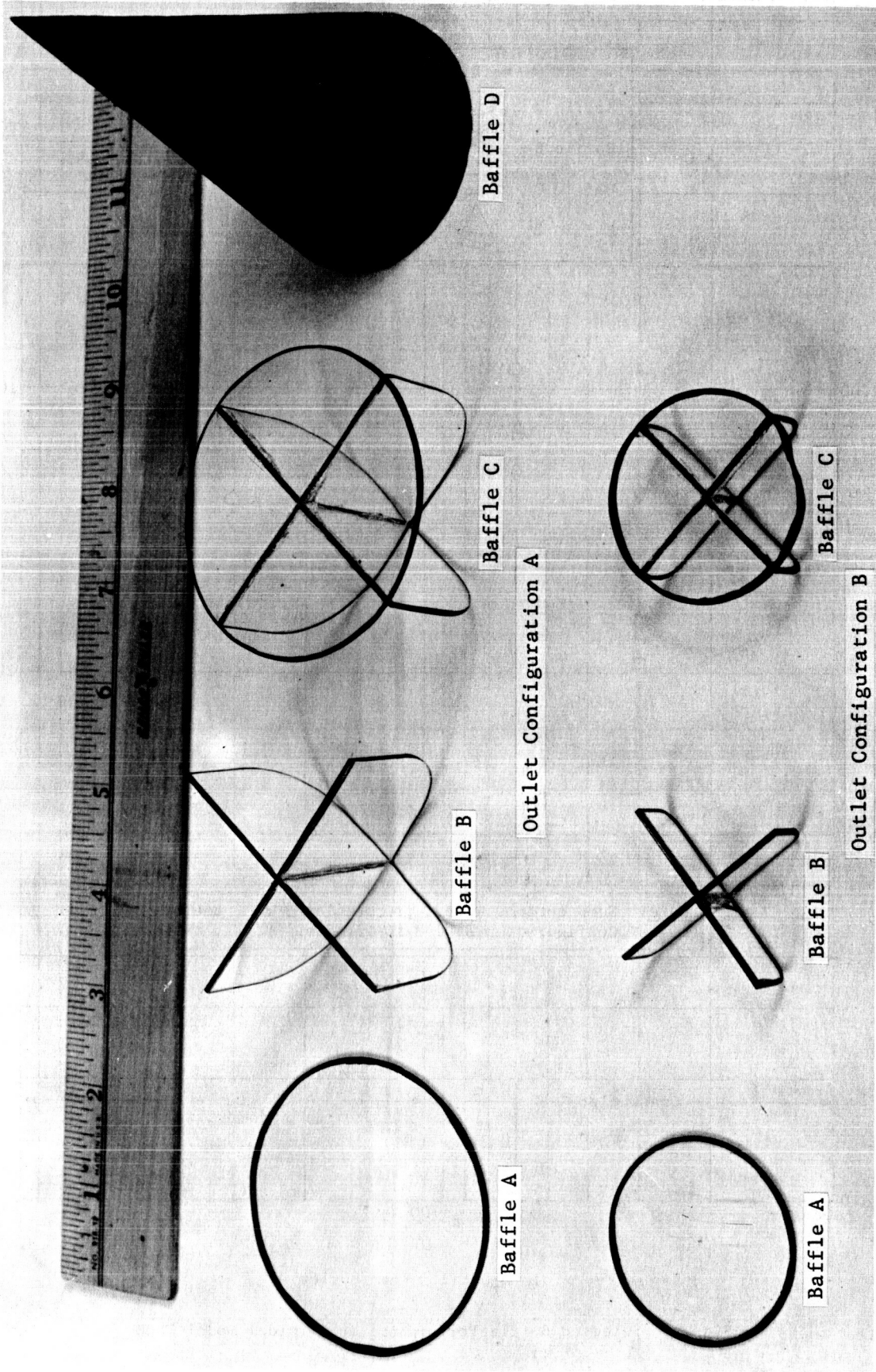


Fig. 25 Toroidal Tank Baffle Configurations

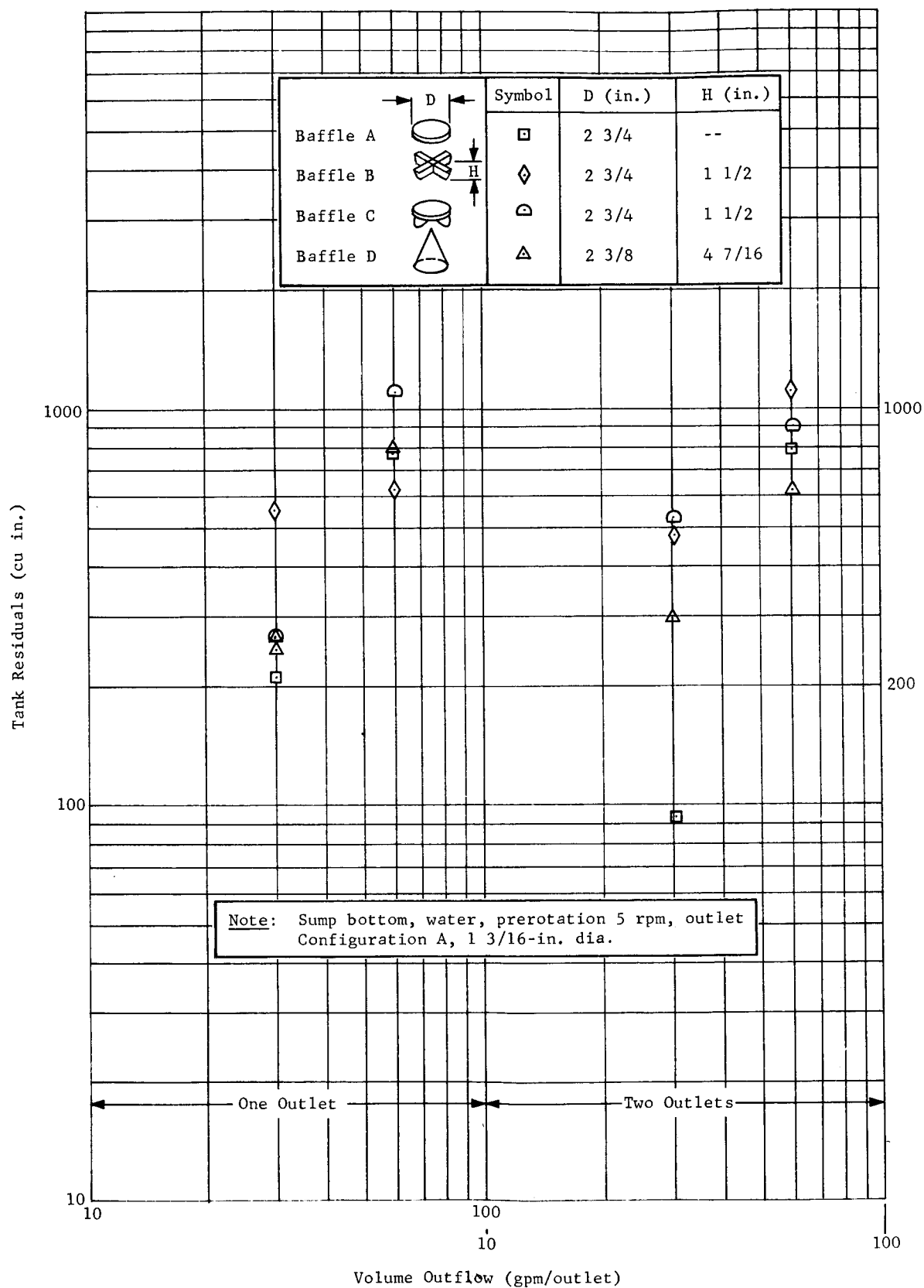


Fig. 26 Selected Baffle Performance in Toroidal Model Tank

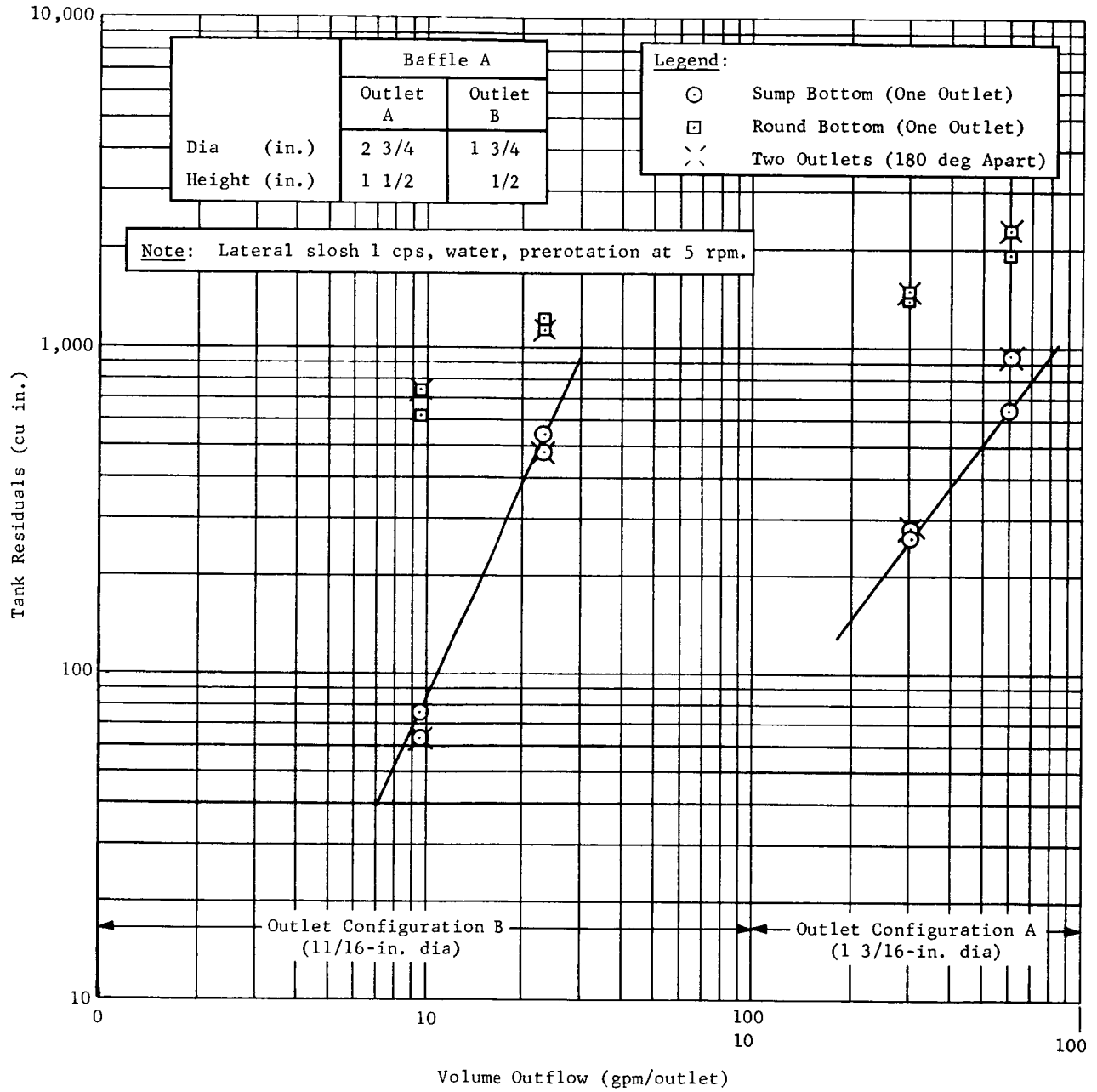


Fig. 27 Toroidal Tank Residuals as a Function of Bottom Type, Number, and Size of Baffled Outlets

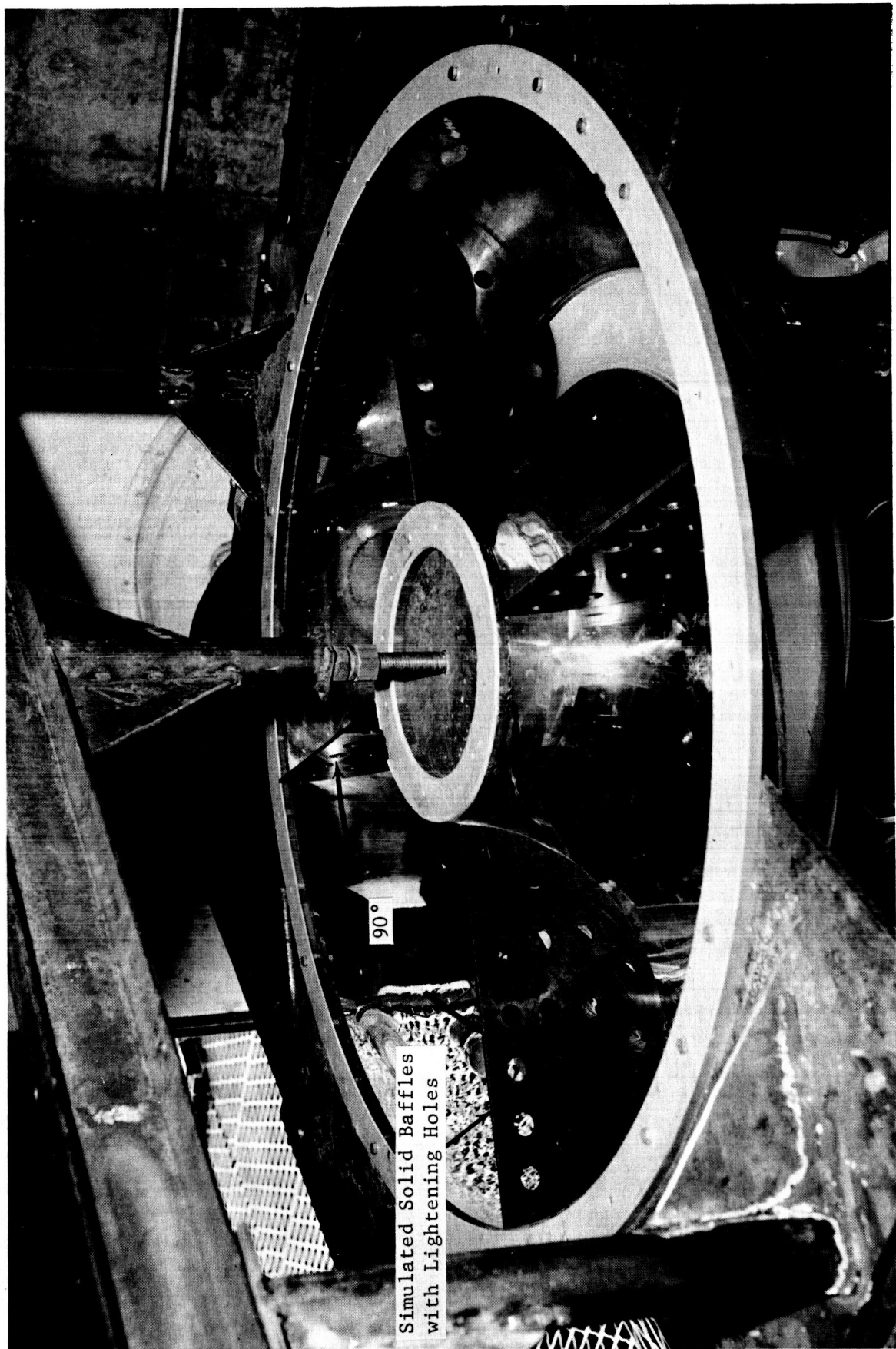


Fig. 28 Antislosh Solid Baffles Installed in Toroidal Model Tank Half

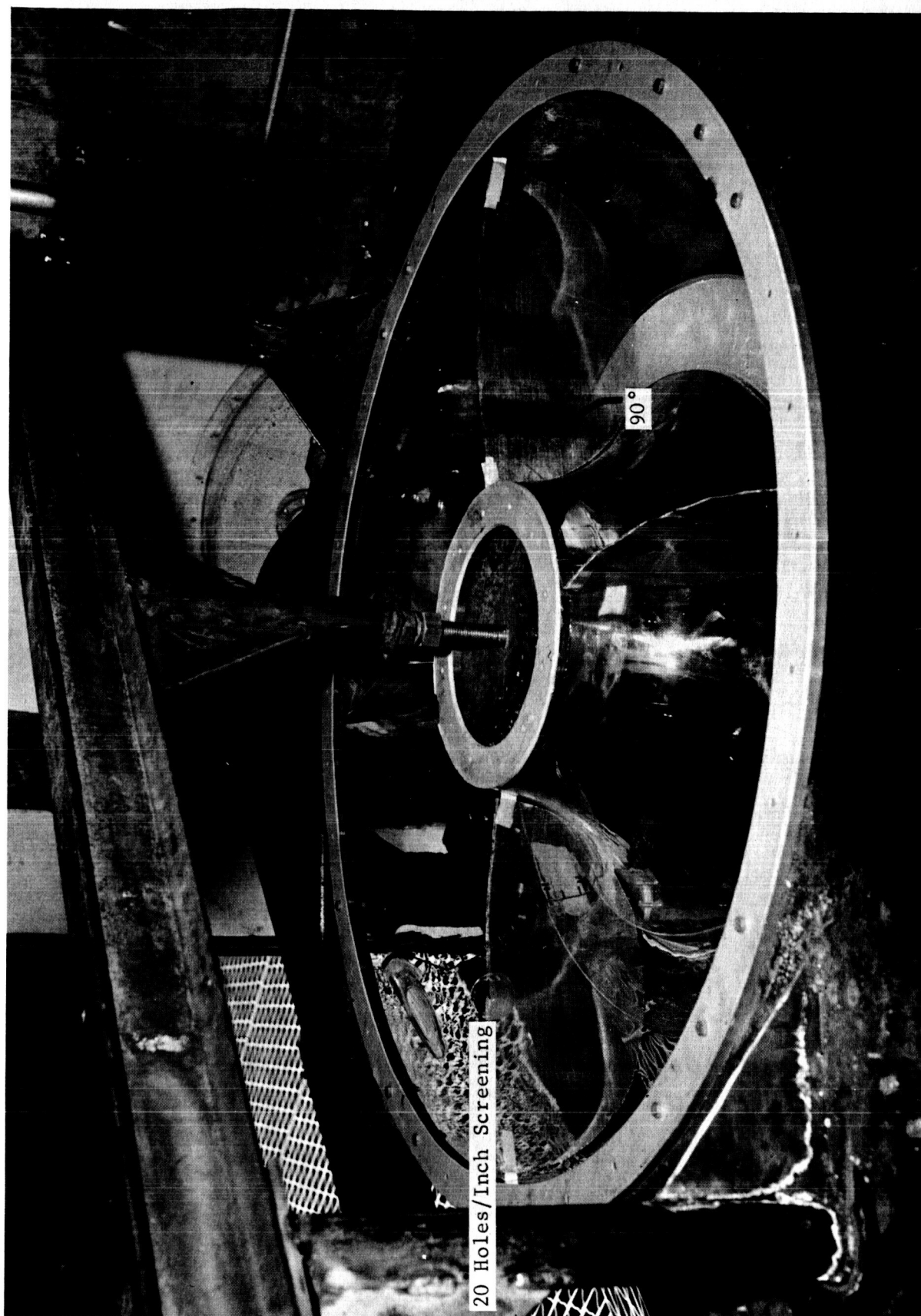


Fig. 29 Antislush Screen Baffles Installed in Toroidal Model Tank Half

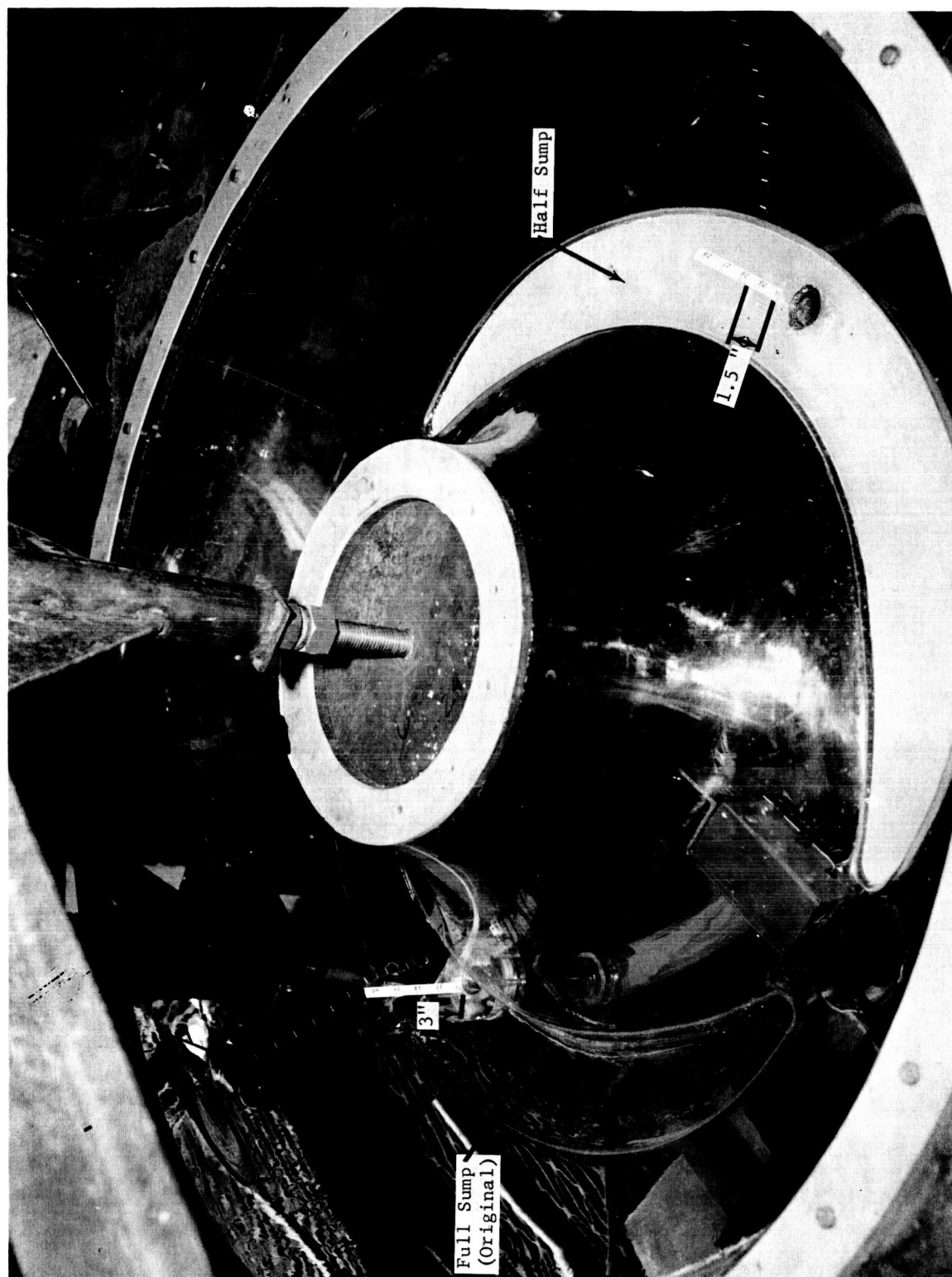


Fig. 30 Sump Bottom Modification Details

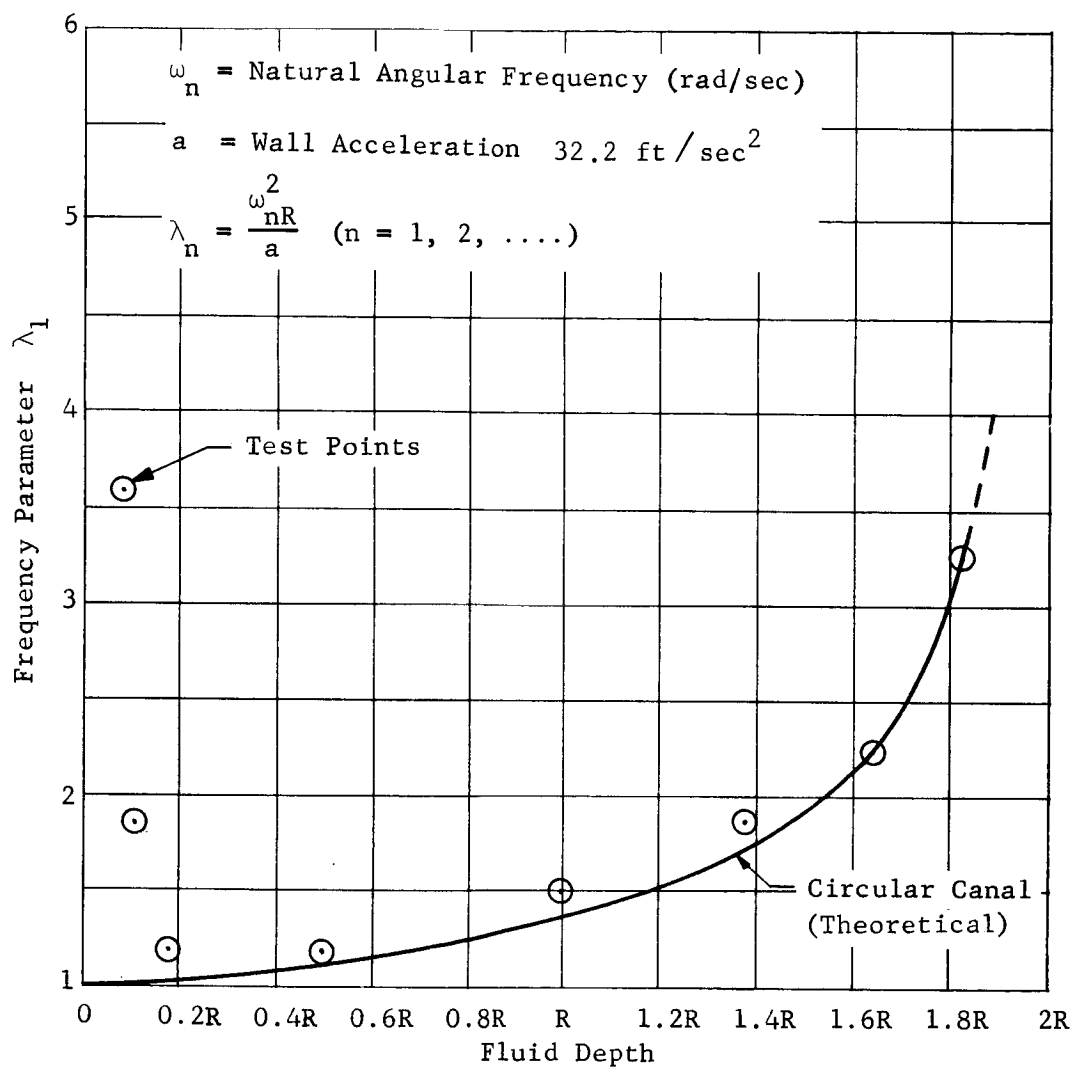


Fig. 31 Predicted and Test Observations, Stable Planar Resonance Mode, Toroidal Model Tank

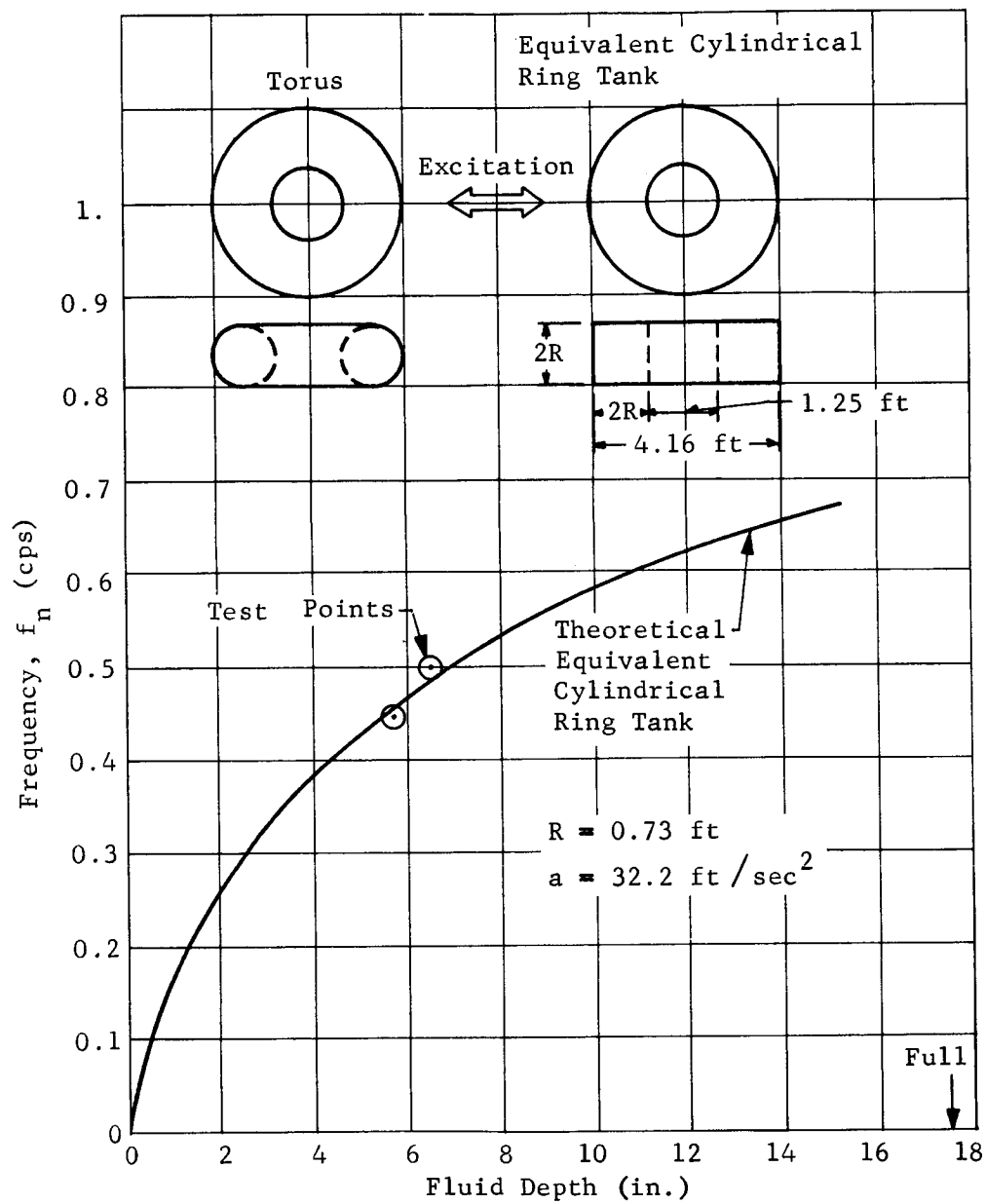


Fig. 32 Predicted and Test Observations, Stable Nonplanar Resonance Mode, Toroidal Model Tank

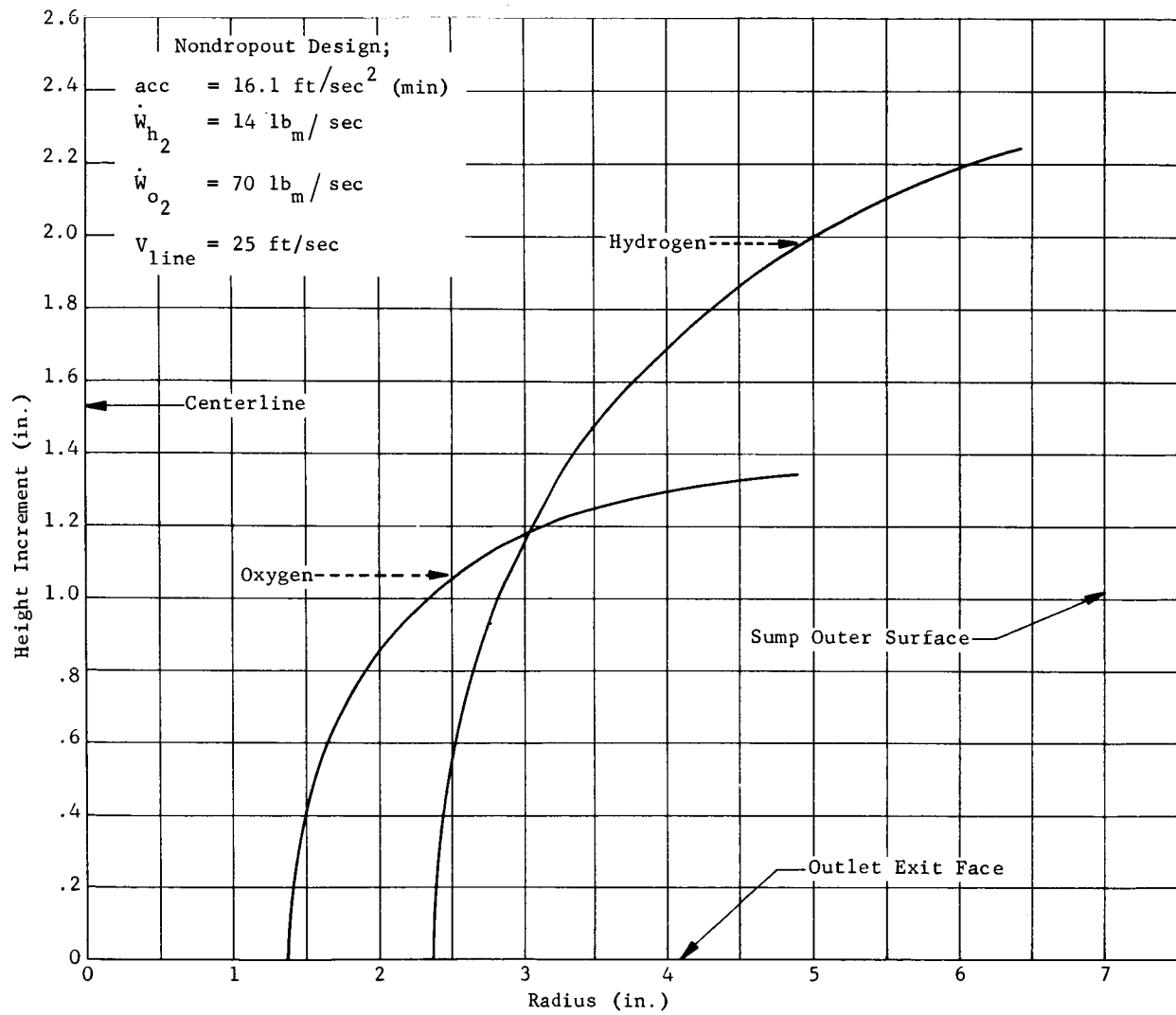


Fig. 33 Toroidal Tank Full-Scale Outlet Contours

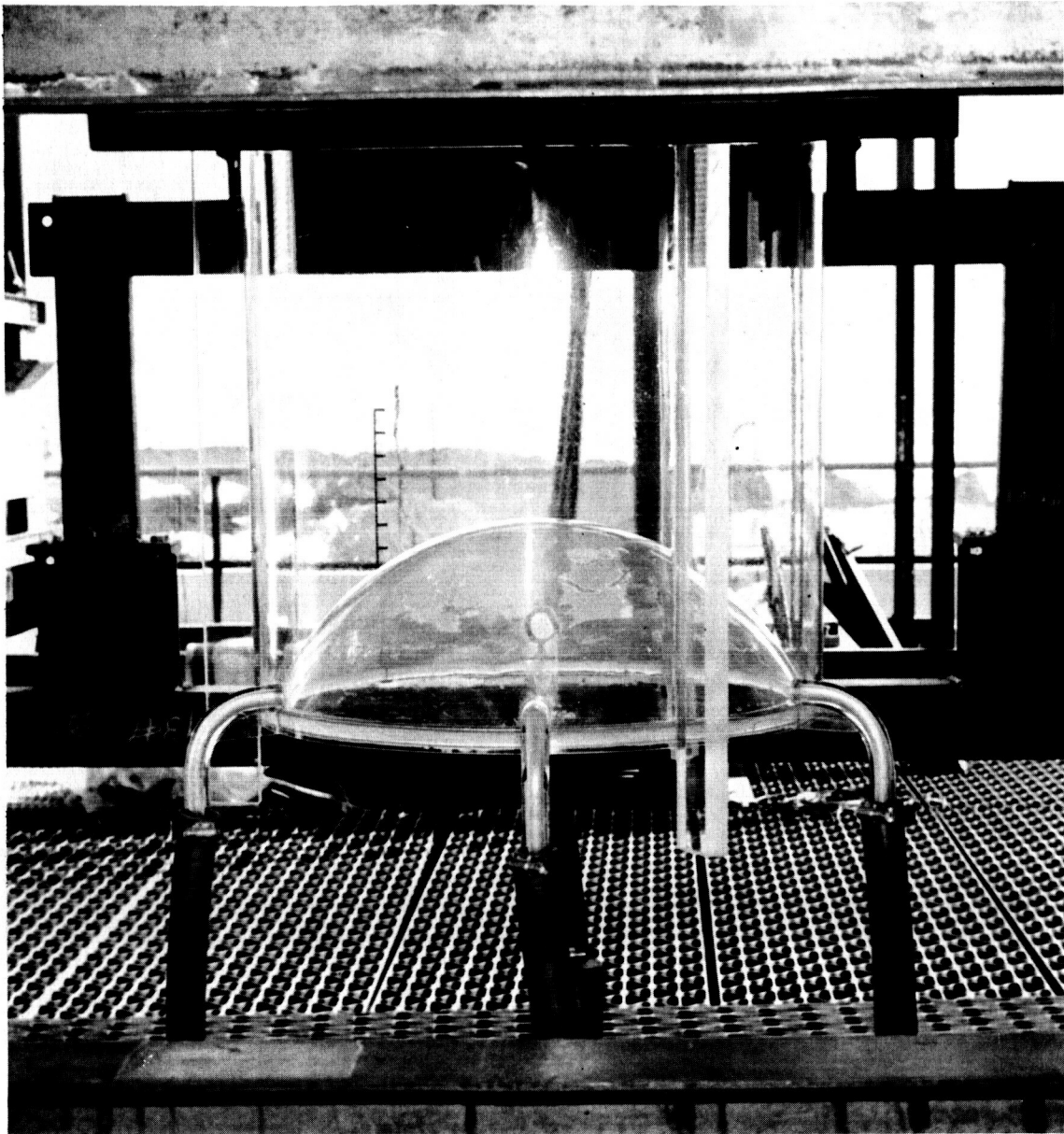


Fig. 34 Cylindrical Tank with Concave Lower Dome Model

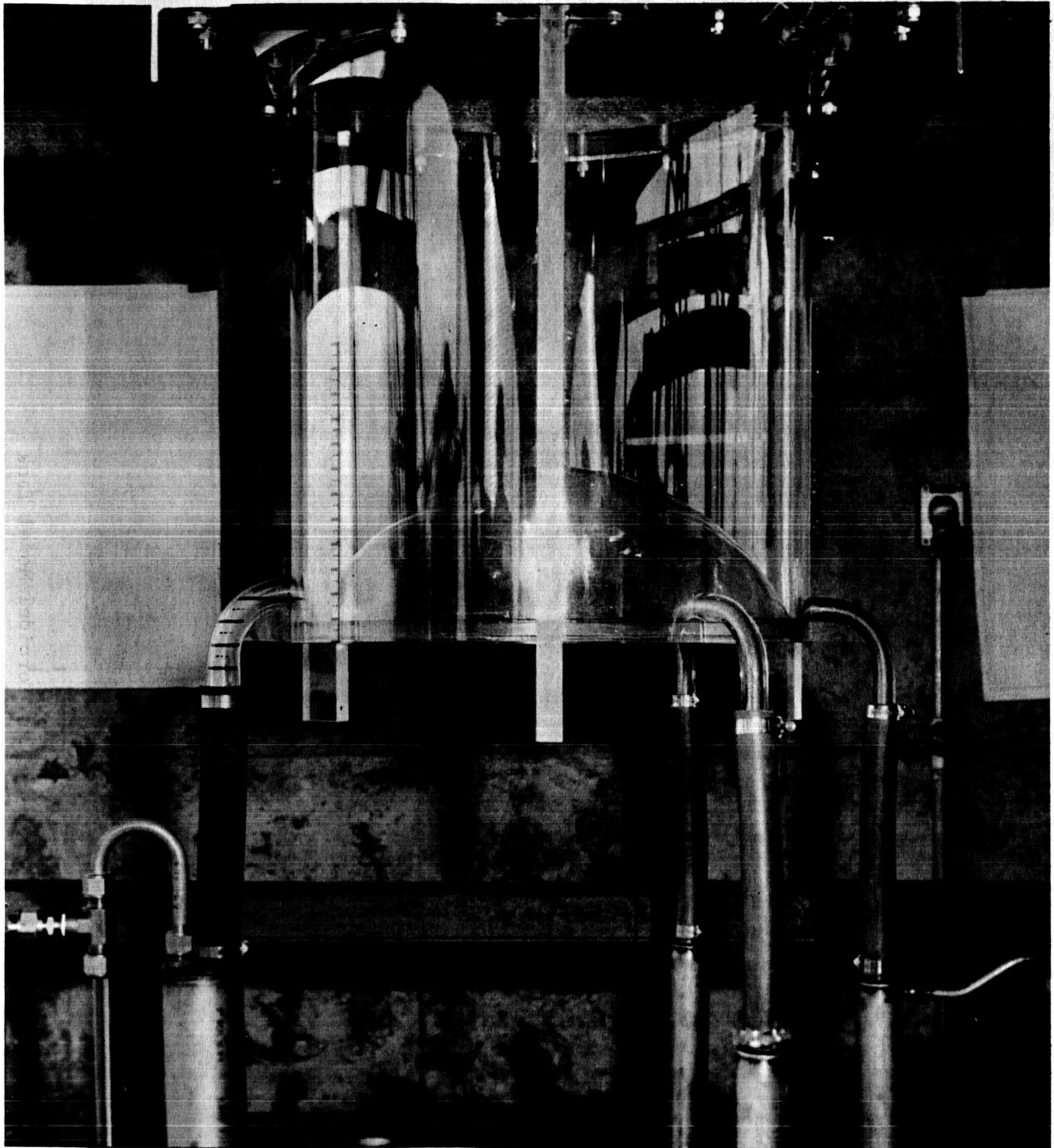


Fig. 35 Calibrated Cylindrical Model Tank

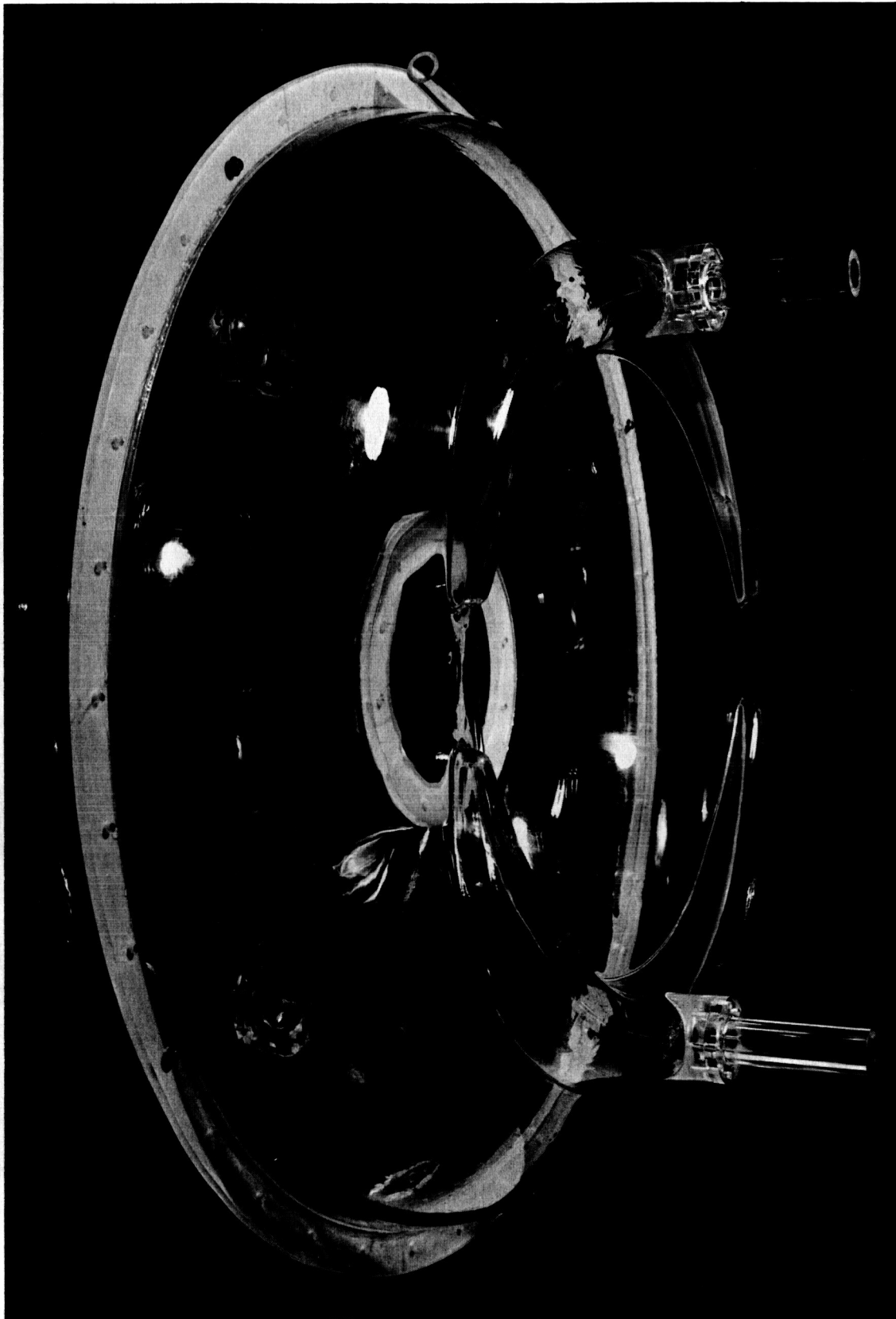


Fig. 36 Toroidal Model Tank

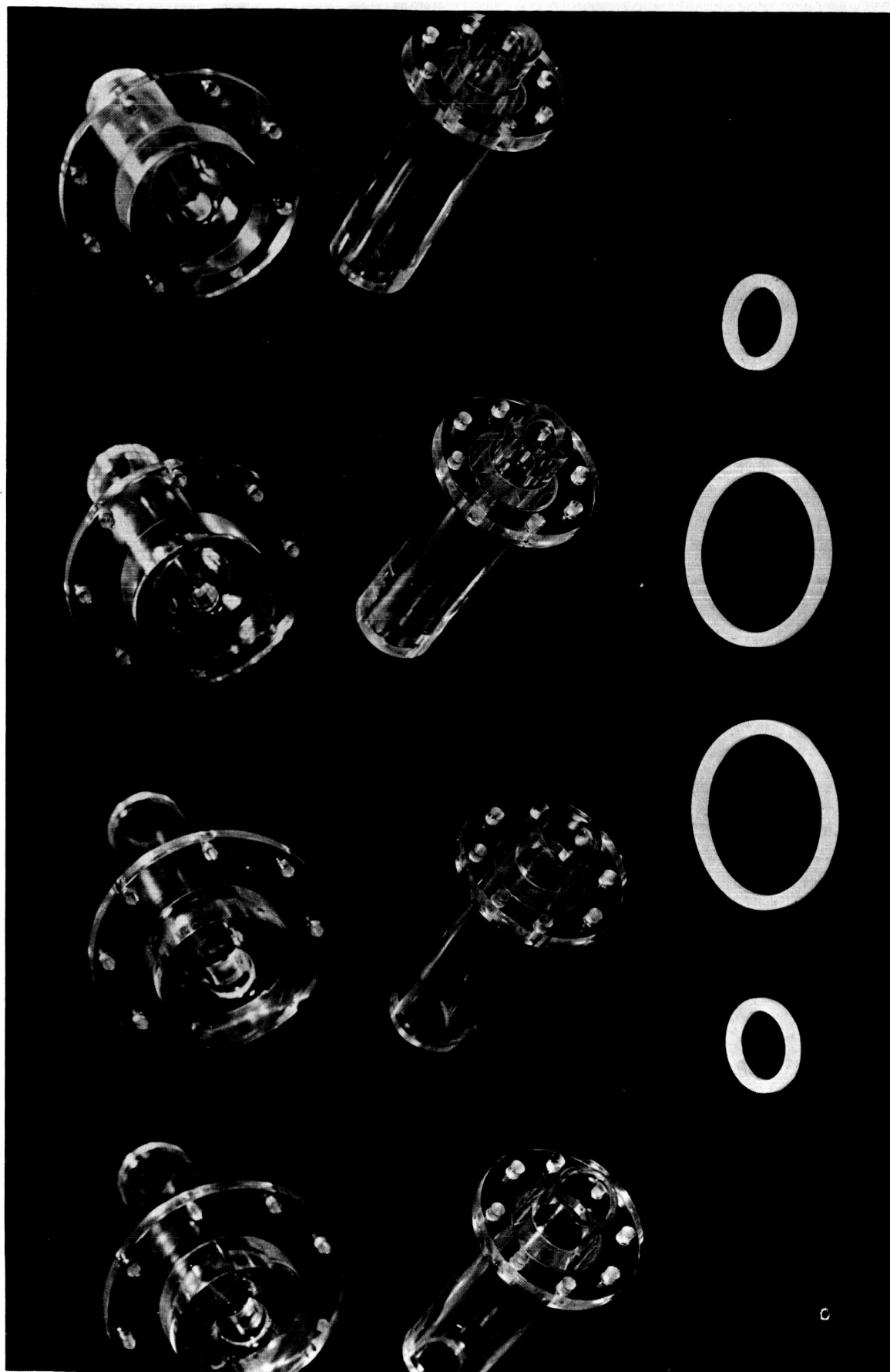


Fig. 37 Outlet Inserts for Toroidal Model Tank

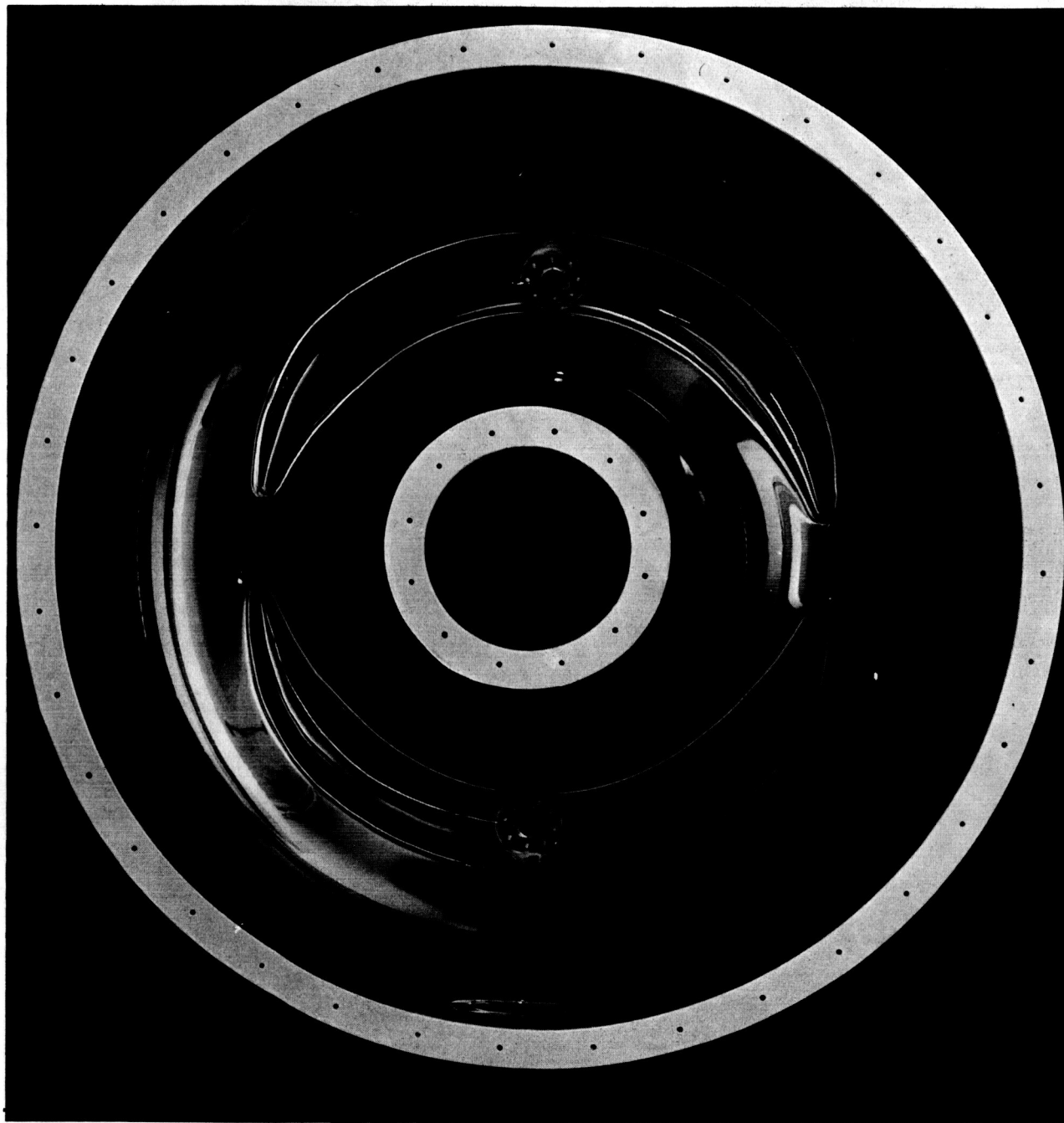


Fig. 38 Toroidal Model Tank-Sump Bottom View

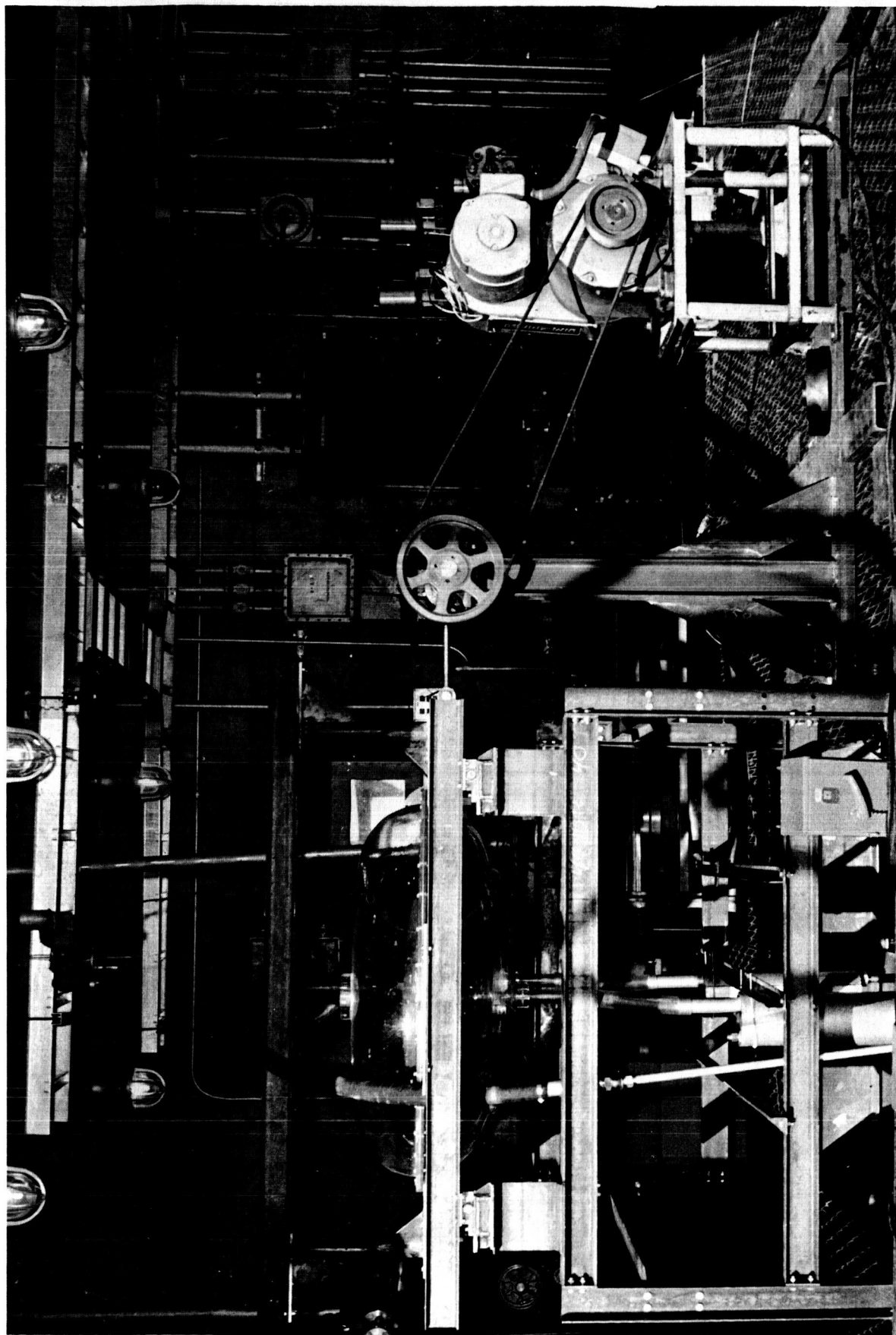


Fig. 39 Terminal Draining Study Test Setup, Toroidal Tank Installed

Table 2 Pertinent Outlet Dropout Parameter Calculations, Cylindrical Tank - Concave Lower Dome

	Outlet Configuration A										Outlet Configuration B													
	1	2	2.5	3	4	5	6	0.405	0.5	1	2	2½	3	4	5		0.405	0.5	1	2	2½	3	4	5
h (in.)	1.5	1.3	1.58	1.9	2.68	3.65	4.96	0.59	0.64	0.83	1.3	1.58	1.9	2.68	3.65		0.59	0.64	0.83	1.3	1.58	1.9	2.68	3.65
$(r_{\max}-C_h)$ (in.)	0.83	1.3	1.58	1.9	2.68	3.65	4.96	0.59	0.64	0.83	1.3	1.58	1.9	2.68	3.65		0.59	0.64	0.83	1.3	1.58	1.9	2.68	3.65
Flow Area (in. ²)	0	0.6	1.2	1.85	2.75	3.7	4.96	0	0.11	0.36	0.96	1.56	2.21	3.11	4.26		0	0.11	0.36	0.96	1.56	2.21	3.11	4.26
A_s (in. ²)	0	1.2	2.4	3.7	5.5	7.9	10.8	0	0.22	0.72	1.92	3.12	4.42	6.22	8.52		0	0.22	0.72	1.92	3.12	4.42	6.22	8.52
(dA_s/dh) (in.)	1.975	2.41	3.27	3.73	5.02	5.67	5.96	1.4	1.48	1.945	2.47	3.17	3.73	5.02	5.67		1.4	1.48	1.945	2.47	3.17	3.73	5.02	5.67
$\frac{A_s^3}{(dA_s/dh)} \times 10^{-5}$ (ft ⁵)	0	0.29	2.01	6.23	18	80.4	1080	0	0.0029	0.0774	4.97	11.07	26.0	99.5	324		0	0.0029	0.0774	4.97	11.07	26.0	99.5	324

Diagram illustrating the geometry of a circular segment. The radius is $R = 11.04$ in. The segment height is $r_{\max} - C_h$. The chord length is C_h . The area of the segment is A_s . The diagram also shows the total height h and the radius R .

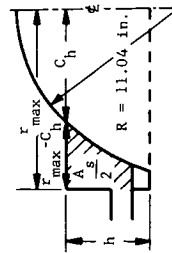


Table 3 ξ_n Factors for Cylindrical Ring Tank

n/k	0	0.1	0.2	0.3	0.4	0.5	0.6	0.7	0.8	0.9
1	1.841	1.803	1.705	1.582	1.462	1.355	1.262	1.182	1.113	1.053
2	5.33	5.137	4.961	5.137	5.66	6.565	8.041	10.592	15.778	31.447
3	8.53	8.20	8.433	9.31	10.68	12.706	15.801	21.004	31.451	62.848

Roots of the Determinant:

$$\Delta_1(\xi) = \begin{vmatrix} J_1'(\xi) & Y_1'(\xi) \\ J_1'(K\xi) & Y_1'(K\xi) \end{vmatrix} = 0$$

Note: $k = \frac{\text{inner radius}}{\text{outer radius}}$.
 $n = \text{no. of mode.}$

Table 4 Natural Frequency Parameter, λ_n , for Circular Canal

Depth (radii)	Mode		
	First	Second	Third
0	1	6	15
0.2	1.045	5.38	10.85
0.4	1.099	4.97	9.13
0.6	1.165	4.74	8.33
0.8	1.249	4.65	7.99
1.0	1.36	4.7	7.96
1.2	1.513	4.91	8.23
1.4	1.742	5.34	8.89
1.6	2.13	6.22	10.28
1.8	3.04	8.42	13.84
2	∞	∞	∞
$\lambda_n = \frac{\omega_n^2 R}{a}$			

Table 5 Prototype and Model Tank Design Parameters

Item	Cylindrical Tank		Toroidal Tank	
	A	B	A	B
Prototype				
Configuration				
Number of Outlets	1	3	1 or 2	1 or 2
Propellant	Hydrogen	Hydrogen	Hydrogen	Oxygen
Propellant Flowrate (lb _m /sec/outlet)	85	14	14	70
Acceleration Range (g)	1½ to 6	1½ to 6	½ to 2	1/3 to 2
Outlet Size (in.)	11 3/4	4 3/4	4 3/4	2 3/4
Model				
Scale	1:11.78	1:11.78	1/4	1/4
Outlet size (in.)	1	13/32	1 3/16	11/16
Simulated Acceleration (g)	1½ to 6	1½ to 6	½ to 2	1/3 to 2
Water Flowrate (gpm/outlet)	14.26 to 7.14	2.34 to 1.174	60.6 to 30.3	23.5 to 9.62

Table 6 Toroidal Tank, Sloshing Resonant Frequency
Stable Planar Resonance

Liquid Depth		Natural Frequency [f_n (cps)]	Frequency Parameter $\left(\lambda_n = \frac{4\pi^2 f_n^2 R}{a} \right)$
(in.)	(radii)		
0.75	0.0856	2	3.50
1	0.1143	1.45	1.875
1.875	0.214	1.15	1.178
4.50	0.514	1.15	1.178
8.75	1.0	1.3	1.503
12.075	1.38	1.45	1.875
14.16	1.619	1.6	2.27
15.928	1.82	1.9	3.22
17.181	1.96	2.3	4.7

Table 7 Toroidal Tank, Sloshing Resonant Frequency
Stable Nonplanar Resonance

Liquid Depth		Natural Frequency [f_n (cps)]	Frequency Parameter $\left(\lambda_n = \frac{4\pi^2 f_n^2 R}{a} \right)$
(in.)	(radii)		
5.5	0.628	0.45	0.181
6.5	0.743	0.50	0.223

Table 8 Comparison of Analytical and Test Results for Residuals of Selected Cylindrical Tank Outflow Tests - No Baffles, No Prerotation

Tank Outlet Configuration	Run No.	Volume Flow		$\frac{Q^2}{a} \times 10^5 \text{ (ft}^5\text{)}$	Predicted		Actual	
		(gpm)	(cfs)		Critical Depth (in.)	Residual (Tank Calibration) (cu in.)	Critical Depth (in.)	Residual (Test measure) (cu in.)
A	101	7.1	0.0158	0.776	1.7	52	2.39	59.6
A	102	14.3	0.0318	3.1	2.15	96	2.67	91.3
B	103	1.2	0.00267	0.0221	0.80	19	1.61	33.9
B	104A	2.35	0.00524	0.0851	1.0	35	1.86	46.5

Table 9 Analytical Predictions for Residuals for Toroidal Tank Outflow Tests - No Sump Bottom, Baffled Outlets, No Prerotation, No Sloss.

Toroidal Tank - Nonsump Bottom						
Outlet Configuration	Volume Flow Per Outlet		$Q^2/a \times 10^5 \text{ (ft}^5\text{)}$	Predicted		
	(gpm)	(cfs)		Critical Depth (in.)	Residuals (cu in.)	
A	30.3	0.0674	14.15	0.84	427	
A	60	0.1333	55.4	1.15	671	
B	9.6	0.0213	1.41	0.46	165	
B	23.5	0.0522	8.46	0.73	353	

Table 10 Selected Toroidal Tank Nonsump Bottom Test Data

Test No.	Flowrate (gpm/outlet)	Outlet No.	Configuration Type	Residuals (cu in.)
310	30.0	1	A	1437
311	61.45	1	A	1927.8
313	29.95	2	A	1427
315	61.45	2	A	2280.6
323X	9.6	1	B	603.6
324	23.5	1	B	1211.72
326	9.55	2	B	731.1
327	22.45	2	B	1187.5

APPENDIX E

COMPUTER PROGRAMS

1. Nondropout Outlet Design

All of the governing differential equations ([18], [23], and [28]) can be treated by the same numerical solution. The similarity of the equation structure is evident, so that a single equation with adjustable input coefficients can be programed for the IBM 1620 computer that will be suitable for all outlet configurations. This generalized equation with appropriate letter coefficients becomes:

$$h_n'' + A \left(h_n'^3 + h_n' \right) \left[\frac{Br_n^{E1}}{r_n^{E2} (r_m^2 - r_n^2)^{E3}} + \frac{C(\delta + 2r_n)^{E4} g_c \sqrt{1 + h_n'^2}}{r_n^{E5} \delta^{E6} (r_m - r_n)^{E7} Ch^2} \right] - \frac{D\pi^{E8} \delta^{E9} r_n^{E10} (r_m^2 - r_n^2)^{E11} a h_n'^4}{Q^2} = 0.$$

The following tabulation presents the value for each coefficient for the three outlet configurations under consideration:

Input Constants																		
Outlet Configuration	A	B	C	D	δ	r_m	E1	E2	E3	E4	E5	E6	E7	E8	E9	E10	E11	
Circular	+1	+2	+2	+1	+1	+1	0	+1	0	0	+1	0	0	+2	0	+4	0	
Annular	-1	+2	+2	+1	+1	r_m	+1	0	+1	0	0	0	+1	+2	0	0	+2	
Rectangular	+1	+1	+1	+4	δ	+1	0	+1	0	+1	+1	+1	0	0	+2	+2	0	

As a simplifying procedure, a transformation of variables was instituted. This transformation changed the independent variable from r to h so that the reciprocal of slope, dr/dh , is now computed.

To arrive at this transformation, let us inspect the original second-order differential equation, which is of the following form:

$$\frac{d^2 h}{dr^2} = F\left(\frac{dh}{dr}, r\right).$$

Let

$$p = \frac{dh}{dr} \text{ and } \frac{dp}{dr} = \frac{d^2 h}{dr^2},$$

$$\frac{dp}{dh} = \frac{dp}{dr} \frac{dr}{dh} = \frac{dp}{dr} \frac{1}{p} = \frac{d^2 h}{dr^2} \frac{1}{p},$$

but,

$$\frac{d^2 r}{dh^2} = \frac{d}{dh} \left(\frac{dr}{dh} \right) = \frac{d}{dh} \left(\frac{1}{p} \right) = -\frac{1}{p^2} \frac{dp}{dh} = -\frac{1}{p^3} \frac{d^2 h}{dr^2}.$$

Therefore, to transform the independent variable from r to h , divide the original equation by $-\left(\frac{dh}{dr}\right)^3$. Performing this operation, the following equation is derived from the general form of the differential equation (letter designations remain unchanged):

$$\begin{aligned} \frac{d^2 r}{dh^2} = & A \cdot \left[1 + \left(\frac{dr}{dh} \right)^2 \right] \left[\frac{B r_n^{E1-E2}}{\left(r_m^2 - r_n^2 \right)} E3 + \right. \\ & \left. + \frac{N \left(\delta + 2r_n \right)^{E4}}{r_n^{E5} \left(r_m - r_n \right)^{E7}} \sqrt{1 + \left(\frac{dr}{dh} \right)^{-2}} \right] - \\ & - M \frac{\left[r_n^{E10} \left(r_m^2 - r_n^2 \right)^{E11} \right]}{dr/dh}, \end{aligned}$$

where,

$$N = \frac{Cg_c}{Ch^2 \delta^{E6}}, \quad M = \frac{D\pi^{E8} \delta^{E9}}{Q^2}.$$

The solution of the above differential equation by the Runge-Kutta method proceeds as follows.* Input initial values of r , h , $\left(\frac{dr}{dh}\right)$, and computing increment (Δh) . For $n = 0$, compute:

$$K_{1_n} = \Delta h F \left[r_n \left(\frac{dr}{dh} \right)_n \right]$$

$$K_{2_n} = \Delta h F \left[r_n + \frac{\Delta h}{2} \left(\frac{dr}{dh} \right)_n + \frac{\Delta h}{8} K_{1_n} \left(\frac{dr}{dh} \right)_n + \frac{K_{1_n}}{2} \right]$$

$$K_{3_n} = \Delta h F \left[r_n + \Delta h/2 \left(\frac{dr}{dh} \right)_n + \frac{\Delta h}{8} K_{2_n} \left(\frac{dr}{dh} \right)_n + \frac{K_{2_n}}{2} \right]$$

$$K_{4_n} = \Delta h F \left[r_n + \Delta h \left(\frac{dr}{dh} \right)_n + \frac{\Delta h}{2} K_{3_n} \left(\frac{dr}{dh} \right)_n + K_{3_n} \right].$$

These constants are now used to compute the changes in r and $\left(\frac{dr}{dh}\right)$ to be used for the succeeding step:

$$\Delta r_n = \Delta h \left[\left(\frac{dr}{dh} \right)_n + \frac{K_{1_n} + K_{2_n} + K_{3_n}}{6} \right],$$

$$r_{n+1} = r_n + \Delta r_n,$$

$$\Delta \left(\frac{dr}{dh} \right)_n = \frac{K_{1_n} + 2K_{2_n} + 2K_{3_n} + K_{4_n}}{6},$$

$$\left(\frac{dr}{dh} \right)_{n+1} = \left(\frac{dr}{dh} \right)_n + \Delta \left(\frac{dr}{dh} \right)_n,$$

$$(n = 0, 1, 2, \dots) \dots$$

*J. B. Scarborough: Numerical Mathematical Analyses. Johns Hopkins University, Baltimore, Maryland, 1955.

The procedure is repeated for succeeding steps until the desired contour is obtained.

The computer program listing for the Runge-Kutta solution of the nondropout outlet design follows this discussion. Several options are allowed to permit a more satisfactory computer operation. These options include:

- 1) Instantaneous examination of K values and slope;
- 2) Ability to change the size of the increments Δh ;
- 3) Ability to input an entirely new set of data without stopping the program.

Energizing sense switch 1 causes the typewriter to print the instantaneous K value and slope of the increment under calculation. The sign of K is a safety check on the operation of the program; positive and negative values indicate the appropriate sense of the contour slope. Slope magnitudes also show the degree of program completion.

Five data cards (including a title card) comprise the primary data for the program. One item of data is Δh , the incremental height change. When the initial point taken is at the minimum tank outlet diameter (where the slope is greatest), a small Δh is desired to adequately describe the outlet contour. To conserve computing time, Δh should be increased when the slope shallows. To accomplish this, data cards consisting of a series of Δh values in successively increasing magnitudes follow the five primary data cards. Energizing switch 4 will result in a new Δh value being fed to the computer. This process can be repeated until the data cards are depleted.

Once the program is started, new data for a new tank outlet contour can be loaded without time-consuming shutdown-reload operations. Energizing switch 3 will result in the loading of new data that has been inserted into the read hopper.

The inherent error in the Runge-Kutta method is not easy to evaluate; it has been estimated* to be approximately $(\Delta h)^\dagger$. This is reasonably acceptable for these calculations.

*Ibid.

†H. F. Bauer: Propellant Sloshing. ABMA DATR-18-58, 5 November 1958.

C TERMINAL DRAINING PROGRAM NON DROPOUT OUTLET DESIGN
 C RUNGE-KUTTA SOLUTION FOR SECOND ORDER DIFFERENTIAL EQUATION
 C

```

    DIMENSION FC(4)
    785 READ 601
    601 FORMAT(40X,40X)
    1 FORMAT(11F5.0)
    2 FORMAT(7F10.0)
    600 READ 2,H,R,R1
    READ 2,A,B,C,D,ACC,XMAX,SLOPE
    READ 2,DEL,Q,CH,GC,RM,DH
    READ 1,E1,E2,E3,E4,E5,E6,E7,E8,E9,E10,E11
    PUNCH 601
    TYPE 601
    XN=C*GC/((CH**2)*(DEL**E6))
    XM=D*(3.1416**E8)*(DEL**E9)*ACC/(Q**Z)
    IMAX=XMAX
    PUNCH 101
    101 FORMAT(/,3X,36H I    RADIUS    HEIGHT    SLOPE    )
    PUNCH 602
    602 FORMAT(8X,6HINCHES,4X,6HINCHES/)
    I=1
    Q=1./R1
    RIN=R*12.
    HIN=H*12.
    PUNCH 100,I,RIN,HIN,G
    80 DO 60 K = 1,4
    IF(SENSE SWITCH 4)350,351
    350 TYPE 375
    375 FORMAT(40HREADY TO READ NEW DH CARD, START READER )
    352 FORMAT(F10.0)
    READ 352,DH
    TYPE 355
    355 FORMAT(34HTURN OFF SWITCH 4, THEN PUSH START )
    PAUSE
    GO TO 351
    351 GO TO (10,20,30),K
    10 V=R
    VP=R1
    GO TO 50
    20 V=R+(DH/2.)*R1+(DH/8.)*FC(K-1)
  
```

```

VP=R1+FC(K-1)/2.
GO TO 50
30 V=R+DH*R1+(DH/2.)*FC(K-1)
VP=R1+FC(K-1)
50 X=B*(V**((E1-E2)/((RM**2-V**2)**E3)
Y=XN*( (DEL+2.*V)**E4)/(V**E5*(RM-V)**E7)
Z=(1.+ (1./ (VP**2)))**.5
T=((V**E10)*(RM**2-V**2)**E11)/VP
FC(K)=(A*(1.+VP**2)*(X+Y*Z))-(XM*T))*DH
60 CONTINUE
IF(SENSE SWITCH 1)300,923
300 TYPE 603,1
603 FORMAT(2H1=,I4)
TYPE 377,Q
377 FORMAT(6 Hslope=,F10.5)
923 R=R+DH*(R1+(FC(1)+FC(2)+FC(3))/6.)
H=H+DH
R1=R1+(FC(1)+2.*FC(2)+2.*FC(3)+FC(4))/6.
Q=1./R1
I=I+1
RIN=R*12.
HIN=H*12.
PUNCH 100,I,RIN,HIN,Q
100 FORMAT(I4,2F10.5,3X,F10.4)
IF(SENSE SWITCH 3)785,786
786 IF(I-IMAX)202,202,201
202 IF(Q-SLOPE)200,200,80
201 TYPE 500
500 FORMAT(36H SATISFIED MAXIMUM BEFORE MAX. SLOPE )
GO TO 600
200 TYPE 501
501 FORMAT(47H MAX. SLOPE EXCEEDED BEFORE LOOP WAS SATISFIED )
GO TO 600
END

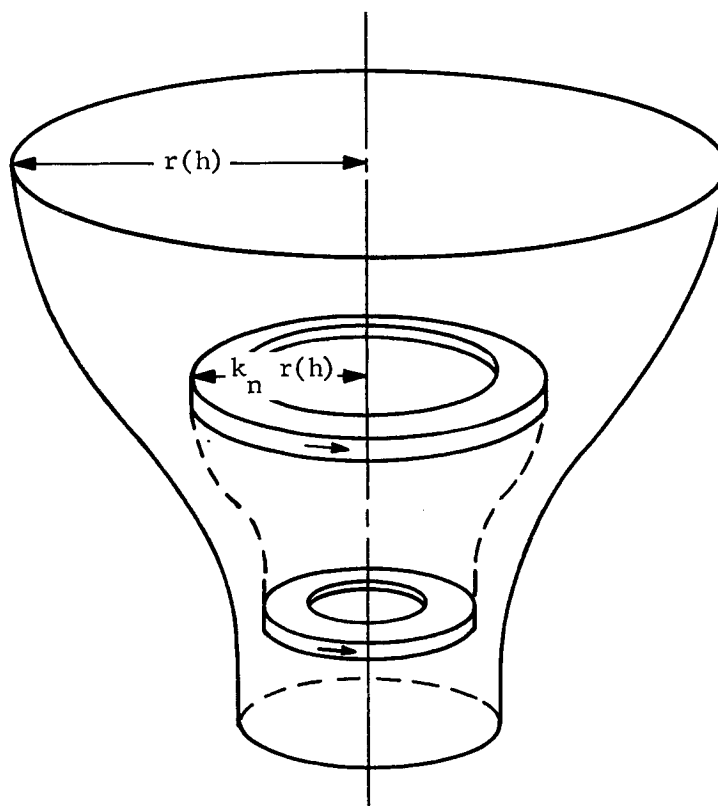
```

2. Vortexing Behavior Analysis

Based on the analysis described in Section B of Chap. II, a computer program has been developed to predict the severity of vortexing in a symmetrical outlet, with or without a symmetrical insert, for any instant of time.

The following theoretical assumptions have been made:

- 1) Kelvin's theorem applies. This is equivalent to assuming that the fluid is both incompressible and non-viscous. For cryogenic propellants, these two assumptions are realistic;
- 2) Any fluid particle path, under a zero-rotation regime, is represented by $k_n r(h)$ (i.e., any particle that is initially at a radius equal to $1/3$ the radius of the tank is finally located at $1/3$ the radius of the outlet, and was at this position during the entire constriction period). Further, under a rotation regime, it is assumed that the path of any vortex tube is such that its radius is $k_n r(h)$ at all times, as in the following sketch;



Path of a Vortex Tube

- 3) It is assumed that either the solid-body rotating core, the vortex air pipe, or the inserted solid-body nonrotating core has the configuration $\delta(h) = C_1 r(h)$, where C_1 is a function of the fluid properties, the potential function, or the insert arrangement. It will probably be empirically determined.

The vortex computer program requires the following inputs: r_o , r_{final} , Q , and $a(t)$. Another input, such as the outlet contour, $r(h)$, is prescribed from noncavitating and nondropout considerations. The remaining inputs, such as $\delta(h)$ and ω_o , are also required.

This program is based on a particulate system. The tank cross section is divided into a number of K horizontal levels, and a number of vertical bands. In any K level, the radius of a particle is defined as:

$$r_n = \left[\frac{r(h) - \delta(h)}{N} \right]_n + \delta(h); \quad [E-1]$$

where N = number of particles in each K level; i.e., each K level has the same number of particles equally distributed across the radial width $[r(h) - \delta(h)]$.

For a given time increment, Δt , the tank outflow volume during this increment is $Q\Delta t$. An empirical factor relating the tank's K level heights can be found by the expression:

$$\pi \int_{K(h)}^{K(h+1)} \left[\frac{r^2(h) - \delta^2(h)}{Q\Delta t} \right] dh = K. \quad [E-2]$$

We now assume a solid body, ω_o , for the entire contents of the tank. The specific kinetic energy of every particle is found by the expression $1/2 r_n^2 \omega_o^2$ and the total kinetic energy of an entire K level is

$$1/2 \sum_{n=1}^N r_n^2 \omega_o^2.$$

The particles now redistribute their kinetic energies according to the relation:

$$\omega_n = \frac{C_K}{r_n^2},$$

where

$$C_K = \omega_0 \sqrt{\frac{\sum_{n=0}^N (r_n)^2}{\sum_{n=0}^N \left(\frac{1}{r_n}\right)^2}}. \quad [E-3]$$

This computation is repeated for each K level.

The vertical bands have been taken to be equal in width, and each band contains certain particles. For any single band, the kinetic energies for any K level are averaged, and then all the K-band-level energies are averaged. This is repeated for each bandwidth. Then, an equivalent weight is calculated for each band, referencing their heights to the band height of the outermost width, which is set equal to zero. This is expressed by:

$$h_B = \frac{\overline{KE}_B - \overline{KE}_1}{g}. \quad [E-4]$$

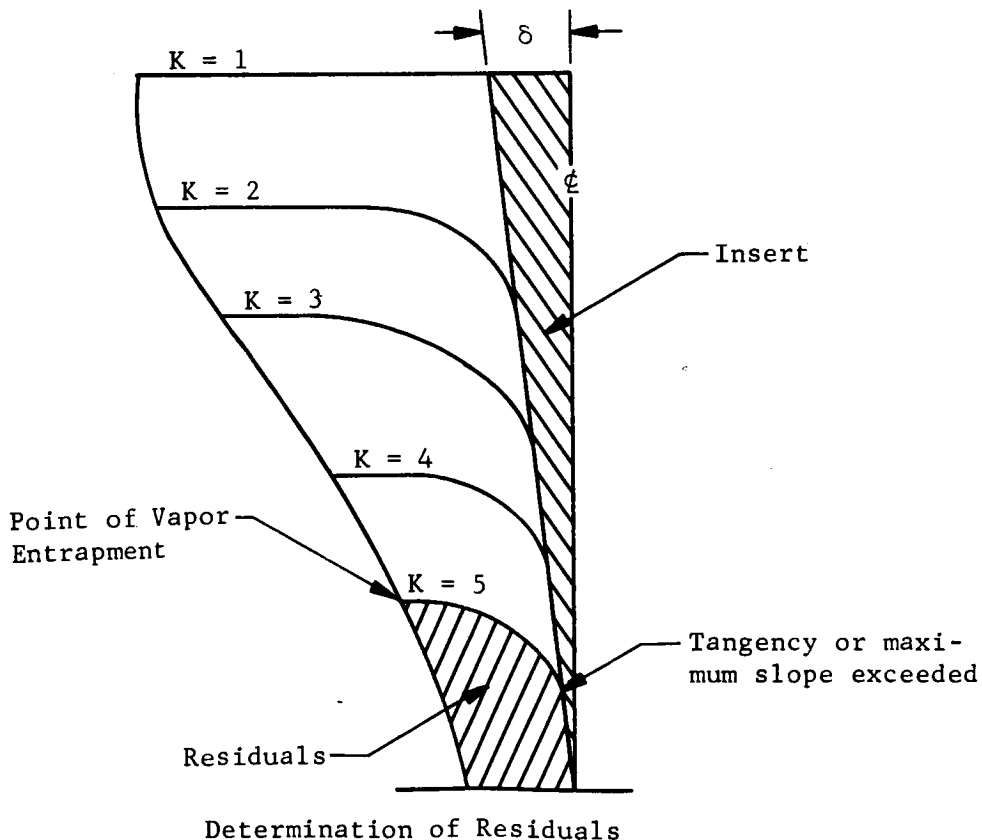
The outflow then starts. The nth particle in any K level moves down and displaces the nth particle in the next K level. Based on the conservation of angular momentum, its new angular rotation is given by:

$$\omega_{K+1, n} = \frac{r^2(K, n) \omega_{K, n}}{r^2(K+1, n)}. \quad [E-5]$$

The particles now redistribute their kinetic energies, and the new equivalent height for each band is recomputed. This process is continued until the tank is emptied.

In this manner, a height cross section of the vortexing fluid is obtained for each interval of time. Vapor is not entrapped as long as the height profile intersects the $\delta(h)$ area as shown in the following sketch. When the height profile begins to lie tangent to the $\delta(h)$ profile (i.e., for $K = 5$), vapor entrapment may be expected, and outflow of propellant must cease. In this manner, an estimate of the residuals is obtained for any particular circular tank outlet, initial perturbation rate, and $\delta(h)$ insert configuration.

Since the exact determination of vapor entrapment is clouded by possible misinterpretation of machine output, an additional section to the program, Data Reduction and Curve Generation, is included. This determines the mean particle radius of each band. A curve is fit to the points most influenced by the vortex (i.e., the three bands nearest the axis). It then determines the point of vapor entrapment by extrapolating the curve to the flow core. The point of entrapment is identified mathematically by either of two ways: as a tangency of the extrapolated line with the flow core or as some condition of excessive slope of the extrapolated line. As a program check, coefficients A, B, and C for the generated curve are a part of the output.



The vortex computer program also requires tank outlet configuration input in tabular form. The program initially undertakes a curve-fitting process wherein the lowest-order polynomial that yields a standard deviation less than some preassigned value is accepted. The same is true for the insert configuration, where applicable. After expressions for these two configurations are found, the program proceeds as previously described.

The complete program listing is shown on the following seven pages.

```

TERMINAL DRAINING PROGRAM  VORTEXING ANALYSIS  ...PHASE 1  OF 3
DIMENSION WRLN(10,20),R(121),DELTA(121),L(10),KLN(10,20),CLN(10)
LIST = 1
DO 500 IP = 1,121
500 READ 100,R(IP)
100 FORMAT(F10.5)
READ 232,OMEGI,TINTR,FLOW,SCALE,CORE,GF
232 FORMAT(6F10.3)
IF(CORE)79,82,82
79 DO 80 K = 1,121
80 READ 100,DELTA(K)
82 TYPE 889,OMEGI,TINTR
889 FORMAT(8H OMEGI= F10.5/8H TINTR= F10.5)
DELH=0.
C LEVEL SETTING
DO 7 IP = 1,10
X=0.
DO 5 K = 1,121
X=R(K)*2 +X
V=FLOW*TINTR*DELH/.31416
LLL=K
IF(X-V)5,5,6
5 CONTINUE
6 L(IP)=LLL
IF(SENSE SWITCH 1)500,604
600 TYPE 779,R(LLL),L(IP)
779 FORMAT(11H RADIUS IS F9.5,11H AT HEIGHT 14)
604 IPX=IP
IF(SENSE SWITCH 3)200,201
200 ACCEPT 423,TINTR
423 FORMAT(F20.0)
GO TO 82
201 I=IPX
IF(L(IP)-121)7,1,1
7 DELH=DELH + 1.
1 CONTINUE
DO 9 IN = 1,I
NUM = L(IN)
IF(CORE)606,83,83
83 DELTA(NUM)=CORE*R(NUM)
606 DO 9 KX = 1,20
X=KX

```

```

9  RLN(IN,KX)=((R(NUM)-DELTA(NUM))/20.)*X )+DELTA(NUM)
DC 12 IN = 1,I
I=IPX
X=0.
DO 10 KX = 1,20
10  X=RLN(IN,KX)**2 +X
Y=0.
DO 11 KX=1,20
11  Y=(1./RLN(IN,KX))**2 +Y
12  CLN(IN) = (SQRT(X/Y))*OMEGI
I=IPX
DO 13 IN = 1,I
DO 13 KX = 1,20
13  WRLN(IN,KX)=(CLN(IN)/RLN(IN,KX)**2)**2
PUNCH 107,IPX,LIST,SCALE,GF
DO 302 LL = 1,I
PUNCH 706,L(LL)
DO 302 MM = 1,20
302  PUNCH 303, RLN(LL,MM),WRLN(LL,MM)
107  FORMAT(2I5,2F10.5)
706  FORMAT(I5)
303  FORMAT(2E20.10)
TYPE 576
576  FORMAT(15H RUN COMPLETED )
END

```

TERMINAL DRAINING PROGRAM VORTEXING ANALYSIS...PHASE 2

C
C

```

DIMENSION B(10),L(10),CLN(10),MSAVE(20),XCLN(10)
DIMENSION R(121),RLN(10,20),      WRLN(10,20),ELBA(10,10)
DO 300 M = 1,121
300 READ 303, R(M)
      READ 500,IPX,LIST,SCALE,GF
      DO 302 LL = 1,IPX
      READ 500, L(LL)
      DO 302 M = 1,20
302 READ 303, RLN(LL,M),WRLN(LL,M)
69 N = L(LIST)
PUNCH 602,LIST
602 FORMAT(//5H BAND,6X,6HRADIUS,6X,6HHEIGHT,5X,7HINSTANT,13)
DO 24 M = 1,10
A=M
B(M)=R(N)*A/10.
DO 20 IN = LIST,IPX
MO=0
DO 15 KX = 1,20
IF (M-1)17,17,558
558 IF(B(M-1)-RLN(IN,20))555,19,19
555 IF(B(M-1)-RLN(IN,KX))17,17,15
17 IF(B(M)-RLN(IN,KX))19,19,16
16 MO=MO+1
MSAVE(MO)=KX
IF (KX-20) 15,19,19
15 CONTINUE
19 X=0.
IF (MO)30,30,31
30 ELBA(M,IN)=0.
GO TO 20
31 DO 20 LF = 1,MO
      KX=MSAVE(LF)
      X=RLN(IN,KX)**2*WRLN(IN,KX) + X
A=MO
20 ELBA(M,IN)=X/A
X=0.
LL=IPX-1
DO 23 IN = LIST,LL
A=L(IN+1)-L(IN)

```

```

      CLN(IN)=ELBA(M,IN)*A
23  X= CLN(IN)+X
    DO 22 KX = N,121
      A=XX-N
      IF(R(KX)-B(M))24,22,22
22  CONTINUE
24  XCLN(M)=X/A
      A=L(LIST)-1
      DO 600 M = 1,10
        BX = (((XCLN(10)-YCLN(M))/(32.17*GF))-(A/10.))*SCALE
        600 PUNCH 117,M,B(M),BX
        117 FORMAT(1X,13,5X,F8.4,4X,E11.5)
        303 FORMAT(2E20.10)
        500 FORMAT(2I5,2F10.5)
        LIST=LIST+1
        IF(LIST-IPX)800,801,801
800  DO 13 IN = LIST,IPX
      X=0.
      DO 10 KX = 1,20
        10 X=((WRLN(IN-1,KX) -*(RLN(IN-1,KX)**4)/RLN(IN,KX)**2)) + X
      Y=0.
      DO 11 KX = 1,20
        11 Y=(1./RLN(IN,KX))**2 +Y
      CLN(IN)=X/Y
      DO 13 KX = 1,20
        13 WRLN(IN,KX)=CLN(IN)/RLN(IN,KX)**4
      GO TO 69
801  END

```

```

C      TERMINAL DRAINING PROGRAM: VORTEXING ANALYSIS...PHASE 3
C      DATA REDUCTION AND CURVE GENERATION
C
C      SWITCH 1 CAUSES GENERATION OF SECOND ORDER CURVE (IF ON)
C      SWITCH 2 CAUSES RADIUS AND HEIGHT VALUES OF CURVE TO BE TYPED OUT (IF ON)
C
C
100 DIMENSION R(10),HITE(10),POINT(10)
    READ 1,INST
    1 FORMAT(/,/4IX,I3)
    IF(INST)21,998,21
    21 DO 20 I = 1,10
    20 READ 2,R(I),HITE(I)
    2 FORMAT(9X,F8.0,4X,E11.0)
    DO 30 I = 1,10
    IF(I-1)40,40,41
    40 POINT(I)=R(I)*.5
    GO TO 30
    41 POINT(I)=(R(I)+R(I-1))* .5
    30 CONTINUE
    PUNCH 31,INST
    31 FORMAT(/,5X,7H POINT /5X,7H RADIUS,5X,7H HEIGHT,8X,8H INSTANT,I3)
    DO 50 I = 1,10
    50 PUNCH 32,POINT(I),HITE(I)
    32 FORMAT(3X,F9.4,4X,E11.4)
    PUNCH 102
    102 FORMAT(/10X,31HNCTE..RADIUS AND HEIGHT IN FEET /)
    IF(SENSE SWITCH 1)150,100
    150 X1=POINT(1)**2
        X2=POINT(2)**2
        X3=POINT(3)**2
        Y1=POINT(1)
        Y2=POINT(2)
        Y3=POINT(3)
        Z1=1.
        Z2=1.
        Z3=1.
        P=X1*Y2*Z3+Y1*Z2*X3+Z1*X2*Y3-X3*Y2*Z1-Y3*Z2*X1-Z3*X2*Y1
        DO 200 I = 1,3
        GO TO ( 201,202,203),I
    201 X1=HITE(1)
        X2=HITE(2)

```



```

X3=HITE(3)
Y1=POINT(1)
Y2=POINT(2)
Y3=POINT(3)
Z1=1.
Z2=1.
Z3=1.
GO TO 500
202 X1=POINT(1)**2
X2=POINT(2)**2
X3=POINT(3)**2
Y1=HITE(1)
Y2=HITE(2)
Y3=HITE(3)
Z1=1.
Z2=1.
Z3=1.
GO TO 500
203 X1=POINT(1)**2
X2=POINT(2)**2
X3=POINT(3)**2
Y1=POINT(1)
Y2=POINT(2)
Y3=POINT(3)
Z1=HITE(1)
Z2=HITE(2)
Z3=HITE(3)
500 Q=X1*Y2*Z3+Y1*Z2*X3+Z1*X2*Y3-X3*Y2*Z1-Y3*Z2*X1-Z3*X2*Y1
GO TO (501,502,503),I
501 A=Q/P
GO TO 200
502 B=Q/P
GO TO 200
503 C=Q/P
200 CONTINUE
XS=1.
601 SLOPE=2.*A*XS+B
YS=A*XS**2+B*XS+C
IF(YS+12.)602,603
603 IF(SLOPE-1000.)609,602,602
609 IF(XS)999,999,604
604 XS=XS-.05

```

```
GO TO 601
602 IF(SENSE SWITCH 2)605,606
605 TYPE 608,XS,YS,SLOPE
608 FORMAT( 2HK=F10.4,10X,3HY=F10.4,10X,6HSLOPE=F10.4/)
606 PUNCH 607,A,B,C
607 FORMAT(2HA=F10.4,5X,2HE=F10.4,5X,2HC=F10.4)
PUNCH 608,XS,YS,SLOPE
GO TO 100
998 TYPE 800
800 FORMAT(13HRUN COMPLETED)
IF(SENSE SWITCH 3)100,876
876 STOP
999 TYPE 801
801 FORMAT(41HRADIUS IS AT ZERO, HEIGHT IS ABOVE BOTTOM /)
GO TO 605
END
```

DISTRIBUTION

Copies

To

1 thru 10
(plus one
reproducible)

Purchasing Office
George C. Marshall Space Flight Center
National Aeronautics and Space Administration
Huntsville, Alabama 35812
Attn: PR-EC

Remaining
Copies

Martin Company
Denver Division
Denver, Colorado 80201
Attn: Libraries Section